AN ABSTRACT OF THE DISSERTATION OF

Paroma Chatterjee for the degree of Doctor of Philosophy in Molecular and Cellular Biology presented on November 18, 2016.

Title: Establishing Larval Zebrafish as an *In Vivo* Model Organism for Characterizing the Roles of Otoferlin, a Sensory Hair Cell Protein Essential for Hearing.

Abstract approved: _____

Colin P. Johnson

Abstract

Auditory defects and disorders are prevalent at all ages and affect 8% of the population in developed nations including newborns and children. Congenital hearing loss is the most common birth defect and it is estimated that 1 in 1000 children are affected by deafness at birth or before the onset of speech. Most of these children suffer from non-syndromic hearing loss, where hearing loss is the sole symptom with no other associated symptoms. More than two-thirds of non-syndromic hearing loss cases are of genetic origin, with approximately 80% inherited in an autosomal recessive mode. Autosomal recessive deafness is attributed to *DFNB* loci. Different *DFNB* loci have been reported and more than 50 genes have been identified to date. One such gene that encodes otoferlin, *OTOF* is responsible for the *DFNB9* nonsyndromic form of deafness, which accounts for up to 8% of all prelingual autosomal recessive nonsyndromic deafness. Patients with mutations in

otoferlin suffer from profound sensorineural prelingual non-syndromic hearing loss.

Otoferlin belongs to the ferlin family of proteins. Ferlins are a group of multi-C2 domain proteins with emerging roles in vesicle fusion, membrane trafficking and repair. Otoferlin has six C2 domains including a C-terminal trans-membrane domain and these C2 domains bind to calcium, phospholipids and SNARE proteins. Otoferlin has been proposed to play a role in exocytosis of synaptic vesicles at the auditory inner hair cell synapse and also contributes to the development of the auditory cell synapse. Ablation of this gene causes abolition of exocytosis and improper targeting of synaptic components in sensory hair cells. More than 60 pathogenic mutations have been reported and are distributed in different C2, non-C2, and transmembrane domains of otoferlin. Despite the fact that otoferlin is a major contributor to sensorineural deafness, very little is known about the actual role of this protein in sensory hair cells.

Currently, the field is restricted by a lack of an *in vivo* model that could facilitate rapid analysis and easy characterization of otoferlin. Most studies have used mouse and rat models where, hair cells are few in number and require harvesting through time-consuming micro-dissections of the animal ear. Given the importance of otoferlin in hair cell development and function, and the lack of an easy genetically manipulatable model, the goal of this thesis was to develop a more tractable organismal model to establish the role of otoferlin.

Over the past years, zebrafish has emerged as an ideal model to study vertebrate development. It allows rapid assessment of gene function *in vivo* because it is amenable to genetic manipulation. Most importantly, the transparency of the zebrafish embryos allows direct visualization of tissue morphogenesis as it occurs in a live organism. Moreover, zebrafish possesss the easily accessible lateral line system, comprised of clusters of sensory hair cells, which are similar to mammalian type II vestibular hair cells and have similar morphological and anatomical structure. These sensory cells possesss synaptic ribbon bodies composed of L-type voltage activated calcium channels, a VGlut3 transporter for glutamate loading in synaptic vesicles, and develop a post-synapse upon maturation. Despite all these structural similarities zebrafish hair cells possesss only 3-5 synapses per hair cell. The aim here is to characterize the role of otoferlin by generating zebrafish models for otoferlinopathy.

Here we show for the first time that otoferlin is conserved in all species including zebrafish. However, due to a zebrafish genome duplication event, the *otoferlin* gene is paralogous, and there are two different subtypes which we named *otoferlin a* (encoded on chromosome 20) and *otoferlin b* (encoded on chromosome 17). Otoferlin a is the longer gene and has all six C2 domains, whereas otoferlin b is the shorter gene and lacks an N-terminal C2 domain. Otoferlin expression starts early during larval development and coincides with the onset of sensory morphogenesis and maturation. The otoferlin a isoform is strictly restricted to the hair cells of the developing otic

region, whereas otoferlin b is distributed in the hair cells of the otic region and lateral line neuromasts. At the cellular level, otoferlin distribution is observed in the supranuclear and basolateral regions of hair cells. Depleting both isoforms of otoferlin results in auditory and vestibular defects in larval zebrafish, and larvae exhibit abnormal swimming behavior. Moreover, larvae fail to develop an inflated swim bladder and develop a curved spine phenotype that becomes more prominent with development and facilitates a circling swimming behavior. These otoferlin-depleted zebrafish morphants belong to a class of 'circler' mutants that possesss similar hearing and balance defects. At the molecular level, sensory hair cells of otoferlin-depleted zebrafish developed atypical synapses comprised of tightly coalesced synaptic ribbon bodies, diffusely distributed VGlut3 and a dense and enlarged post-synapse. However, these hair cells possesssed an intact calcium response to mechanical deflection of hair bundles indicating an absence of mechanotransduction defects upon otoferlin depletion. Furthermore, otoferlin- depleted zebrafish exhibited severe defects in endocytotic dye uptake predominantly in the basolateral region of neuromast hair cells.

Studies have identified several otoferlin-interacting partners, however, a comprehensive study on otoferlin mutants is lacking. Also lacking is a more vivid description of the genes regulating the circler phenotype during development and maturation. For the first time we report a high-throughput transcriptomic analysis of otoferlin-depleted zebrafish in an attempt to

characterize the circler phenotype in larvae that also exhibit abnormal synaptic development. This study validates zebrafish as a model for high-throughput studies of the auditory and vestibular circler motility mutants, including otoferlin mutants. In this high-throughput transcriptomic study we identify several novel transcripts that are up or downregulated due to otoferlin depletion in zebrafish larvae. Some of these transcripts are very specific to the lateral line neuromasts and otic vesicle and have been shown to play roles during morphogenesis and development of the zebrafish sensory and neuronal regions. Moreover, there is a correlation between altered levels of some of these novel transcripts in otoferlin-depleted sensory cells and their synaptic morphology; hair cells with reduced levels of identified transcripts show an abnormal synaptic morphology indicated by coalesced distribution of synaptic ribbons when compared with control siblings.

Finally, this is also the first study that shows that the rescue of gross phenotypic loss due to otoferlin depletion is possible by co-injecting otoferlin-depleted larvae with the *p5E-pmyo6b* hair cell specific vector containing full length (FL) and truncated versions of mouse otoferlin constructs. This further reiterates that otoferlin is indeed conserved across species and that gross rescue of the phenotype can be achieved with either mouse otoferlin FL or truncated constructs that contains as little as just one C-terminal C2 domain with the trans-membrane region. This also provides a sense of which otoferlin domains are sufficient to rescue synaptic activity. Furthermore, we also see rescue in levels of reduced transcripts that are derived from the transcriptomic

analysis when otoferlin-depleted larvae are coinjected with the *p5E-pmyo6b* mouse FL vector construct.

Overall, these studies successfully establish zebrafish as an *in vivo* model organism to characterize defects associated with otoferlin loss, both at the molecular and transcriptomic levels in a much shorter span of time compared to mouse-based studies. They also show a promising application of otoferlin trans-species rescue using hair-cell-specific otoferlin rescue contructs that correct for loss of overall auditory and vestibular defects associated with otoferlin depletion in larval zebrafish.

Establishing Larval Zebrafish as an *In Vivo* Model Organism for Characterizing the Roles of Otoferlin, a Sensory Hair Cell Protein Essential for Hearing.

by
Paroma Chatterjee

A DISSERTATION

submitted to

Oregon State University

in partial fulfillment of
the requirements for the
degree of

Doctor of Philosophy

Presented November 18, 2016
Commencement June 2017

Doctor of Philosophy dissertation of Paroma Chatterjee presented on November 18, 2016

APPROVED:

Major Professor, representing Molecular and Cellular Biology

Director of the Molecular and Cellular Biology Graduate Program

Dean of the Graduate School

I understand that my dissertation will become part of the permanent collection of Oregon State University libraries. My signature below authorizes release of my dissertation to any reader upon request.

Paroma Chatterjee, Author

ACKNOWLEDGEMENTS

Any accomplishment requires the effort of many people and my thesis is no exception to this and I would like to take this opportunity to thank each and every person who has made this possible. First of all, I would like to express my sincere thanks to my advisor and graduate mentor Prof. Colin P. Johnson for his tireless help, support and motivation. Thank you for always taking out time to share new and novel research ideas and broadening my research perspectives. I would like to express my sincere gratitude to Prof. Robert L. Tanguay, Director, Sinnhuber Aquatic Research Laboratory (SARL) for his continued support and for giving me an opportunity to accomplish my research at SARL. I am also thankful to Prof. Katie S. Kindt, NIDCD, NIH for her help and feedback and granting me an opportunity to work in her lab. I am grateful to all my fellow group members at the Johnson lab and the Tanguay lab for all their support and feedbacks. This acknowledgement section will be incomplete if I do not thank Jane LaDu and Carrie Barton, Faculty Research Assistant, SARL, for their constant help. I would like to thank Lisa Truong, Deputy Director, SARL for all her support. I would also like to thank my other committee members – Prof. Kathy Magnusson, Prof. Thomas Wolpert and my Grad Rep Dr. Sue-Ann Bottoms for their guidance.

I am really thankful to my parents – Mr. Goutam Chatterjee and Mrs. Sanghamitra Chatterjee for their immense enthusiasm, support, motivation and unconditional love; my in-laws – Late Dr. Sumit Kumar Roy (father-in-law) and Mrs. Swapna Roy (mother-in-law) and my sister-in-law (Dr. Debaleena

Das Chakraborty) for their constant support, motivation and unconditional love. Finally, this acknowledgement section will be incomplete without thanking my husband, Dr. Ananda Sankar Roy for his constant support, enthusiasm, guidance and companionship. Overall, it has been an excellent experience during my Ph.D. career at Oregon State University, Corvallis.

CONTRIBUTION OF AUTHORS

Chapter 1: Paroma Chatterjee wrote the chapter with editing by Prof. Colin P. Johnson.

Chapter 2: Prof. Colin P. Johnson has designed the research experiments. Prof. Colin P. Johnson and Paroma Chatterjee have written the manuscript. Paroma Chatterjee has performed all the principal experiments with help from Murugesh Narayanappa, Nazish Abdullah and Jane LaDu. Paroma Chatterjee has analyzed all the data and prepared graphs. Prof. Robert L. Tanguay has given feedbacks on experiments and done critical analysis of the manuscript.

Chapter 3: Paroma Chatterjee has designed the experiments, analyzed the data and written the manuscript with help from Derik Haggard, Prof. Robert L. Tanguay and Prof. Colin P. Johnson. Paroma Chatterjee has performed all the principle experiments with help from Aayushi Manchanda. Derik Haggard helped with the transcriptomic data analysis. Prof. Katie S. Kindt has helped with the calcium imaging experiments. Prof. Robert L. Tanguay has done the critical analysis of the manuscript.

Chapter 4: Paroma Chatterjee wrote the chapter with editing by Prof. Colin P. Johnson.

TABLE OF CONTENTS

Page

TABLE OF CONTENTS (Continued)

Page

TABLE OF CONTENTS (Continued)

LIST OF FIGURES

Figures Page

LIST OF FIGURES (Continued)

Figures Page

LIST OF TABLES

Tables Page

Dedicated to *my beloved parents, in-laws and husband.*

Chapter 1 – General Introduction: Hereditary Non-Syndromic Hearing loss; DFNB loci, and the Involvement of Otoferlin in Hearing

Paroma Chatterjee

1.1 Abstract:

Auditory impairment is prevalent at all ages and is a major health concern in developed nations, affecting around 8% of the population (1). The most commonly afflicted are children at birth, and it is estimated that 1 in 1000 newborns are deaf, one in 300 infants suffer from congenital hearing loss of a lesser degree and an additional 1 in 1000 are affected by profound hearing loss before they reach adulthood (2-3). Approximately 25% of hearing loss in children is environmental; more than 50% is caused by genetic change and, in the remaining 25%, the cause remains unknown (4). Of the causes with a genetic basis, the most frequent is the auditory recessive non-syndromic form of hearing loss (NSHL) attributable to the *DFNB* gene loci. The *DFNB* gene loci include several genes including *OTOF,* which encodes otoferlin. Affected individuals suffer from profound prelingual deafness that affects children before the onset of speech and manifests as auditory neuropathy or a condition where effective encoding and transmission of sound from the inner ear to the brain is impaired. However, very little is known about the actual contribution and function of this protein in the inner ear primarily due to lack of an adequate and easy-to-use animal model. Currently, cochlear implants are the only treatment option available to patients with mutations in DFNB genes including OTOF. However, cochlear implants do not fully restore hearing. Thus, there is a need to develop additional treatment for DFNB. Finding a cure also necessitates the development of appropriate animal models that can be used to understand the functions of the DFNB genes. We aim to better understand the role of otoferlin by establishing a

facile animal model that can be used for high throughput analyses to discover networks and pathways regulating the function of this protein. Additionally we aim to develop and test methods that could rescue the phenotypic changes associated with otoferlin-loss-of functions.

1.2 Hereditary hearing loss

Genetic causes account for the largest percentage of hearing loss in children. Hereditary hearing loss can be autosomal dominant, autosomal recessive, X-linked, or by mitochondrial inheritance. Of the 50% of cases caused by genetic mutations, more than 70% are non-syndromic and approximately 80% of the non-syndromic cases are inherited in an autosomal recessive manner **(FIGURE 1.1)** (5). In non-syndromic hearing loss (NSHL), the sole symptom is hearing loss. Most NHSL manifest as a sensorineural defect, primarily attributable to malfunctioning of the cochlea or to nerve pathways from the cochlea to the brain.To date, 105 *DFNB* genetic loci and 72 genes have been identified that cause autosomal recessive NSHL (http://hereditaryhearingloss.org/ ; Hereditary Hearing Loss Homepage). A full genotype-phenotype correlation is a great challenge due to the extreme genetic heterogeneity and the fact that mutations in broad subsets of genes confer NSHL. Another important concern is the complication caused by the wide variability in epidemiology of non-syndromic hearing impairments among different groups of populations (6-7). It is important to develop efficient high-throughput studies to deduce gene networks that are responsible for the DFNB phenotype.

1.3 The *DFNB* non-syndromic hearing loci and identification of otoferlin

The systematic elucidation of NSHL genes over the past two decades has identified a total of more than 105 *DFNB* genetic loci http://hereditaryhearingloss.org/ ; Hereditary Hearing Loss Homepage). This has been made possible by the establishment of massively parallel next gen sequencing technologies. More than 70 genes corresponding to the different *DFNB* loci have been identified to date. Some of these genes include – CX26 (*DFNB1),* encoding gap junction protein connexin 26 (8-9); MYO7A (*DFNB2)* and MYO15 (*DFNB3),* which encode the unconventional myosins, myosin VIIA and myosin XV (10-11); SLC26A4 (*DFNB4)*, which encodes the solute carrier family 26, member 4 an anion transporter (12); TMIE (*DFNB6)* encoding the transmembrane inner ear expressed gene (13). All these genes are expressed in the inner ear. At the turn of the century, Yasunaga S et al. (14-15), identified the OTOF gene corresponding to the *DFNB9* locus that encodes a trans-membrane protein called otoferlin. OTOF encodes multiple long and short isoforms of the protein generated by alternative splicing events and several translation initiation sites 14-15. Otoferlin is homologous to dysferlin, another ferlin protein, which was identified a year earlier (16). Both otoferlin and dysferlin belong to the family of ferlin proteins. Ferlins, including otoferlin, are large proteins (200-240 kDa) with multiple calcium-binding C2-domains (five to seven) and are anchored to the plasma membrane by a single C-terminal transmembrane domain **(FIGURE 1.2)** (17). Otoferlin is made up of six predicted C2 domains and a C-terminal transmembrane region. Genetic evidence suggests that a longer isoform of otoferlin with all six predicted C2 domains including the transmembrane domain, is

associated with *DFNB9 (*15). The C2 domains of otoferlin have been predicted to share high sequence homologies to other ferlins (18), but their similarity with non-ferlin C2 domain containing proteins like synaptotagmin 1, a conventional neuronal calcium sensing protein, is rather low (15).

1.4 Spectrum of mutations in different domains of otoferlin

Human patients with mutations in otoferlin suffer from auditory neuropathy and otoferlin accounts for up to 8% of all autosomal recessive NSHL (19). More than 60 pathogenic mutations have been identified in otoferlin, and these mutations are distributed in the C2, non C2 and transmembrane domains of the protein. Most of these pathogenic mutations lead to profound prelingual deafness. (19-20) **(FIGURE 1.3)**. The non-pathogenic mutations are mostly found in the C2A domain or in the linker region between the different C2 domains. There is no hotspot for the pathogenic mutations in the otoferlin C2 domains; however, most of the missense pathogenic mutations are distributed in the C2C-C2F domains (19). Of note is the Spanish mutation (Q829X) that results in a premature stop codon with affected individuals suffering from profound prelingual hearing loss (19,21). Other missense mutations were identified in a Turkish family, and include a L1011P substitution resulting in non-syndromic hearing loss (22); a P1825A substitution in a Spanish family afflicted with sensorineural deafness (21); a R1939Q substitution in Japanese patients resulting in an early onset auditory neuropathy (23). There are other kinds of mutations affecting different domains of otoferlin. Of note is the frameshift mutation caused by 1-bp deletion (1778G) leading to generation of a stop codon and formation of a truncated protein that causes auditory neuropathy in children (24).

Besides the prelingual non-syndromic form of hearing loss, there is a less frequent temperature–sensitive non-syndromic auditory neuropathy (TS-NSAN) phenotype also observed in patient with mutations in the OTOF gene. These patients suffer from normal-to-mild hearing loss when the individual is afebrile. However, with the onset of fever affected individuals suffer from severe to profound hearing loss. Hearing returns to normal when the fever subsides. Varga R. et al. (25), reported the I515T mutation that causes the temperature sensitive auditory neuropathy. Matsunaga et al., (23) identified the G541S substitution that renders a similar temperature sensitive phenotype in the affected individual. Given the widespread distribution of mutations in different domains of otoferlin, it is becoming increasingly important to decipher the structure and function of different domains including the overall function of the protein. Moreover, there is dire need to develop animal models of otoferlinopathy and study how the mutations can impact the overall protein function.

1.5 Otoferlin expression, mechanism of sound processing and proposed functions

1.5.1 Otoferlin expression

Most cases of DFNB9 deafness that is caused by mutations in otoferlin leads to dysfunction of the cochlea. Cochlea of the inner ear is made up of sound detecting sensory inner hair cells, sound amplifying outer hair cells, and neurons that innervate the cochlear cells and conduct the sound to the brain for processing. The main site of damage in DFNB9 deafness can be attributed to the sensory inner hair

cells, the auditory afferents and the synapses between them (26-27). In agreement with the regions affected in the DFNB9 deafness it was found that otoferlin is expressed mainly in the affected regions of the cochlea. There are two different isoforms of the *OTOF* gene that are detected in human tissues – the longer isoform with all the six C2 domains and the transmembrane region (7kb) was detected in the brain, whereas the shorter isoform, possesssing only the last three C2 domains and the C-terminal transmembrane region (5kb), was detected mainly in the inner ear and also other tissues. However, in mice, only the longer isoform (7kb) was detected, primarily in the brain, inner ear and vestibular organ (15). In agreement with previous studies, a more recent study found otoferlin protein expression was restricted to the rat brain, cochlear inner hair cells and also vestibular hair cells. Additionally, otoferlin expression was detected in the outer hair cells of the cochlea and also in the auditory afferent fibres (28). Moreover, in the outer, inner and vestibular hair cells, otoferlin was found at the synaptic terminal and was also subcellularly distributed throughout the sensory cell soma and even at a considerable distance from the neurotransmitter release site (28). This indicates broader roles of otoferlin beyond sound transmission (29). Given that otoferlin is primarily expressed in the cochlear and vestibular hair cells and otoferlin deficient patients primarily suffer from dysfunctioning of the inner ear, it is important that we get a better understanding of the structure of the inner ear and mechanism of sound processing.

1.5.2 Structure of inner ear and mechanism of sound processing and transmission

The cochlea of the inner ear is the most critical structure in the auditory pathway. It perceives and amplifies sound waves and also transforms them into neural impulses. The cochlea is made up of two different kinds of hair cell populations that encode acoustic signals with high precision. These cells are the inner hair cells (IHC) or sound sensors and the outer hair cells (OHC) or sound amplifiers **(FIGURE 1.4A).** Hair cells are flask-shaped epithelial cells that possess a bundle of hair like processes at the apical end. The hair bundles are arranged in an organ-pipe like structure and serve as mechanotransducers. At the opposite basolateral end of mammalian hair cells, there are 15-20 presynaptic specialized ribbon bodies. Ribbon bodies tether multiple synaptic vesicles, which are loaded with the excitatory neurotransmitter glutamate, and ensures a sustained release for effective sound encoding and transmission. Each of the presynaptic ribbon bodies synapse onto a post-synaptic afferent neuron and communicates the signal to the dendrites of the primary auditory nerve. Displacement of hair bundles towards the tallest stereocilium depolarizes the hair cell. The resulting depolarization event causes voltage gated calcium channels to open at the presynaptic active zone located in the basolateral end. Multiple vesicles that are tethered to the synaptic ribbon body fuse at the active zone and release neurotransmitter. Neurotransmitter release activates the post-synaptic receptors and conveys the signal to the auditory nerve (30-31).

Besides the sound detection system, the inner ear also possessses a system for perception of balance. This system is referred to as the vestibular system. The sensory receptor cells of the vestibular system are located in the otolith organ and the semicircular canals of the inner ear. The vestibular hair cells are like the cochlear

hair cells and function in a similar fashion in perceiving and transmitting balance signals to the vestibular nerve **(FIGURE 1.4B).** Both the auditory and vestibular sensory cells have specialized synapses that are different in both structure and composition compared to the conventional neuronal synapses. Hence, it is important to understand the composition, maturation and function of hair cell synapses to get a better understanding of otoferlin function during sensory development.

1.5.3 Organization and maturation of the hair cell ribbon synapses; Sub-cellular otoferlin localization in relation to the synapse

The inner, outer and vestibular hair cells have specialized synapses called ribbon synapses in the basal portion. The synaptic ribbons in sensory hair cells are phylogenetically old structures and are present in not only mammals but also in the fishes, amphibians and birds. Ribeye is the main structural component of the synaptic ribbons and tethers multiple synaptic vesicles at the synapses. Ribeye was isolated from mouse cochlear hair cells (32), frog saccular hair cells (33), and zebrafish neuromast hair cells (34), thus highlighting conservation of ribbon synapses in vertebrate evolution. Active research is underway to explore the still largely unexplored components of the active zone of the hair cell synaptic ribbons. Some of the basic components of vertebrate conventional CNS synapses that are actually involved in the regulation of the synaptic vesicle fusion events are absent at the hair cell synapses. In fact, studies have shown that, inner hair cell synapses operate without Munc-13 like priming factors (35); Rab-3 (36), and RIM (37) like vesicle tethering, docking and fusion factors. Furthermore, inner hair cell exocytosis is insensitive to genetic ablation of neural SNAREs (38) and hence a role of syntaxin

1, VAMP 1 and 2, as well as SNAP-25, in the the inner hair cell exocytosis is questionable. Moreover, SNARE regulators synaptotagmins 1 and 2 (39-40) and complexins (41-42) seem to be absent from the matured and fully functional inner hair cells. Currently, the demonstrated active zone components of inner hair cells include, scaffold proteins Bassoon and Piccolo (32), the glutamate solute carrier (SLC) transporter VGlut3 (43-44), voltage gated CaV1.3 calcium channel (45) and otoferlin, which is hypothesized to play a central role in hair cell exocytosis (29, 46, 47, 20).

As the hair cells of the inner ear develop and mature, the synaptic ribbons undergo several morphological, electrophysiological and compositional changes (48). The synaptic ribbons of mouse cochlear hair cells transform from a round to a more oval shape on maturation and develop a tighter post-synaptic density region compared to the immature hair cells. Moreover, the spontaneous depolarization in immature inner hair cells switches to more graded action potentials upon maturity. This is achieved by reductions in the number of CaV1.3 voltage gated calcium channels, which reduces regenerative depolarization responsible for spontaneous depolarization events. Moreover there is pruning of both the afferent and efferent neurons innervating the hair cell synaptic ribbons upon maturity. In conclusion, during development from pre-hearing to hearing, hair cell ribbon synapses undergo major morphological and functional refinements that results in a much tighter spatial coupling between Ca^{2+} influx and exocytosis. Besides the morphological and functional changes, the protein composition of hair cell synapses also changes during maturation and development; particularly the calcium sensors and vesicle

fusion regulators - synaptotagmins 1 and 2, are absent in the mature hair cells and there is predominant expression of the multi-C2 domain protein otoferlin, which is proposed to play a role similar to that of synaptotagmin 1 and 2 at the sensory hair cell synapses (48, 29, 20, 49).

Structural and domain analysis of otoferlin suggests that the protein is primarily localized to the basolateral membrane due to the presence of the C-terminal transmembrane domain. Furthermore, due to the presence of the C2 calcium binding domains (14), it is presumed to play a crucial role at the synaptic ribbons and proposed to primarily affect vesicle fusion events by regulating calcium sensing and downstream vesicle fusion (29,39, 47, 20). However, more recent studies have shown that in mouse cochlear hair cells, otoferlin is not exclusively localized to the active zone membrane and ribbons, is more diffusely distributed in the cytoplasm (29). Moreover, it was found that otoferlin colocalizes with the endosomal marker EEA1 and the golgi marker GM130 in mouse cochlear outer and inner hair cells (28). Also, otoferlin colocalizes with the endocytotic marker AP-2 in the apical region of mouse cochlear hair cells and a predominant expression of otoferlin was detected in the supranuclear region of cochlear hair cells (50). Furthermore, otoferlin co-localizes with the unconventional myosinVI in the apical and supranuclear region, in addition to the basolateral domain (51). All these data suggest a role for otoferlin that extends beyond the proposed exocytosis and vesicle fusion.

1.5.4 Current hypotheses of otoferlin function

Because otoferlin associates with synaptic vesicles and loss of the protein causes impairment of vesicle exocytosis at the synaptic ribbon (29), and given the

structural and biochemical similarities of otoferlin to synaptotagmin 1 (15), it is currently hypothesized that otoferlin functions as a synaptotagmin 1-like calcium sensor that regulates vesicle fusion at the cochlear hair cell synapses.

In vitro studies have indeed shown that otoferlin directly interacts with SNARE proteins, Syntaxin 1 and SNAP-25, and the otoferlin C2 domains also bind to calcium and phospholipids (29, 52-54). Also, presence of SNARE proteins was detected in the cochlear hair cells by immunolabeling and western blotting experiments (55, 42). Additionally, otoferlin was shown to play an indispensible role in hair cell exocytosis, both at the mature and immature hair cell synapses (29, 39, 47, 20). These data support a role of otoferlin in synaptic vesicle exocytosis at inner hair cell synapses. However, a more recent study has cast doubt on the role of SNARE proteins in vesicle fusion and exocytosis at the cochlear hair cell synapses by demonstrating that neuronal SNAREs are not required for exocytosis at cochlear hair cells (38). Furthermore, transgenic expression of synaptotagmin1 failed to restore cochlear hair cell exocytosis in otoferlin knockout mice (40). Together these findings suggest that otoferlin possibly binds with yet unidentified SNARE equivalents and regulates exocytosis at inner hair cells. These data also argue against a simple functional equivalence of otoferlin with it's structurally and biochemically related counterpart synaptotagmin 1 for inner hair cell function. More recently, Brandt N. et al., (56), demonstrated that immature cochlear hair cell exocytosis proceeds without the presence of otoferlin, which contradicts all previous studies that suggested the absolute requirement of otoferlin for hair cell exocytosis and vesicle fusion events. Therefore, there is an unquestionable need to clarify the

function of otoferlin in inner hair cells of the cochlea from a developmental perspective and also focus on detecting pathways and partners that regulate otoferlin function during maturation.

Beyond the hypothesized role in exocytosis and vesicle fusion events at the hair cell synapses, studies have also implicated a role for otoferlin in vesicle replenishment (20), endocytosis (50, 57), and development and maintenance of basolateral cochlear hair cell synapses (51). Moreover, auditory nerves of otoferlin mutant mice show a reduction in volume in comparison to control siblings suggesting a role of otoferlin in neural development (58). Additionally, otoferlin couples with GAD65 and modulates GABA levels in hippocampal neurons (59). All these data indicate a broader role of otoferlin that extends beyond just regulation of exocytosis at the hair cell synapses.

1.6 **Animal models of otoferlinopathy**

1.6.1 Animal models in otoferlin study

Most of the above findings on otoferlin are based on *in vitro* studies and using *in vivo* murine models. While mammalian murine models are insightful, share a comparable hearing range to humans, and exhibit high degrees of homology, one of the major challenges in hair cell research is the difficulty in harvesting sufficient hair cells to perform molecular experiments (60). A mouse ear contains only 10-30000 hair cells, which are buried in the cochlear bone. One has to burrow through the cochlear bone to reach the hair cells. This is a huge impediment to hair cell research.

Some of the popular mouse models of otoferlinopathy include, the *deaf5* mutant mice carrying a missense mutation in the C2B domain of otoferlin (51, 61). These mice exhibit a hearing loss phenotype which grossly phenocopies DFNB9 deafness. At the molecular level, these mice have defective exocytosis and the inner hair cells show signs of developmental defect and appear immature. The other otoferlin mutant is the *Pachanga* mouse with a missense mutation in the C2F domain of otoferlin that recapitulates the DFNB9 mutations. The *Pachanga* mutant mice are deaf at the systems level, exhibit defective startle reflex and, at the molecular level they have defective vesicle recycling and replenishment at the active zone of the inner hair cell synapse (20). In a most recent study, Strenzke N. et al., (62) has generated a temperature sensitive mouse model of otoferlinopathy ($Otof^{I515T}$), which recapitulates the otoferlin hearing loss caused by the rise of core body temperature in human patients. These mice exhibit a moderate hearing loss, have enlarged synaptic vesicles, and show reduced exocytosis at the ribbon synapses upon sustained stimulation. Some of the other otoferlin mice knockouts include the $Otof^{tm1.1.Erei}$, a targeted mutation created with the Cre-Lox method that results in an intragenic deletion/insertion of exon 14-15 encoding most of the C2C domain of mouse otoferlin. This mutant has been used in a couple of studies (40,35).

However, development of mouse models of otoferlinopathy is an extremely time consuming process and it takes years to develop a knockout mouse model. Moreover, the embryos are opaque and disallow direct visualization and morphogenesis of the ear and vestibular organ during development. In addition,

mouse models are low-throughput and cannot be successfully used to run a transcriptomic assay.

1.6.2 Zebrafish as an alternative model to study hearing and hearing related genes including otoferlin

Since its identification over almost two decades ago, overall progress on the study of otoferlin has been slow because micro-dissection and isolation of hair cells from mammalian ears is cumbersome and mammalian hair cells are almost impossible to transfect. Over the years, zebrafish have emerged as a model to study vertebrate development and diseases (63). Zebrafish allow rapid assessment of gene function *in vivo* because they are amenable to genetic manipulation, including rescue experiments. Most importantly, zebrafish embryos are optically clear and allow direct visualization of tissue morphogenesis. Yet, zebrafish have not been exploited to date for studying otoferlin. Additionally, zebrafish are an attractive candidate for studying development and function of the vertebrate sensory system because of the presence of the lateral line – a system composed of a series of hair cells on the surface of the fish that operate in a similar fashion to mammalian inner hair cells. Zebrafish have been previously used to characterize other inner hair cell proteins that include Ribeye (64), Cav1.3 (65) and VGlut3 (66), to mention a few. Thus, if it can be determined that zebrafish can be used as a model for otoferlin, it would help advance the study of otoferlin and associated disorders for many researchers currently limited in their choice of organismal models. Moreover, it would permit transcriptomic studies on otoferlin mutants and help to identify new interacting partners of otoferlin. Finally, it

would also allow possible rescue experiments on otoferlin mutants within a much shorter frame of time compared to rescue experiments on mice.

We aim to establish zebrafish as an *in vivo* model organism and characterize the function of otoferlin by generating otoferlin-depleted zebrafish models. We also aim to utilize the zebrafish model for transcriptomic assay in order to get a better understanding of the overall function of otoferlin. Finally we aim to develop and use the zebrafish for rescue experiments in an otoferlin-depleted background.

1.7 References

1) **Petit C, Levilliers J, Marlin S, Hardelin J-P**. Hereditary hearing loss. Scriver CR, Beaudet AL, Sly WS, Valle D, editors. New York: McGraw-Hill;2001:6281–6328

2) **Mason JA**, **Herrmann KR**. Universal infant hearing screening by automated auditory brainstem response measurement. Pediatrics. 1998;101:221–228

3) **Parving A.** The need for universal neonatal hearing screening: some aspects of epidemiology and identification. Acta Paediatr Suppl. 1999;88:69–72.

4) **Marres HA.** Congenital abnormalities of the inner ear. Ludman H, Wright T Bath, editors. Arnold & Oxford University Press; Diseases of the Ear.1998:288–296.

5) ACMG Genetics evaluation guidelines for the etiologic diagnosis of congenital hearing loss. Genetic Evaluation of Congenital Hearing Loss Expert Panel: ACMG statement. Genet Med.2002;4:162–171.

6) **Petit C, Levilliers J, Hardelin JP.** 2001. Molecular genetics of hearing loss. Annual review of genetics **35:**589-646.

7) **Friedman TB, Griffith AJ.** 2003. Human nonsyndromic sensorineural deafness. Annual review of genomics and human genetics **4:**341-402.

8) **Guilford P, Ben Arab S, Blanchard S, Levilliers J, Weissenbach J, Belkahia A, Petit C.** 1994. A non-syndrome form of neurosensory, recessive deafness maps to the pericentromeric region of chromosome 13q. Nature genetics **6:**24-28.

9) **Kelsell DP, Dunlop J, Stevens HP, Lench NJ, Liang JN, Parry G, Mueller RF, Leigh IM.** 1997. Connexin 26 mutations in hereditary non-syndromic sensorineural deafness. Nature **387:**80-83.

10) **Guilford P, Ayadi H, Blanchard S, Chaib H, Le Paslier D, Weissenbach J, Drira M, Petit C.** 1994. A human gene responsible for neurosensory, non-syndromic recessive deafness is a candidate homologue of the mouse sh-1 gene. Human molecular genetics **3:**989-993.

11) **Friedman TB, Liang Y, Weber JL, Hinnant JT, Barber TD, Winata S, Arhya IN, Asher JH, Jr.** 1995. A gene for congenital, recessive deafness DFNB3 maps to the pericentromeric region of chromosome 17. Nature genetics **9:**86-91.

12) **Baldwin CT, Weiss S, Farrer LA, De Stefano AL, Adair R, Franklyn B, Kidd KK, Korostishevsky M, Bonne-Tamir B.** 1995. Linkage of congenital, recessive deafness (DFNB4) to chromosome 7q31 and evidence for genetic heterogeneity in the Middle Eastern Druze population. Human molecular genetics **4:**1637-1642.

13) **Fukushima K, Ramesh A, Srisailapathy CR, Ni L, Chen A, O'Neill M, Van Camp G, Coucke P, Smith SD, Kenyon JB, et al.** 1995. Consanguineous nuclear families used to identify a new locus for recessive non-syndromic hearing loss on 14q. Human molecular genetics **4:**1643-1648.

14) **Yasunaga S, Grati M, Cohen-Salmon M, El-Amraoui A, Mustapha M, Salem N, El-Zir E, Loiselet J, Petit C.** 1999. A mutation in OTOF, encoding otoferlin, a FER-1-like protein, causes DFNB9, a nonsyndromic form of deafness. Nature genetics **21:**363-369.

15) **Yasunaga S, Grati M, Chardenoux S, Smith TN, Friedman TB, Lalwani AK, Wilcox ER, Petit C.** 2000. OTOF encodes multiple long and short isoforms: genetic evidence that the long ones underlie recessive deafness DFNB9. American journal of human genetics **67:**591-600.

16) **Liu J, Aoki M, Illa I, Wu C, Fardeau M, Angelini C, Serrano C, Urtizberea JA, Hentati F, Hamida MB, Bohlega S, Culper EJ, Amato AA, Bossie K, Oeltjen J, Bejaoui K, McKenna-Yasek D, Hosler BA, Schurr E, Arahata K, de Jong PJ, Brown RH, Jr.** 1998. Dysferlin, a novel skeletal muscle gene, is mutated in Miyoshi myopathy and limb girdle muscular dystrophy. Nature genetics **20:**31-36.

17) **Rizo J, Sudhof TC.** 1998. C2-domains, structure and function of a universal Ca2+-binding domain. The Journal of biological chemistry **273:**15879-15882.

18) **Jimenez JL, Bashir R.** 2007. In silico functional and structural characterisation of ferlin proteins by mapping disease-causing mutations and evolutionary information onto three-dimensional models of their C2 domains. Journal of the neurological sciences **260:**114-123.

19) **Rodriguez-Ballesteros M, Reynoso R, Olarte M, Villamar M, Morera C, Santarelli R, Arslan E, Meda C, Curet C, Volter C, Sainz-Quevedo M, Castorina P, Ambrosetti U, Berrettini S, Frei K, Tedin S, Smith J, Cruz Tapia M, Cavalle L, Gelvez N, Primignani P, Gomez-Rosas E, Martin M, Moreno-Pelayo MA, Tamayo M, Moreno-Barral J, Moreno F, del Castillo I.** 2008. A multicenter study on the prevalence and spectrum of mutations in the otoferlin

gene (OTOF) in subjects with nonsyndromic hearing impairment and auditory neuropathy. Human mutation **29:**823-831.

20) **Pangrsic T, Lasarow L, Reuter K, Takago H, Schwander M, Riedel D, Frank T, Tarantino LM, Bailey JS, Strenzke N, Brose N, Muller U, Reisinger E, Moser T.** 2010. Hearing requires otoferlin-dependent efficient replenishment of synaptic vesicles in hair cells. Nature neuroscience **13:**869-876.

21) **Migliosi V, Modamio-Hoybjor S, Moreno-Pelayo MA, Rodriguez-Ballesteros M, Villamar M, Telleria D, Menendez I, Moreno F, Del Castillo I.** 2002. Q829X, a novel mutation in the gene encoding otoferlin (OTOF), is frequently found in Spanish patients with prelingual non-syndromic hearing loss. Journal of medical genetics **39:**502-506.

22) **Tekin M, Akcayoz D, Incesulu A.** 2005. A novel missense mutation in a C2 domain of OTOF results in autosomal recessive auditory neuropathy. American journal of medical genetics. Part A **138:**6-10.

23) **Matsunaga T, Mutai H, Kunishima S, Namba K, Morimoto N, Shinjo Y, Arimoto Y, Kataoka Y, Shintani T, Morita N, Sugiuchi T, Masuda S, Nakano A, Taiji H, Kaga K.** 2012. A prevalent founder mutation and genotype-phenotype correlations of OTOF in Japanese patients with auditory neuropathy. Clinical genetics **82:**425-432.

24) **Varga R, Kelley PM, Keats BJ, Starr A, Leal SM, Cohn E, Kimberling WJ.** 2003. Non-syndromic recessive auditory neuropathy is the result of mutations in the otoferlin (OTOF) gene. Journal of medical genetics **40:**45-50.

25) **Varga R, Avenarius MR, Kelley PM, Keats BJ, Berlin CI, Hood LJ, Morlet TG, Brashears SM, Starr A, Cohn ES, Smith RJ, Kimberling WJ.** 2006. OTOF mutations revealed by genetic analysis of hearing loss families including a potential temperature sensitive auditory neuropathy allele. Journal of medical genetics **43:**576-581.

26) **Cone-Wesson B, Vohr BR, Sininger YS, Widen JE, Folsom RC, Gorga MP, Norton SJ.** 2000. Identification of neonatal hearing impairment: infants with hearing loss. Ear and hearing **21:**488-507.

27) **Starr A, Sininger YS, Pratt H.** 2000. The varieties of auditory neuropathy. Journal of basic and clinical physiology and pharmacology **11:**215-230.

28) **Schug N, Braig C, Zimmermann U, Engel J, Winter H, Ruth P, Blin N, Pfister M, Kalbacher H, Knipper M.** 2006. Differential expression of otoferlin in brain, vestibular system, immature and mature cochlea of the rat. The European journal of neuroscience **24:**3372-3380.

29) **Roux I, Safieddine S, Nouvian R, Grati M, Simmler MC, Bahloul A, Perfettini I, Le Gall M, Rostaing P, Hamard G, Triller A, Avan P, Moser T, Petit C.** 2006. Otoferlin, defective in a human deafness form, is essential for exocytosis at the auditory ribbon synapse. Cell **127:**277-289.

30) **Hudspeth AJ.** 1997. How hearing happens. Neuron **19:**947-950.

31) **Hudspeth AJ.** 2000. Hearing and deafness. Neurobiology of disease **7:**511-514.

32) **Khimich D, Nouvian R, Pujol R, Tom Dieck S, Egner A, Gundelfinger ED, Moser T.** 2005. Hair cell synaptic ribbons are essential for synchronous auditory signalling. Nature **434:**889-894.

33) **Zenisek D, Davila V, Wan L, Almers W.** 2003. Imaging calcium entry sites and ribbon structures in two presynaptic cells. The Journal of neuroscience **23:**2538-2548.

34) **Sheets L, Hagen MW, Nicolson T.** 2014. Characterization of Ribeye subunits in zebrafish hair cells reveals that exogenous Ribeye B-domain and CtBP1 localize to the basal ends of synaptic ribbons. PloS one **9:**e107256.

35) **Vogl C, Cooper BH, Neef J, Wojcik SM, Reim K, Reisinger E, Brose N, Rhee JS, Moser T, Wichmann C.** 2015. Unconventional molecular regulation of synaptic vesicle replenishment in cochlear inner hair cells. Journal of cell science **128:**638-644.

36) **Geppert M, Goda Y, Stevens CF, Sudhof TC.** 1997. The small GTP-binding protein Rab3A regulates a late step in synaptic vesicle fusion. Nature **387:**810-814.

37) **Schoch S, Castillo PE, Jo T, Mukherjee K, Geppert M, Wang Y, Schmitz F, Malenka RC, Sudhof TC.** 2002. RIM1alpha forms a protein scaffold for regulating neurotransmitter release at the active zone. Nature **415:**321-326.

38) **Nouvian R, Neef J, Bulankina AV, Reisinger E, Pangrsic T, Frank T, Sikorra S, Brose N, Binz T, Moser T.** 2011. Exocytosis at the hair cell ribbon synapse apparently operates without neuronal SNARE proteins. Nature neuroscience **14:**411-413.

39) **Beurg M, Michalski N, Safieddine S, Bouleau Y, Schneggenburger R, Chapman ER, Petit C, Dulon D.** 2010. Control of exocytosis by synaptotagmins and otoferlin in auditory hair cells. The Journal of neuroscience **30:**13281-13290.

40) **Reisinger E, Bresee C, Neef J, Nair R, Reuter K, Bulankina A, Nouvian R, Koch M, Buckers J, Kastrup L, Roux I, Petit C, Hell SW, Brose N, Rhee JS, Kugler S, Brigande JV, Moser T.** 2011. Probing the functional equivalence of otoferlin and synaptotagmin 1 in exocytosis. The Journal of neuroscience **31:**4886-4895.

41) **Strenzke N, Chanda S, Kopp-Scheinpflug C, Khimich D, Reim K, Bulankina AV, Neef A, Wolf F, Brose N, Xu-Friedman MA, Moser T.** 2009. Complexin-I is required for high-fidelity transmission at the endbulb of Held auditory synapse. The Journal of neuroscience **29:**7991-8004.

42) **Uthaiah RC, Hudspeth AJ.** 2010. Molecular anatomy of the hair cell's ribbon synapse. The Journal of neuroscience **30:**12387-12399.

43) **Seal RP, Akil O, Yi E, Weber CM, Grant L, Yoo J, Clause A, Kandler K, Noebels JL, Glowatzki E, Lustig LR, Edwards RH.** 2008. Sensorineural deafness and seizures in mice lacking vesicular glutamate transporter 3. Neuron **57:**263-275.

44) **Ruel J, Emery S, Nouvian R, Bersot T, Amilhon B, Van Rybroek JM, Rebillard G, Lenoir M, Eybalin M, Delprat B, Sivakumaran TA, Giros B, El Mestikawy S, Moser T, Smith RJ, Lesperance MM, Puel JL.** 2008. Impairment of SLC17A8 encoding vesicular glutamate transporter-3, VGLUT3, underlies nonsyndromic deafness DFNA25 and inner hair cell dysfunction in null mice. American journal of human genetics **83:**278-292.

45) **Brandt A, Khimich D, Moser T.** 2005. Few CaV1.3 channels regulate the exocytosis of a synaptic vesicle at the hair cell ribbon synapse. The Journal of neuroscience **25:**11577-11585.

46) **Beurg M, Safieddine S, Roux I, Bouleau Y, Petit C, Dulon D.** 2008. Calcium- and otoferlin-dependent exocytosis by immature outer hair cells. The Journal of neuroscience **28:**1798-1803.

47) **Dulon D, Safieddine S, Jones SM, Petit C.** 2009. Otoferlin is critical for a highly sensitive and linear calcium-dependent exocytosis at vestibular hair cell ribbon synapses. The Journal of neuroscience **29:**10474-10487.

48) **Safieddine S, El-Amraoui A, Petit C.** 2012. The auditory hair cell ribbon synapse: from assembly to function. Annual review of neuroscience **35:**509-528.

49) **Pangrsic T, Reisinger E, Moser T.** 2012. Otoferlin: a multi-C2 domain protein essential for hearing. Trends in neurosciences **35:**671-680.

50) **Duncker SV, Franz C, Kuhn S, Schulte U, Campanelli D, Brandt N, Hirt B, Fakler B, Blin N, Ruth P, Engel J, Marcotti W, Zimmermann U, Knipper M.** 2013. Otoferlin couples to clathrin-mediated endocytosis in mature cochlear inner hair cells. The Journal of neuroscience **33:**9508-9519.

51) **Heidrych P, Zimmermann U, Kuhn S, Franz C, Engel J, Duncker SV, Hirt B, Pusch CM, Ruth P, Pfister M, Marcotti W, Blin N, Knipper M.** 2009. Otoferlin interacts with myosin VI: implications for maintenance of the basolateral synaptic structure of the inner hair cell. Human molecular genetics **18:**2779-2790.

52) **Ramakrishnan NA, Drescher MJ, Drescher DG.** 2009. Direct interaction of otoferlin with syntaxin 1A, SNAP-25, and the L-type voltage-gated calcium channel Cav1.3. The Journal of biological chemistry **284:**1364-1372.

53) **Johnson CP, Chapman ER.** 2010. Otoferlin is a calcium sensor that directly regulates SNARE-mediated membrane fusion. The Journal of cell biology **191:**187-197.

54) **Padmanarayana M, Hams N, Speight LC, Petersson EJ, Mehl RA, Johnson CP.** 2014. Characterization of the lipid binding properties of Otoferlin reveals specific interactions between PI(4,5)P2 and the C2C and C2F domains. Biochemistry **53:**5023-5033.

55) **Safieddine S, Wenthold RJ.** 1999. SNARE complex at the ribbon synapses of cochlear hair cells: analysis of synaptic vesicle- and synaptic membrane-associated proteins. The European journal of neuroscience **11:**803-812.

56) **Brandt N, Kuhn S, Munkner S, Braig C, Winter H, Blin N, Vonthein R, Knipper M, Engel J.** 2007. Thyroid hormone deficiency affects postnatal spiking activity and expression of Ca2+ and K+ channels in rodent inner hair cells. The Journal of neuroscience **27:**3174-3186.

57) **Jung S, Maritzen T, Wichmann C, Jing Z, Neef A, Revelo NH, Al-Moyed H, Meese S, Wojcik SM, Panou I, Bulut H, Schu P, Ficner R, Reisinger E, Rizzoli SO, Neef J, Strenzke N, Haucke V, Moser T.** 2015. Disruption of adaptor protein 2mu (AP-2mu) in cochlear hair cells impairs vesicle reloading of synaptic release sites and hearing. The EMBO journal **34:**2686-2702.

58) **Wright S, Hwang Y, Oertel D.** 2014. Synaptic transmission between end bulbs of Held and bushy cells in the cochlear nucleus of mice with a mutation in Otoferlin. Journal of neurophysiology **112:**3173-3188.

59) **Wu W, Rahman MN, Guo J, Roy N, Xue L, Cahill CM, Zhang S, Jia Z.** 2015. Function coupling of otoferlin with GAD65 acts to modulate GABAergic activity. Journal of molecular cell biology **7:**168-179.

60) **Monroe JD, Rajadinakaran G, Smith ME.** 2015. Sensory hair cell death and regeneration in fishes. Frontiers in cellular neuroscience **9:**131.

61) **Longo-Guess C, Gagnon LH, Bergstrom DE, Johnson KR.** 2007. A missense mutation in the conserved C2B domain of otoferlin causes deafness in a new mouse model of DFNB9. Hearing research **234:**21-28.

62) **Strenzke N, Chakrabarti R, Al-Moyed H, Muller A, Hoch G, Pangrsic T, Yamanbaeva G, Lenz C, Pan KT, Auge E, Geiss-Friedlander R, Urlaub H, Brose N, Wichmann C, Reisinger E.** 2016. Hair cell synaptic dysfunction, auditory fatigue and thermal sensitivity in otoferlin Ile515Thr mutants. The EMBO journal.

63) **Whitfield TT.** 2002. Zebrafish as a model for hearing and deafness. Journal of neurobiology **53:**157-171.

64) **Sheets L, Trapani JG, Mo W, Obholzer N, Nicolson T.** 2011. Ribeye is required for presynaptic Ca(V)1.3a channel localization and afferent innervation of sensory hair cells. Development **138:**1309-1319.

65) **Sheets L, Kindt KS, Nicolson T.** 2012. Presynaptic CaV1.3 channels regulate synaptic ribbon size and are required for synaptic maintenance in sensory hair cells. The Journal of neuroscience **32:**17273-17286.

66) **Obholzer N, Wolfson S, Trapani JG, Mo W, Nechiporuk A, Busch-Nentwich E, Seiler C, Sidi S, Sollner C, Duncan RN, Boehland A, Nicolson T.** 2008. Vesicular glutamate transporter 3 is required for synaptic transmission in zebrafish hair cells. The Journal of neuroscience **28:**2110-2118.

Figure 1.1

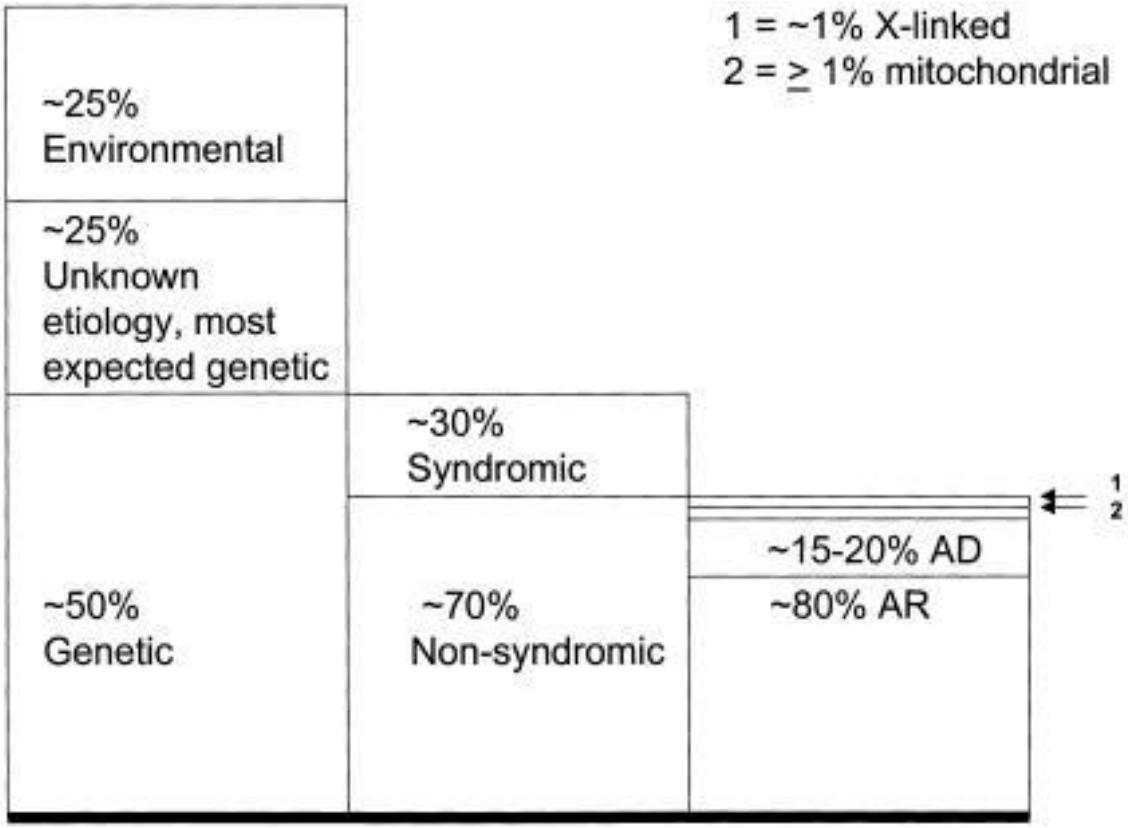

Prevalence of hereditary hearing loss. AD, autosomal dominant; AR, autosomal recessive (*Adapted from Iris Schrijver, The Journal of Molecular Diagnostics:JMD, 2004)*

Figure 1.2

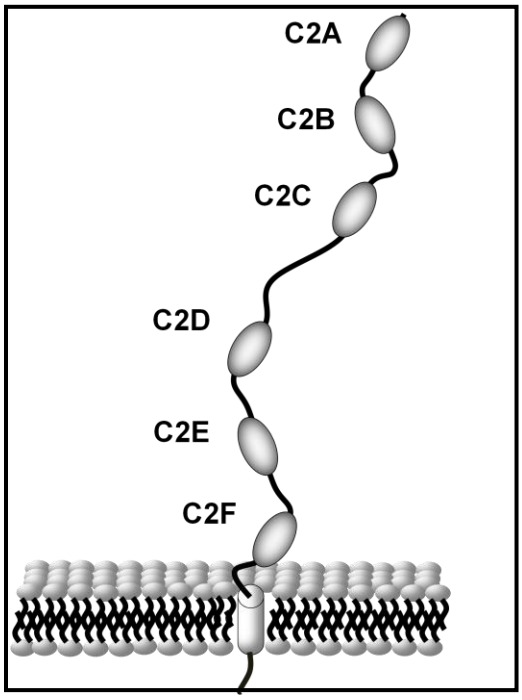

Proposed orientation of otoferlin C2 and transmembrane domains *(Adapted from Padmanarayana M, et al., Biochemistry, 2014)*

Figure 1.3

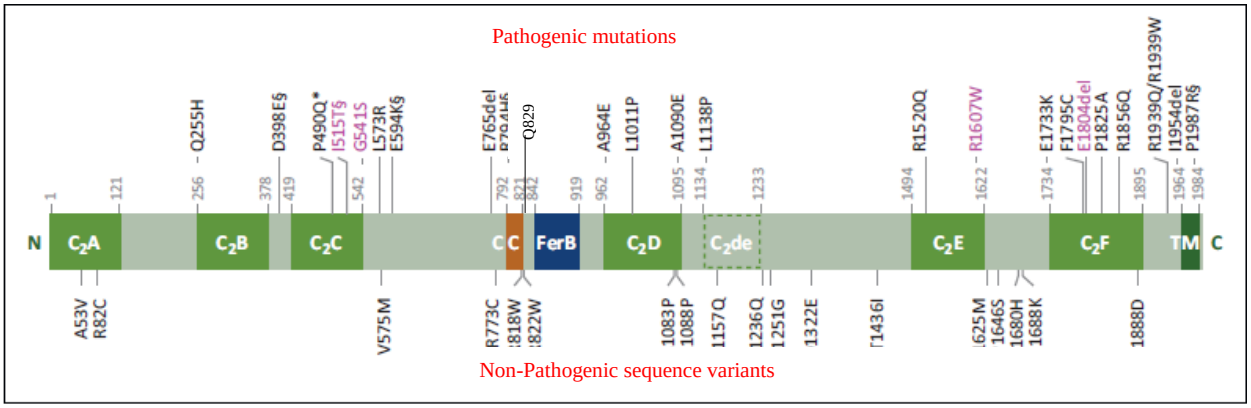

Distribution of pathogenic mutations and non-pathogenic sequence variants in different C2, non-C2 and transmembrane domains of otoferlin. *(Adapted from Pangrsic T, et al., Trends in Neurosciences, 2012)*

Figure 1.4

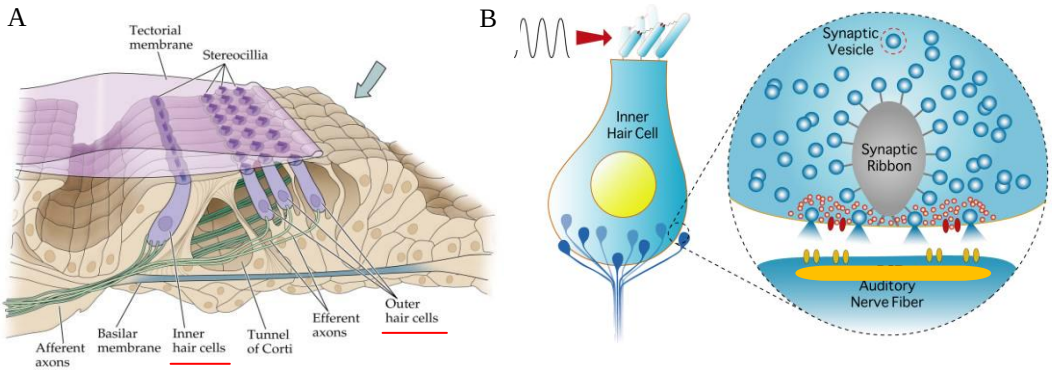

Structure of the inner ear cochlea and morphology of an inner hair cell (A) Cross section of the cochlea showing the arrangement of the inner and outer hair cells; Inner hair cells receive afferent input form the auditory nerve whereas outer hair cells mostly receive efferent inputs (*Image adapted from Neuroscience, 3rd edition)*.(B) Inner hair cell with apical hair bundles and 15-20 presynaptic ribbon bodies with afferent connections. The apical hair bundles receive the sound wave and undergoes depolarization causing calcium entray at the basolateral presynaptic active zone marked by the presence of the synaptic ribbon that tethers multiple glutamate filled vesicles. Glutamate release trasnmits the transduced sound to the post synaptic density (PSD) which has receptors that transmit the signal to the auditory afferent nerve fiber *(Adapted from Nouvian et al, Journal of Membrane Biology, 2006).*

Chapter 2 - Otoferlin Deficiency In Zebrafish Results In Defects In Balance And Hearing: Rescue Of The Balance And Hearing Phenotype With Full-length And Truncated Forms Of Mouse Otoferlin.

Paroma Chatterjee, Murugesh Padmanarayana, Nazish Abdullah, Chelsea L. Holman, Jane LaDu, Robert L. Tanguay, Colin P. Johnson.

Published in Molecular and Cellular Biology, March, 2015

2.1 Abstract

Sensory hair cells convert mechanical motion into chemical signals. Otoferlin, a six-C2 domain transmembrane protein linked to deafness in humans, is hypothesized to play a role in exocytosis at hair cell ribbon synapses. To date however, otoferlin has been studied almost exclusively in mouse models, and no rescue experiments have been reported. Here we describe the phenotype associated with morpholino-induced otoferlin knockdown in zebrafish, and report the results of rescue experiments conducted with full length and truncated forms of otoferlin. We find that expression of otoferlin occurs early in development, and is restricted to hair cells and the midbrain. Immunofluorescence microscopy reveals localization to both apical and basolateral regions of hair cells. Knockdown of otoferlin results in hearing and balance defects, as well as locomotion deficiencies. Further, otoferlin morphants had uninflated swim bladders. Rescue experiments conducted with mouse otoferlin restored hearing, balance and inflation of the swim bladder. Remarkably, truncated forms of otoferlin retaining the C-terminal C2F domain also rescued the otoferlin knockdown phenotype, while the individual N-terminal C2A domain did not. We conclude that otoferlin plays an evolutionarily conserved role in vertebrate hearing, and that truncated forms of otoferlin can rescue hearing and balance.

2.2 Introduction

Hair cells couple mechanical motion to neurotransmitter release at synapses (1). In contrast to conventional neural synapses, hair cell synapses release neurotransmitter continuously and in a graded manner, (2) possesss synaptic ribbons (2-4), and lack synaptophysin (5), complexin (6-9), Munc13 (10) and the calcium sensors synaptotagmin I and II (11). In place of synaptotagmin, it is believed that otoferlin may confer calcium sensitivity to evoke neurotransmitter release (12-13). Otoferlin is a six-C2 domain transmembrane protein expressed in inner, outer, and vestibular hair cells, as well as restricted regions of the brain (13-16). In humans, missense mutations in otoferlin have been linked to hearing loss (17, 18), and biochemical studies have determined that otoferlin binds calcium and lipids (12, 19), as well as membrane trafficking proteins (12, 20-23). Further, *in vitro* assays have demonstrated that otoferlin accelerates SNARE mediated membrane fusion (12). Based upon this evidence, it is hypothesized that otoferlin functions as a calcium sensitive regulator of neurotransmitter release in sensory hair cells.

However the results of several studies have raised questions related to otoferlin's function. For instance, despite otoferlin expression in vestibular hair cells, knockout mice show no balance defects (24-25) despite reduced exocytosis in vestibular type I hair cells (24, 26). This raises questions as to the importance of otoferlin in this system. Further, otoferlin did not rescue synchronous neurotransmitter release in synaptotagmin I knockout cultured neurons, indicating that otoferlin and synaptotagmin are not functionally redundant (27). It is also unclear as to whether otoferlin related deafness can be rescued by introduction of a functional copy of the otoferlin gene, and no rescue

experiments have been reported. Related to this, it is currently unknown as to which domains of the protein are critical for hearing, and whether truncated otoferlin protein can recapitulate the function of wild-type otoferlin. To date, almost all studies on otoferlin have used a mouse model (28), and while insightful, current mammalian models present obstacles to progress in understanding otoferlin, including the challenge of hair cell isolation and difficulties in transfection. To circumvent such difficulties, and to add to the general body of knowledge of otoferlin across species, we have turned to zebrafish for the study of otoferlin. In this study we characterized otoferlin expression in zebrafish as well as the phenotype associated with knockdown. We also present rescue experiments using full-length and truncated forms of otoferlin.

2.3 Materials and methods

Fish strains.

Tropical 5D strains of zebrafish (*Danio rerio*) were used for this study and reared according to Institutional Animal Care and Use Committee protocols at the Sinnhuber Aquatic Research Laboratory, Oregon State University. Adult fish were raised on a recirculating water system (28 + 1°C) with a 14:10 hour light-dark schedule. Spawning and embryo collection were followed as described in (29).

Bioinformatic tools.

Protein sequences were obtained from Ensembl (Ensembl accession numbers: ENSP00000272371(human);ENSMUSP00000073803(mouse);ENSDARP00000123935 ,ENSDARP00000118166(zebrafish);ENSRNOP00000046997(rat);ENSOCUP00000013 417 (rabbit); ENSCPOP00000000288 (guinea pig); and ENSXETP00000007211 (Frog). NCBI blastp tool was used to detect percent identity in the peptide sequences across

different species with human as the query sequence. The blastp tool was further used to obtain percent identity across the different C2 domains of otoferlin keeping the human C2s as the query sequences. ClustalW and PRALINE tools were used for sequence alignments. SMART and SWISS-MODEL tools were used for domain analysis. R-software was used to create the dot-plot.

Real-time Quantitative Reverse Transcription Polymerase Chain Reaction (qPCR).

Total RNA was extracted from wild type (WT) embryos collected at different hours post fertilization (hpf) with RNAzol (Molecular Research Centre, OH, USA) and cDNA was synthesized using iScript cDNA synthesis kit (Bio-Rad, CA, USA). Gene-specific primers **(Table 2.1)** were designed from genomic sequences for otoferlin b and otoferlin a found in Ensembl (Ensembl accession numbers: ENSDART00000149773 and ENSDART00000136255) and relative abundance assessed by qPCR performed using Power Sybr Green PCR master mix (Applied Biosystems, CA, USA). The data was normalized to otoferlin expression at 24 hpf for both isoforms. Also, the expression of myosinVIb (Ensembl accession number- ENSDART00000088801),vglut3 (Ensembl accession number- ENSDART00000080454) and sonic hedgehog a, shha (NCBI accession number – NM_131063.3) were examined in the otoferlin single and double KDs with gene-specific primers **(Table 2.1)**. The data was normalized relative to expression of the control and beta-actin genes. Graphs were plotted with the Prism software version 5.0.

Whole-mount Immunohistochemistry.

WT and microinjected zebrafish embryos were collected at different hpf and fixed in 4% paraformaldehyde overnight at 4°C. Mouse monoclonal anti-otoferlin and 3A10 (anti-

Mauthner neurons) primary antibodies (dilution: 1:500, and 1:200, Developmental Studies Hybridoma Bank, University of Iowa, Iowa City, IA, USA) and rabbit polyclonal anti-myosinVI (dilution: 1:800, Proteus Biosciences, CA, USA) were used. AlexaFluor 488 and 555 goat anti-mouse (dilution: 1:1000, Molecular Probes, Invitrogen, Eugene, OR, USA) and AlexaFluor Goat anti-rabbit 494 (dilution: 1:500, Molecular Probes, Invitrogen, Eugene, OR, USA) secondary antibodies were used. Fixed embryos were washed with PBST and UltraPure distilled water (Invitrogen, CA, USA). Collagenase (0.0001g/ ml PBST, C9891; Sigma-Aldrich, MO, USA) treatment was performed to permeabilize the embryos, followed by rinsing with phosphate buffer saline. Permeabilized embryos were blocked with 10% normal goat serum (G6767; Sigma-Aldrich, MO, USA) for an hour and incubated with primary antibody overnight at 4°C. The following day samples were rinsed in phosphate buffer saline and incubated with secondary antibody. Embryos were imaged with an inverted Zeiss Axiovert 200M epifluorescence microscope fitted with a Zeiss Axiocam HRm camera and 5x objective.

Whole-mount *In Situ* Hybridization.

In situ hybridization (ISH) of otoferlin was performed with digoxygenin-labeled antisense RNA probes specific to zebrafish otoferlin a and otoferlin b on WT zebrafish embryos collected at different hpf as described in (30). Furthermore, ISH was performed as described in (43) with digoxygenin-labeled antisense RNA probes specific to the mouse otoferlin (NCBI accession number – NM_001100395.1) to detect expression of the hair-cell specific mouse otoferlin construct in larval zebrafish double morphants. To synthesize the probe, gene-specific primers **(Table 2.2)** with RNA polymerase promoter were designed for amplifying the probe templates, and cDNA was prepared from RNA

isolated as described from whole zebrafish at 48 hpf. Embryos were labeled with either Fast Red (31) or NBT/BCIP stain. Stained embryos were imaged using an inverted Zeiss Axiovert 200M epi-fluorescence microscope and Nikon SMZ 1500 stereomicroscope mounted with a Coolpix E500 digital camera for NBT/BCIP.

***In Situ* Hybridization on larval zebrafish paraffin sections.**

WT 120 hpf larval zebrafish were fixed in 10% neutral buffer formalin overnight at 4°C. The fish was rinsed in phosphate buffer saline and dehydrated in graded ethanol. Agar blocks were prepared using zebrafish metal molds (32) and pre-fixed zebrafish were arranged in the agar blocks. The agar blocks were sent to the Veterinary Diagnostic Lab, Oregon State University, Corvallis, OR for paraffin embedding and sectioning. Five micrometer sections were obtained and these sections were used for *in situ* hybridization (ISH) with digoxygenin-labeled antisense RNA probes specific to otoferlin a as described in (30, 33).

Plasmids and constructs.

The cDNA encoding mouse otoferlin was a gift from Christine Petit (Institut Pasteur, Paris, France). The *p5E-pmyo6b* vector used in cloning was a gift from Teresa Nicolson (Oregon health and Science University, OR, USA). The *p5E-pmyo6b* vector contains hair cell specific promoter for myosin VIb. Full length (FL) and truncated constructs of otoferlin **(Table 2.3)** were cloned downstream to the promoter at SacII and NotI sites. Clones were screened by colony PCR and verified by sequencing.

Microinjections.

A pair of morpholinos (MOs) targeting exon/intron boundaries of otoferlin a and otoferlin b **(Table 2.4)** and a standard negative control were obtained from GeneTools,

Philomath, OR, USA (Supplementary table D). Approximately 2nl of 0.6 mM of otoferlin a MO, 0.7 mM of otoferlin b MO and both MOs diluted with RNAse-free ultrapure distilled water and 3% phenol red were pressure-injected in WT embryos at one-cell stage. For verification of splicing pattern and efficacy of knockdown, total RNA was extracted and cDNA was synthesized from injected and WT zebrafish embryos collected at different hpf as described. Gene-specific primers **(Table 2.5)** were used for PCR with KOD Hot Start DNA Polymerase (Novagen, USA) and the products were separated on a 1.25% agarose gel.

For the rescue, approximately 600 pg of the vector construct with either mouse full-length (FL) otoferlin or truncated mouse otoferlin (construct with mouse putative C2DEF domains with the transmembrane, C2F domain with the transmembrane, C2EF domains with the transmembrane and C2A) were co-injected with the morpholinos. Capped RNA was synthesized with the mMessage mMachine transcription kit (Ambion, TX, USA) and PCR template. PCR template was amplified from pcDNA3 vector with the coding region for mouse full-length otoferlin using primers containing a T7-RNA polymerase promoter site. The amplified PCR template was purified with QIAquick PCR purification kit (Qiagen, CA, USA). Approximately 250 pg of synthesized mRNA were co-injected with the morpholinos. Larvae were screened for rescue of the balance phenotype, acoustic startle response including rescue of un-inflated swim bladder for further analysis.

Staining with vital dyes.

FM1-43FX dye (Life Technologies, NY, USA) labeling of neuromast hair cells was performed on live zebrafish at 120 hpf. Zebrafish larvae were immersed in 3 uM of FM1-43FX dye in embryo medium and rinsed off. The fish were washed several times with

embryo medium and anaesthetized with 0.2 mg/ml tricaine solution for confocal imaging.

YO-PRO-1 (Life Technologies, NY, USA) staining of the neuromast hair cells was performed on live morpholino injected fish at 120 hpf. Zebrafish larvae were incubated for an hour at 28 deg C in 2uM YO-PRO-1 dye in embryo medium. The fish were washed three times with the embryo medium and anaesthetized with 0.2mg/ml tricaine solution for imaging with the inverted Zeiss Axiovert 200M epifluorescence microscope fitted with a Zeiss Axiocam HRm camera and 5x, 10x, 20x objectives.

Confocal image acquisition and processing.

Whole-mount immunohistochemistry preparations were mounted with 1% agar on 35 mm glass-bottomed petri dish and imaged with a confocal laser-scanning microscope fitted with a 40x oil-immersion objective (Zeiss LSM 510 Meta) with Alexa-Fluor 555 filter sets. For live zebrafish stained with vital dye FM1-43, fish were immobilized with 1% agarose containing 0.2 mg/ml tricaine on glass-bottomed petri dish and imaged with a 63x water-immersion objective (Zeiss LSM 510 Meta) with appropriate filter sets. Stacks of confocal images were taken and reconstructed with ImageJ software.

Larval behavior tests.

Injected zebrafish larvae were tested in a 96-well plate with the Viewpoint Zebrabox (Viewpoint Life Sciences, Lyon, France). Locomotor activity was measured using the Viewpoint tracker by subjecting the larvae to alternate phases of light and dark. Behavioral differences between the different injected groups were determined by comparing the distance moved during the dark period. Briefly, 96 hpf zebrafish larvae were loaded in a 96-well plate at least 3 hours prior to the experiment to give them

sufficient time to acclimatize. Larvae were subjected to alternate phases of light followed by dark and finally light during which Viewpoint tracker recorded fish movement from the individual wells. Raw data files obtained from the Viewpoint were processed using a python script and JMP software to average the total distance travelled during the dark phase for each group. Graphs were plotted and statistically analyzed with the Graphpad Prism software version 5.0.

Acoustic Startle Response.

Injected zebrafish larvae from different groups were subjected to a startle stimulus assay at 120 hpf. Larvae were individually placed on a 100 mm petri dish filled with embryo medium and startled with a push-solenoid that generated a sudden tap when activated. Movement was recorded with a digital video camera (Sony,HDR CX22) for 30 secs after startling. The distance moved from the point of origin by different groups of larvae were compared by analyzing the video outputs from the camera with Noldus EthoVision XT(version 8.5) tracking software. Graphs were plotted and statistically analyzed with the Graphpad Prism software version 5.0.

2.4 Results

Zebrafish have two copies of otoferlin:

Contrary to mammals, the zebrafish genome contains two copies of otoferlin, located on chromosomes 17 and 20. The transcript (~8 kb) encoded by chromosome 17 will be referred to as otoferlin b with otoferlin a referring to the transcript encoded by chromosome 20 (~7 kb). A comparative study between the human otoferlin amino acid sequence with sequences from other species indicated that otoferlin is highly conserved **(Figure 2.1 A, B)**. Overall, the zebrafish otoferlin isoforms show 74% (otoferlin b) and

76% (otoferlin a) identity with human otoferlin **(Figure 2.1B**). Even higher identity was found when the comparison was restricted to sequences predicted to form C2 domains (**Figure 2.1A**). Comparison of the sequence identity between zebrafish otoferlin a and human otoferlin is 77% in the C2A domain, 91% in the C2B domain, 89% in C2C, 83% in C2D, 92% in C2E and 95% in C2F. Zebrafish otoferlin b is 91% identical in the C2B, 89% in the C2C, 83% in C2D, 88% in C2E, and 94% in C2F domains with human otoferlin. Zebrafish otoferlin a appeared to be a closer representation of the human otoferlin because of the presence of all six C2 domains, unlike otoferlin b that lacked the C2A domain **(Figure 2.1A, Figure 2.1C)**. The identity between amino acid sequences of the two zebrafish otoferlin isoforms is ~80%. From the diagonal in the center of the dot-plot (**Figure 2.1D**) it can be discerned that the zebrafish otoferlin peptide sequences are identical in most regions except in the first ~200 amino acids. On further comparison by sequence alignments (data not shown) it was confirmed that the peptide sequence of otoferlin b was ~180 amino acids shorter on the N-terminal than otoferlin a. In summary, the sequences of the C2 domains are more conserved than the non-C2 domain regions, and the C2A domain is the least conserved of the C2 domians.

Otoferlin expression and localization in zebrafish:

The amino acid sequence of otoferlin is similar across species including zebrafish, suggesting a conserved function. Given the ease with which the organism can be genetically manipulated, we chose zebrafish as our model for use in the study of otoferlin. To ascertain the developmental expression profile of otoferlin we conducted qPCR on wild-type (WT) zebrafish samples collected every 24 hours during the first 120 hours post fertilization (hpf). We found that 24 hpf zebrafish larvae express both copies

of otoferlin (**Figure 2.2A)** with an increase in relative abundance of both transcripts at 48 hpf **(Figure 2.2 A).** Expression plateaus after 72 hpf. The rise in otoferlin expression during the first 72 hours of embryonic development coincided with the deposition of neuromasts and formation of the aLL (anterior lateral line) and pLL (posterior lateral line). It also coincided with formation of the semicircular canals and otic vesicle occurring during this stage of development (34). We next sought to characterize the spatial pattern of otoferlin expression in zebrafish larvae using whole-mount *in situ* hybridization (**Figure 2.2B).** Transcripts of otoferlin b were detected in the otic placode of 24-hour old larvae **(Figure 2.2B).** The otic placode eventually forms sensory patches and develops as the zebrafish inner ear (35). There was also weak expression of otoferlin b in primordial cells that form neuromasts of the zebrafish lateral line organ system **(Figure 2.2B)**. The expression of otoferlin b became pronounced in the neuromasts of pLL, aLL and the inner ear region as the zebrafish larvae continued to develop through 120 hpf **(Figure 2.2B**). Transcripts of otoferlin a were detected at around 24 hpf in the otic placode **(Figure 2.2B)** and is restricted to the sensory patches of the inner ear as the larvae continues to develop through 120 hpf **(Figure 2.2 B).** We observed a relatively weak and diffuse expression in the zebrafish brain region and in the retina starting at around 48 hpf that became prominent at 120 hpf **(Figure 2.2C).** Analyses of sectioned 120 hpf larval zebrafish confirmed expression of otoferlin transcripts in the mid-brain and the retinal ganglion cell layer **(Figure 2.S1).** However, no expression of the otoferlin a transcript were detected in the hair cells of the aLL and pLL neuromasts **(Figure 2.2B).**

Whole-mount immunohistochemistry on WT zebrafish larvae with the anti-otoferlin HCS-1 antibody were consistent with the mRNA expression profile in the inner ear and lateral line **(Figure 2.2B)** during the first 120 hours of zebrafish development (36). Strong immunoreactivity in the nascent hair cells of the zebrafish otic region at 24 hpf were detected **(Figure 2.3A),** and immunoreactivity was detectable in the hair cells of both the pLL and aLL at 48 hpf **(Figure 2.3B)** becoming more pronounced between 72-120 hpf **(Figures 2.3C, D, F).** Negative controls at 72 hpf **(Figure 2.3E)** with no primary antibody confirmed that the labeling observed is due only to binding of the secondary antibody to the HCS-1 antibody. Overall the onset and increase of otoferlin expression correlated with the formation and development of the zebrafish inner ear and the pLL and aLL system (34).

To examine the sub-cellular localization of otoferlin in zebrafish hair cells, confocal images of 120 hpf larvae were collected. Pronounced immunolabeling in both the supranuclear and basolateral compartments including a punctate distribution throughout the cytoplasm were observed in hair cells of the neuromast **(Figure 2.3G).** This subcellular distribution is similar to observations made on mouse hair cells (20, 23, 37). Probing 120 hour wild-type zebrafish with the FM1-43 dye **(Figure 2.3H)** showed uptake in the apical end of the hair cells of a posterior lateral line neuromast cluster indicating active vesicle recycling (38). This overlap in otoferlin distribution and FM1-43 dye uptake in the apical hair cell compartment raises the possibility of another role of otoferlin in the apical region in addition to the established function in synaptic transmission at the basolateral region (13, 37). To validate expression of otoferlin in the zebrafish hair cells, dual immunofluorescence was performed on wild-type 120 hpf

larval zebrafish with anti-otoferlin and anti-myosin VI antibodies. Myosin VI is a marker for hair cells, and fluorescence images confirmed that otoferlin co-localizes with myosinVI in larval zebrafish hair cells **(Figure 2.3I)** (39, 40).

Knockdown of otoferlin in the zebrafish hair cells:

To determine the function of otoferlin *in vivo,* we used anti-sense splice-blocking morpholinos that targeted both isoforms including their splice variants. Two splice-blocking MOs for each otoferlin gene targeting exon-intron boundaries (otoferlin b MOs– e2i2 and e38i38; otoferlin a MOs- i6e7, e11i11) **(Figure 2.4A)** were designed and microinjected at the one–cell stage. Comparable phenotypes were observed with each pair of morpholinos, and the e38i38 MO targeting otoferlin b, and i6e7 MO targeting otoferlin a were used for subsequent experiments in this study. We evaluated mRNA expression to assess knockdown of the otoferlin a and b transcripts in the single and double morphants. Analysis of qPCR data indicated that the expression of otoferlin a is significantly reduced in the otoferlin a and otoferlin b+a KD groups (p-value <0.001) **(Figure 2.4D).** Similarly, otoferlin b is significantly reduced in the otoferlin b and otoferlin b+a KD groups (p-value <0.001) **(Figure 2.4D).** RT-PCR further supported the conclusion that both the single and double knockdowns were effective at 96 hpf **(Figure 2.4B; lanes 4, 5, 6 and 7)** when compared with age-matched microinjected controls **(Figure 4C, lanes 1 and 2)** and lasted up to 120 hpf **(Figure 2.S2A).** As the otoferlin b and a sequences are ~80% identical **(Figure 2.1C),** it was necessary to validate the specificity of MOs that were designed to target each isoform separately. Analysis of qPCR data indicated that knockdown of otoferlin b did not significantly affect the expression of otoferlin a and vice versa **(Figure 2.4D).** RT-PCR further supported the

conclusion that each MOs specifically blocked the targeted otoferlin without affecting expression of the other isoform at up to 120 hpf **(Figure 2.4C and Figure 2.S2B).**

Since otoferlin interacts with the hair cell marker myosinVI (21, 40), and a reduction in otoferlin decreases the immunofluorescence of synaptic vesicle marker VGlut3 (37), qPCR were conducted on otoferlin single and double morphants to measure the relative expression changes of both myosin VI and VGlut3. Analyses indicated that otoferlin knockdown does not significantly affect the expression of myosin VI or VGlut3 in larval zebrafish at 96 hpf **(Figure 2.4D).**

Immunohistochemistry on 120 hpf injected control **(Figure 2.5A)** and morphant larvae **(Figures 2.5B-D)** were also conducted. Embryos injected with the otoferlin b morpholino showed staining in the hair cells of the inner ear **(Figure 2.5B).** However, there were no detectable signal in the hair cells of the neuromasts of the pLL and aLL **(Figure 2.5B).** Contrary to otoferlin b, the otoferlin a morphants showed staining in the hair cells of the inner ear with strong immunolabeling in the hair cells of the neuromasts of pLL and aLL **(Figure 2.5C).** Visual inspection of the otic region revealed that in comparison to the control zebrafish larvae **(Figure 2.5E),** otoferlin a were distributed in the hair cells of the sensory patches of the anterior macula. It was also present in the hair cells of the posterior, anterior and medial cristae **(Figure 2.5F).** However, otoferlin b is distributed in hair cells of the sensory patches of both the anterior and posterior maculae but absent from the cristae **(Figure 2.5G).** This suggested that the otoferlin isoforms might play distinctive roles in the otic region. Finally, otoferlin b and a double morphants showed no anti-otoferlin signal in any of the sensory patches of the inner ear and neuromasts of the lateral line **(Figure 2.5D).** Confocal microscopy images of

immunolabeled 120 hpf injected controls and double morphants were also collected **(Figures 2.S3A and 3B**). In contrast to control siblings, a compressed z-stack image of the head region of double morphants showed absence of anti-otoferlin in the otic region. This indicates a complete knockdown of both isoforms of the zebrafish otoferlin in the otoferlin b+a double morphants to the limits of detection.

Phenotypic analysis of the otoferlin single and double knockdowns:

Compared to age-matched injected controls **(Figure 2.6A),** otoferlin single knockdowns showed no noticeable defects in gross morphology at 120 hpf **(Figures 2.6B and C).** However, after 96 hpf the double morphants failed to develop an inflated swim bladder **(Figure 2.6D)** compared to single knockdowns and injected controls. These phenotypic defects were visible around 72 hpf in the double morphants when they failed to maintain an upright position compared to injected control siblings **(Figures 2.6E and F).** This suggested a balance defect (41) and indicated a critical contribution of otoferlin to balance and vestibular function. Moreover about 80% of the 96 and 120 hour double morphants swam on their sides or back, landed head-on and often floated vertically with head-up. On touching with a hair, double KDs exhibited a circling and looping motion, but swam back to the source of the stimulus rather than escaping. Beyond 120 hpf, double morphants gradually developed a curved spine compared to injected controls **(Figures 2.6G and H)** that enhanced the circling movement. These phenotypic abnormalities are comparable to the 'circler mutants' (39, 41, 42) that were determined to be mutations in sensory hair cell related genes. Since we observed a defective escape response with the double morphants, we examined the morphological differences in the patterning of the lateral line with hair cell marker YO-PRO-1. We did

not observe differences in staining between the control and otoferlin b+a double morphants **(Figure 2.7A).** Further, bright-field images of the otic region indicated that, compared to controls, the semicircular canal folds and otolith formed normally in 120 hpf otoferlin double morphants **(Figure 2.7B).** A similar swim bladder phenotype were observed in the double morphants that had been injected with a second set of morpholinos, e11i11 - otoferlin a and e2i2- otoferlin b **(Figure 2.S4A).**

Given that the double morphants show an uninflated swim bladder phenotype we tested whether otoferlin knockdown affected swim bladder development using qPCR analysis of shha in double morphants at 72 hpf. shha is a swim bladder developmental marker (43) , and our results indicated that relative to control, the expression level of the shha gene do not change in the double morphants **(Figure 2.S4B).**

Since both isoforms of otoferlin are expressed in hair cells of the otic region and lateral line, both copies may play a role in hearing and balance. To test whether otoferlin knockdown impaired hearing, acoustic startle reflex assays were conducted on 120 hpf single and double morphants. Acoustic startle assays are widely used to evaluate hearing induced escape response in larval zebrafish (41). As shown in **Figure 2.8C**, the distance travelled by control larvae (n=23) was 63.94 mm, while otoferlin b KD (n=18) was 66.03 mm and otoferlin a KD (n=17) was 66.79 mm. When the single KDs were compared to control using Dunn's multiple comparison with standard 5% significance level, the test showed no significant difference. By contrast, double KDs (n= 16) travelled only 22.92 mm after startling. This value is significantly lower (Dunn's multiple comparison, p-value < 0.001) when compared with the distance moved by the single KD and age-matched controls. A summary comparing the startle between otoferlin single

and double morphants as well as the control group has been included in **Figure 2.S5**. These results suggested that there is redundancy of function between the two isoforms and the startle escape was significantly attenuated when expression of both the isoforms were reduced. To ensure that the larval zebrafish movement is not random but coincided with the startle stimuli, the average startle velocity as a function of time were plotted. The movement of the larval fish coincided with the startle stimuli for both the control and the double morphants (**Figure 2.8D**). Furthermore, the control fish showed a marked increase in velocity after startling followed by a decrease, while the double morphants show some slight movement after startling which quickly declines relative to control **(Figure 2.8D).** These data are consistent with the defective escape response observed in the double morphants when compared to age-matched controls.

Studies on mouse models have established a link between otovestibular defects and locomotion using a dark-light test (44, 45). Upon finding that zebrafish otoferlin morphants exhibited balance defects and an abnormal startle escape response, dark-light locomotory tests were conducted on control and KD larval fish. 96 hpf otoferlin single (n=72) and double (n=72) morphants, as well as age-matched controls (n=72) were used for the dark-light assay. Compared to controls, single KD traveled less during the dark phase (Mean distance travelled; control = 62.73 mm, otoferlin b KD= 45.67mm, otoferlin a KD = 46.68 mm; Dunn's multiple comparison test, p-value <0.05) **(Figure 2.S6)**, and double KD fish travel even less (otoferlin double KD = 35.61 mm; Dunn's multiple comparison test, p-value <0.001) **(Figure 2.S6).** Since the zebrafish single and double morphants showed a defective dark-light response, this indicated a possible direct or indirect role of otoferlin on neuronal wiring in the larval zebrafish. However,

comparison of immunofluorescently labeled Mauthner cells that mediate the escape response (46-48), did not reveal any gross defects in the double morphants (n=3) as compared to age-matched controls (n=2) **(Figures 2.S5E and F)**.

Rescue of zebrafish otoferlin knockdown with mouse otoferlin:

From comparison it is evident that there is a high sequence identity between otoferlin of different species, which suggests functional conservation **(Figures 2.1A and B).** To test for functional conservation we co-injected double morphants with a *p5E-pmyo6b* vector encoding mouse otoferlin and a hair cell specific myosin VIb promoter, and tested for rescue of the knockdown phenotype. Several constructs including the full length mouse otoferlin (FL-otoferlin), as well as truncated forms of the protein were used in this study to identify the domain(s) critical for otoferlin function **(Figure 2.8A).** Expression of mouse otoferlin was validated by performing whole-mount immunohistochemistry on zebrafish double morphants co-injected with the FL-otoferlin construct. **Figure 2.8B** showed that the expression of the FL-otoferlin construct is restricted only in the hair cells of the otic region and the lateral line thereby confirming that the myosin VIb promoter recapitulates endogenous otoferlin expression. We also performed whole mount *in situ* hybridization experiments on zebrafish double morphants co-injected with the mouse FL-otoferlin construct. **Figures 2.S5A, B, and C** shows the presence of otoferlin transcripts in the otic region, pLL, and aLL**. Figures 2.8C, 2.8D and 2.S6** show that the FL-otoferlin was able to rescue the startle escape response (mean distance moved =59.58 mm, n= 18, no significant difference with control group in Dunn's multiple comparison test with standard 5% significance level) and dark-light behavior in the zebrafish double morphants (mean distance travelled during dark-phase = 59.89 mm,

n=72, no significant difference with control group in Dunn's multiple comparison test with standard 5% significance level). Mouse FL-otoferlin also rescued the swim bladder defects observed in 120 hpf zebrafish double morphants **(Figure 2.9A).** Furthermore, FM1-43 uptake in the rescue larvae was indistinguishable from WT larvae (data not shown). These results suggested that the mouse otoferlin was sufficient to correct for the disorders associated with depletion of both otoferlin isoforms found in larval zebrafish.

Remarkably, we were able to rescue the double morphants with a truncated form of mouse otoferlin lacking the first three putative C2 domains (ΔABC). Zebrafish double morphants co-injected with the ΔABC construct were found to have inflated swim bladders as observed at 120 hpf **(Figure 2.9B).** The startle reflex abnormalities **(Figures 2.8C and 2.8D)** were also rescued (mean distance moved =63.32 mm, n=19, no significant difference with control group in Dunn's multiple comparison test with standard 5% significance level). In addition, dark-light behavior was also rescued (mean distance travelled during dark-phase = 59.81 mm, n=48, no significant difference with control group in Dunn's multiple comparison test with standard 5% significance level) **(Figure 2.S6).** This suggests that the first three C2 domains are not required to correct for the balance and hearing deficits that were observed with the zebrafish double morphants.

Several additional truncated constructs **(Figure 2.8A)** lacking either the first 4 or 5 C2 domains (Δ-ABCD, Δ-ABCDE) or consisting of only the N-terminal C2A domain (Δ-BCDEF) were also tested for recovery of the uninflated swim bladder **(Figures 2.S7A and 7B)** and acoustic startle response **(Figure 2.8C).** The ΔABCD (n = 25, mean

distance = 53.94 mm) and ΔABCDE (n = 23, mean distance = 52.00 mm) displayed no significant difference relative to the control group in Dunn's multiple comparison test with standard 5% significance level **(Figure 2.8C).** Co-injection of the double morphants with the ΔBCDEF construct did not rescue the acoustic startle responses however (n = 16, mean distance = 26.57 mm, no significant difference with otoferlin b+a KD group in Dunn's multiple comparison test with standard 5% significance level) **(Figure 2.8C).**

Finally, as an alternative method of rescue, zebrafish double morphants were co-injected with mouse otoferlin mRNA encoding the full-length protein. The mRNA injection completely rescued the swim bladder defect **(Figure 2.9C)** including recovery of the startle escape response (mean distance moved = 65.55 mm, n = 17, no significant difference with control group in Dunn's multiple comparison test with standard 5% significance level), **(Figure 2.8C)** supporting the conclusion that mouse otoferlin can rescue morpholino knockdown in zebrafish. A table showing percentage of larvae with inflated swim bladder rescue phenotype for the double morphants co-injected with the different otoferlin constructs is included in **Figure 2.9D.**

2.5 Discussion

Based upon sequence, expression patterns, knockout phenotype, as well as rescue studies, we conclude that otoferlin plays a conserved role in hair cells. Despite divergence of the zebrafish and mammalian genomes approximately 420 million years ago (49), the amino acid sequences of otoferlin are highly similar, and mouse otoferlin successfully compensates for loss of endogenous otoferlin expression in zebrafish. This suggests both a conserved function of the protein in hair cells, and a conserved set of binding partners for neurotransmitter release. Indeed, the loss in hearing we observed

in otoferlin knockdown zebrafish matches mouse knockout models. We also note that while zebrafish have two otoferlin genes and mammals have one, multiple splice isoforms of the gene have been reported for mice and humans (23, 50).

Analysis of sequence identity of the C2 domains between species show greater conservation among the C-terminal C2D, C2E, and C2F domains compared to the N-terminal C2A domain. We speculate that these C-terminal domains may play a functionally conserved or redundant role in otoferlin function. Indeed, functional redundancy among the C2 domains has been noted in reconstituted membrane fusion assays (12). Experiments we report indicate that shortened forms of otoferlin lacking the N-terminal domains rescue the knockdown phenotype, in agreement with the idea of functional redundancy. However, it is possible that the N-terminal C2 domains play a role that was not detected in our assays or a function found in mammals but not in zebrafish. Indeed, our results seem to conflict with reports of missense mutations in the C2B and C2C domains that have been linked to hearing loss in mammals (51-52). We speculate that these missense mutations may reduce the structural stability of the protein, resulting in lower levels of protein expression. Knockdown of both zebrafish otoferlin genes was required for an observable phenotype in our studies, despite differing in the first N-terminal 183 amino acids, corresponding to the C2A domain, again suggesting that some domains may be dispensable. Interestingly, biophysical studies on the C2A domain have determined that this is the only domain in otoferlin that does not bind calcium (12, 53). However, studies on the otoferlin orthologues myoferlin and dysferlin have found that the C2A domain of these proteins do bind calcium,

supporting the idea that the calcium binding activity of the C2A domain may have diverged among the ferlins (12, 19, 54, 55).

Unexpectedly, otoferlin knockdown zebrafish displayed severe deficits in balance and uninflated swim bladders, suggesting a critical role for otoferlin in balance. While expressed in vertebrate vestibular hair cells, neither otoferlin knockout mice nor human patients with otoferlin mutations suffer from balance deficits (24). Our results clearly demonstrate a critical role for otoferlin in zebrafish balance and vestibular hair cell function. That calcium dependent neurotransmitter release is attenuated but not completely abrogated in knockout mouse vestibular hair cells (24) may indicate that compensatory or redundant calcium sensors exist in mammalian hair cells that are not active in zebrafish cells. Thus zebrafish may serve as a model for future characterization of otoferlin's contribution to vestibular hair cells.

Despite the loss of morpholino knockdown efficiency and expression of both otoferlin genes around 120 hpf, most zebrafish did not show any signs of swim bladder inflation or recovery of balance even at 10 dpf, and many developed a curved spine. This suggests that otoferlin may play a developmental role, and that the lack of otoferlin during a certain developmental window may have permanent effects on zebrafish physiology. In support of this, a recent study reported abnormally small ventral cochlear nuclei in otoferlin knockout mice (56). Future studies should focus on the developmental effects linked to otoferlin loss-of-function.

2.6 Acknowledgements: This work was supported by a Medical Research Foundation (MRF) grant to CPJ, as well as Oregon State University, and NIH P30 000210 (RLT). We thank Prof. Teresa Nicolson for providing us with the p5E-pmyo6b vector, Prof. Christine Petit for providing us with mouse otoferlin cDNA, Veterinary Diagnostic Lab, Oregon State University, OR, for help with the paraffin sections, Carrie Barton for help with fish maintenance and embryo collection, Mike T. Simonich for assembling the startle apparatus, Anne-Marie Girard for help with confocal microscopy, Siba R. Das for advice on the Noldus software, Sean M. Bugel for advice on molecular biology, Pamela Noyes for advice on Graphpad software, Leah Wehmas for advice on agar block preparation, Jacob Thomas Huegel for help with co-localization images, Justin Sanders for advice on in situ hybridization on zebrafish paraffin sections, Ananda S. Roy for help with R-program.

2.7 References

1. **LeMasurier M, Gillespie PG.** 2005. Hair-cell mechanotransduction and cochlear amplification. Neuron **48:**403-415.

2. **Nouvian R, Beutner D, Parsons TD, Moser T.** 2006. Structure and function of the hair cell ribbon synapse. J. Membr. Biol. **209:**153-165.

3. **Fuchs PA.** 2005. Time and intensity coding at the hair cell's ribbon synapse. J Physiol-London. **566:**7-12.

4. **Khimich D, Nouvian R, Pujol R, Tom Dieck S, Egner A, Gundelfinger ED, Moser T.** 2005. Hair cell synaptic ribbons are essential for synchronous auditory signalling. Nature **434:**889-894.

5. **He S, Yang J.** 2011. Maturation of neurotransmission in the developing rat cochlea: immunohistochemical evidence from differential expression of synaptophysin and synaptobrevin 2. Eur. J. Histochem. **55:**1-9.

6. **Mcmahon HT, Missler M, Li C, Sudhof TC.** 1995. Complexins – Cytosolic Proteins That Regulate Snap Receptor Function. Cell **83:**111-119.

7. **Reim K, Mansour M, Varoqueaux F, McMahon HT, Sudhof TC, Brose N, Rosenmund C.** 2001. Complexins regulate a late step in Ca2+-dependent neurotransmitter release. Cell **104:**71-81.

8. **Reim K, Wegmeyer H, Brandstatter JH, Xue MS, Rosenmund C, Dresbach T, Hofmann K, Brose N.** 2005. Structurally and functionally unique complexins at retinal ribbon synapses. J. Cell Biol. **169:**669-680.

9. **Strenzke N, Chanda S, Kopp-Scheinpflug C, Khimich D, Reim K, Bulankina AV, Neef A, Wolf F, Brose N, Xu-Friedman MA, Moser T.** 2009. Complexin-I Is Required for High-Fidelity Transmission at the Endbulb of Held Auditory Synapse. J. Neurosci. **29:**7991-8004.

10. **Uthaiah RC, Hudspeth AJ.** 2010. Molecular anatomy of the hair cell's ribbon synapse. J. Neurosci **30:**12387-12399.

11. **Beurg M, Michalski N, Safieddine S, Bouleau Y, Schneggenburger R,Chapman ER, Petit C, Dulon D.** 2010. Control of exocytosis by synaptotagmins and otoferlin in auditory hair cells. J. Neurosci. **30:**13281-13290.

12. **Johnson CP, Chapman ER.** 2010. Otoferlin is a calcium sensor that directly regulates SNARE-mediated membrane fusion. J. Cell. Biol. **191:**187-197.

13. **Roux I, Safieddine S, Nouvian R, Grati M, Simmler MC, Bahloul A, Perfettini I, Le Gall M, Rostaing P, Hamard G, Triller A, Avan P, Moser T, Petit C.** 2006. Otoferlin, defective in a human deafness form, is essential for exocytosis at the auditory ribbon synapse. Cell **127:**277-289.

14. **Schug N, Braig C, Zimmermann U, Engel J, Winter H, Ruth P, Blin N, Pfister M, Kalbacher H, Knipper M.** 2006. Differential expression of otoferlin in brain, vestibular system, immature and mature cochlea of the rat. Eur. J. Neurosci. **24:**3372-3380.

15. **Valiyaveettil M, Alamneh Y, Miller SA, Hammamieh R, Wang Y, Arun P, Wei Y, Oguntayo S, Nambiar MP.** 2012. Preliminary studies on differential expression of auditory functional genes in the brain after repeated blast exposures. J. Rehabil. Res. Dev. **49:**1153-1162.

16. **Zak M, Bress A, Brandt N, Franz C, Ruth P, Pfister M, Knipper M, Blin N.** 2012. Ergic2, a brain specific interacting partner of Otoferlin. Cell. Physiol. Biochem. **29:**941-948.

17. **Rodriguez-Ballesteros M, Reynoso R, Olarte M, Villamar M, Morera C, Santarelli R, Arslan E, Meda C, Curet C, Volter C, Sainz-Quevedo M, Castorina P, Ambrosetti U, Berrettini S, Frei K, Tedin S, Smith J, Cruz Tapia M, Cavalle L, Gelvez N, Primignani P, Gomez-Rosas E, Martin M, Moreno-Pelayo MA, Tamayo M, Moreno-Barral J, Moreno F, del Castillo I.** 2008. A multicenter study on the prevalence and spectrum of mutations in the otoferlin gene (OTOF) in subjects with nonsyndromic hearing impairment and auditory neuropathy. Hum. Mutat. **29:**823-831.

18. **Yasunaga S, Grati M, Cohen-Salmon M, El-Amraoui A, Mustapha M, Salem N, El-Zir E, Loiselet J, Petit C.** 1999. A mutation in OTOF, encoding otoferlin, a FER-1-like protein, causes DFNB9, a nonsyndromic form of deafness. Nat. Genet. **21:**363-369.

19. **Marty NJ, Holman CL, Abdullah N, Johnson CP.** 2013. The C2 domains of otoferlin, dysferlin, and myoferlin alter the packing of lipid bilayers. Biochemistry **52:**5585-5592.

20. **Duncker SV, Franz C, Kuhn S, Schulte U, Campanelli D, Brandt N, Hirt B, Fakler B, Blin N, Ruth P, Engel J, Marcotti W, Zimmermann U, Knipper M.** 2013. Otoferlin couples to clathrin-mediated endocytosis in mature cochlear inner hair cells. J. Neurosci **33:**9508-9519.

21. **Heidrych P, Zimmermann U, Kuhn S, Franz C, Engel J, Duncker SV, Hirt B, Pusch CM, Ruth P, Pfister M, Marcotti W, Blin N, Knipper M.** 2009. Otoferlin interacts with myosin VI: implications for maintenance of the basolateral synaptic structure of the inner hair cell. Hum. Mol. Genet. **18:**2779-2790.

22. **Ramakrishnan NA, Drescher MJ, Drescher DG.** 2009. Direct interaction of otoferlin with syntaxin 1A, SNAP-25, and the L-type voltage-gated calcium channel Cav1.3. J. Biol. Chem. **284:**1364-1372.

23. **Ramakrishnan NA, Drescher MJ, Morley BJ, Kelley PM, Drescher DG.** 2014. Calcium Regulates Molecular Interactions of Otoferlin with SNARE Proteins Required for Hair Cell Exocytosis. J. Biol. Chem. **289(13):** 8750-66.

24. **Dulon D, Safieddine S, Jones SM, Petit C.** 2009. Otoferlin Is Critical for a Highly Sensitive and Linear Calcium-Dependent Exocytosis at Vestibular Hair Cell Ribbon Synapses. J. Neurosci. **29:**10474-10487.

25. **Schwander M, Sczaniecka A, Grillet N, Bailey JS, Avenarius M, Najmabadi H, Steffy BM, Federe GC, Lagler EA, Banan R, Hice R, Grabowski-Boase L, Keithley EM, Ryan AF, Housley GD, Wiltshire T, Smith RJH, Tarantino LM, Muller U.** 2007. A forward genetics screen in mice identifies recessive deafness traits and reveals that pejvakin is essential for outer hair cell function. J. Neurosci. **27:**2163-2175.

26. **Vincent PF, Bouleau Y, Safieddine S, Petit C, Dulon D.** 2014. Exocytotic machineries of vestibular type I and cochlear ribbon synapses display similar intrinsic otoferlin-dependent Ca2+ sensitivity but a different coupling to Ca2+ channels. J. Neurosci. **34:**10853-10869.

27. **Reisinger E, Bresee C, Neef J, Nair R, Reuter K, Bulankina A, Nouvian R, Koch M, Buckers J, Kastrup L, Roux I, Petit C, Hell SW, Brose N, Rhee JS,**

Kugler S, Brigande JV, Moser T. 2011. Probing the functional equivalence of otoferlin and synaptotagmin 1 in exocytosis. J. Neurosci **31:**4886-4895.

28. **Leibovici M, Safieddine S, Petit C.** 2008. Mouse models for human hereditary deafness. Curr. Top. Dev. Biol. **84:**385-429.

29. **Westerfield M**. 2000. The zebrafish book. A guide for the laboratory use of zebrafish (Danio rerio). 4th ed., Univ. of Oregon Press, Eugene.

30. **Thisse C, Thisse B.** 2008. High-resolution in situ hybridization to whole-mount zebrafish embryos. Nat. Protoc. **3:**59-69.

31. **Novak AE, Ribera AB.** 2003. Immunocytochemistry as a tool for zebrafish developmental neurobiology. Methods Cell Sci. **25:**79-83.

32. **Sabaliauskas NA, Foutz CA, Mest JR, Budgeon LR, Sidor AT, Gershenson JA, Joshi SB, Cheng KC.** 2006. High-throughput zebrafish histology. Methods **39:**246-254.

33. **Javelle M, Marco CF, Timmermans M.** 2011. In situ hybridization for the precise localization of transcripts in plants. J. Vis. Exp. **57:**1-11

34. **Kimmel CB, Ballard WW, Kimmel SR, Ullmann B, Schilling TF.** 1995. Stages of embryonic development of the zebrafish. Dev. Dyn. **203:**253-310.

35. **Waterman RE, Bell DH.** 1984. Epithelial fusion during early semicircular canal formation in the embryonic zebrafish, Brachydanio rerio. Anat. Rec. **210:**101-114.

36. **Goodyear RJ, Legan PK, Christiansen JR, Xia B, Korchagina J, Gale JE, Warchol ME, Corwin JT, Richardson GP.** 2010. Identification of the hair cell soma-1 antigen, HCS-1, as otoferlin. J. Assoc. Res. Otolaryngol. **11:**573-586.

37. **Pangrsic T, Lasarow L, Reuter K, Takago H, Schwander M, Riedel D, Frank T, Tarantino LM, Bailey JS, Strenzke N, Brose N, Muller U, Reisinger E, Moser T.** 2010. Hearing requires otoferlin-dependent efficient replenishment of synaptic vesicles in hair cells. Nat. Neurosci. **13:**869-876.

38. **Griesinger CB, Richards CD, Ashmore JF.** 2002. Fm1-43 reveals membrane recycling in adult inner hair cells of the mammalian cochlea. J. Neurosci. **22:**3939-3952.

39. **Kappler JA, Starr CJ, Chan DK, Kollmar R, Hudspeth AJ.** 2004. A nonsense mutation in the gene encoding a zebrafish myosin VI isoform causes defects in hair-cell mechanotransduction. Proc. Natl. Acad. Sci. USA **101:**13056-13061.

40. **Roux I, Hosie S, Johnson SL, Bahloul A, Cayet N, Nouaille S, Kros CJ, Petit C, Safieddine S.** 2009. Myosin VI is required for the proper maturation and function of inner hair cell ribbon synapses. Hum. Mol. Genet. **18:**4615-4628.

41. **Nicolson T, Rusch A, Friedrich RW, Granato M, Ruppersberg JP, Nusslein-Volhard C.** 1998. Genetic analysis of vertebrate sensory hair cell mechanosensation: the zebrafish circler mutants. Neuron **20:**271-283.

42. **Obholzer N, Wolfson S, Trapani JG, Mo W, Nechiporuk A, Busch-Nentwich E, Seiler C, Sidi S, Sollner C, Duncan RN, Boehland A, Nicolson T.** 2008. Vesicular glutamate transporter 3 is required for synaptic transmission in zebrafish hair cells. J. Neurosci. **28:**2110-2118.

43. **Winata CL, Korzh S, Kondrychyn I, Zheng W, Korzh V, Gong Z.** 2009. Development of zebrafish swimbladder: The requirement of Hedgehog signaling in specification and organization of the three tissue layers. Dev. Biol. **331:**222-236.

44. **Khan Z, Carey J, Park HJ, Lehar M, Lasker D, Jinnah HA.** 2004. Abnormal motor behavior and vestibular dysfunction in the stargazer mouse mutant. Neuroscience **127:**785-796.

45. **Lindema S, Gernet M, Bennay M, Koch M, Loscher W.** 2008. Comparative analysis of anxiety-like behaviors and sensorimotor functions in two rat mutants, ci2 and ci3, with lateralized rotational behavior. Physiol. Behav. **93:**417-426.

46. **Burgess HA, Granato M.** 2007. Sensorimotor gating in larval zebrafish. J. Neurosci. **27:**4984-4994.

47. **Faber DS, Fetcho JR, Korn H.** 1989. Neuronal networks underlying the escape response in goldfish. General implications for motor control. Ann. N. Y. Acad. Sci. **563:**11-33

48. **Zottoli SJ , Faber DS.** 2000. The Mauthner cell: what has it taught us? Neuroscientist **6**: 26-38

49. **Howe K, Clark MD, Torroja CF, Torrance J, Berthelot C, Muffato M, Collins JE, Humphray S, McLaren K, Matthews L, McLaren S, Sealy I, Caccamo M, Churcher C, Scott C, Barrett JC, Koch R, Rauch GJ, White S, Chow W, Kilian B, Quintais LT, Guerra-Assuncao JA, Zhou Y, Gu Y, Yen J, Vogel JH, Eyre T, Redmond S, Banerjee R, Chi J, Fu B, Langley E, Maguire SF, Laird GK, Lloyd D, Kenyon E, Donaldson S, Sehra H, Almeida-King J, Loveland J, Trevanion S, Jones M, Quail M, Willey D, Hunt A, Burton J, Sims S, McLay K, Plumb B, Davis J, Clee C, Oliver K, Clark R, Riddle C, Elliot D, Threadgold G, Harden G, Ware D, Mortimore B, Kerry G, Heath P, Phillimore B, Tracey A, Corby N, Dunn M, Johnson C, Wood J, Clark S, Pelan S, Griffiths G, Smith M, Glithero R, Howden P, Barker N, Stevens C, Harley J, Holt K, Panagiotidis G, Lovell J, Beasley H, Henderson C, Gordon D, Auger K, Wright D, Collins J, Raisen C, Dyer L, Leung K, Robertson L, Ambridge K, Leongamornlert D, McGuire S, Gilderthorp R, Griffiths C, Manthravadi D, Nichol S, Barker G, Whitehead S, Kay M, Brown J, Murnane C, Gray E, Humphries M, Sycamore N, Barker D, Saunders D, Wallis J, Babbage A, Hammond S, Mashreghi-Mohammadi M, Barr L, Martin S, Wray P, Ellington A, Matthews N, Ellwood M, Woodmansey R, Clark G, Cooper J, Tromans A, Grafham D, Skuce C, Pandian R, Andrews R, Harrison E, Kimberley A, Garnett J, Fosker N, Hall R, Garner P, Kelly D, Bird C, Palmer S, Gehring I, Berger A, Dooley CM, Ersan-Urun Z, Eser C, Geiger H, Geisler M, Karotki L, Kirn A, Konantz J, Konantz M, Oberlander M, Rudolph-Geiger S, Teucke M, Osoegawa K, Zhu B, Rapp A, Widaa S, Langford C, Yang F, Carter NP, Harrow J, Ning Z, Herrero J, Searle SM, Enright A, Geisler R, Plasterk RH, Lee C, Westerfield M, de Jong PJ, Zon LI, Postlethwait JH, Nusslein-Volhard C, Hubbard TJ, Roest Crollius H, Rogers J, Stemple DL, Begum S, Lloyd C, Lanz C, Raddatz G, Schuster SC.** 2013. The zebrafish reference genome sequence and its relationship to the human genome. Nature **496:**498-503.

50. **Yasunaga S, Grati M, Chardenoux S, Smith TN, Friedman TB, Lalwani AK, Wilcox ER, Petit C.** 2000. OTOF encodes multiple long and short isoforms: genetic evidence that the long ones underlie recessive deafness DFNB9. Am. J. Hum. Genet. **67:**591-600.

51. **Longo-Guess C, Gagnon LH, Bergstrom DE, Johnson KR.** 2007. A missense mutation in the conserved C2B domain of otoferlin causes deafness in a new mouse model of DFNB9. Hearing research **234:**21-28.

52. **Mirghomizadeh F, Pfister M, Apaydin F, Petit C, Kupka S, Pusch CM, Zenner HP, Blin N.** 2002. Substitutions in the conserved C2C domain of otoferlin cause DFNB9, a form of nonsyndromic autosomal recessive deafness. Neurobiology of disease **10:**157-164.

53. **Helfmann S, Neumann P, Tittmann K, Moser T, Ficner R, Reisinger E.** 2011. The crystal structure of the C(2)A domain of otoferlin reveals an unconventional top loop region. J. Mol. Biol. **406:**479-490.

54. **Abdullah N, Padmanarayana M, Marty NJ, Johnson CP.** 2014. Quantitation of the calcium and membrane binding properties of the C2 domains of dysferlin. Biophys. J. **106:**382-389.

55. **Therrien C, Di Fulvio S, Pickles S, Sinnreich M.** 2009. Characterization of lipid binding specificities of dysferlin C2 domains reveals novel interactions with phosphoinositides. Biochemistry **48:**2377-2384.

56. **Wright S, Hwang Y, Oertel D.** 2014. Synaptic Transmission between End Bulbs of Held and Bushy Cells in the Cochlear Nucleus of Mice with a Mutation in Otoferlin. J. Neurophysiol jn 00522 02014.

Figure 2.1

A)

Species	Otoferlin C2 domains (% identity with human)					
	C2A	C2B	C2C	C2D	C2E	C2F
Mouse	91	100	100	100	98	98
Rat	92	100	100	99	98	98
Rabbit	95	99	99	99	100	-
Guinea-Pig	94	99	98	100	99	98
Frog	-	78	91	91	94	96
Zebrafish						
1)otoferlin	-	91	89	83	88	94
2)otoferlin	77	91	89	83	92	95

B)

Species	% identity with **human** otoferlin peptide sequence
Mouse	95
Rat	93
Rabbit	93
Guinea-Pig	94
Frog	79
Zebrafish	
1) otoferlin	74
2) otoferlin	76

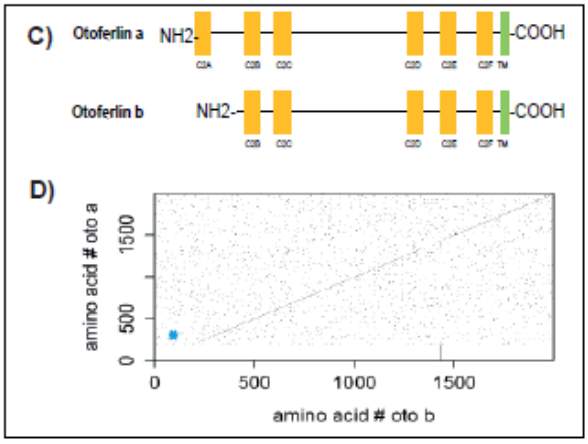

Sequence identity of otoferlin across different species. A) Percent identity of predicted otoferlin C2 domains of various species compared to human otoferlin. **B)** Comparison of overall sequence identity of otoferlin with human otoferlin. **C)** Zebrafish otoferlin isoforms with putative C2 domains. Otoferlin b lacks the C2A domain. **D)** Dot-plot showing the identity of amino acid sequence between the two zebrafish otoferlin proteins: otoferlin a and otoferlin b. The diagonal across the plot indicates highly identical sequnces. Breaks along the diagonal indicate regions which are non-identical. The asterisk (*) designates the absence of the C2A domain (amino acid = 3- 97).

Figure 2.2

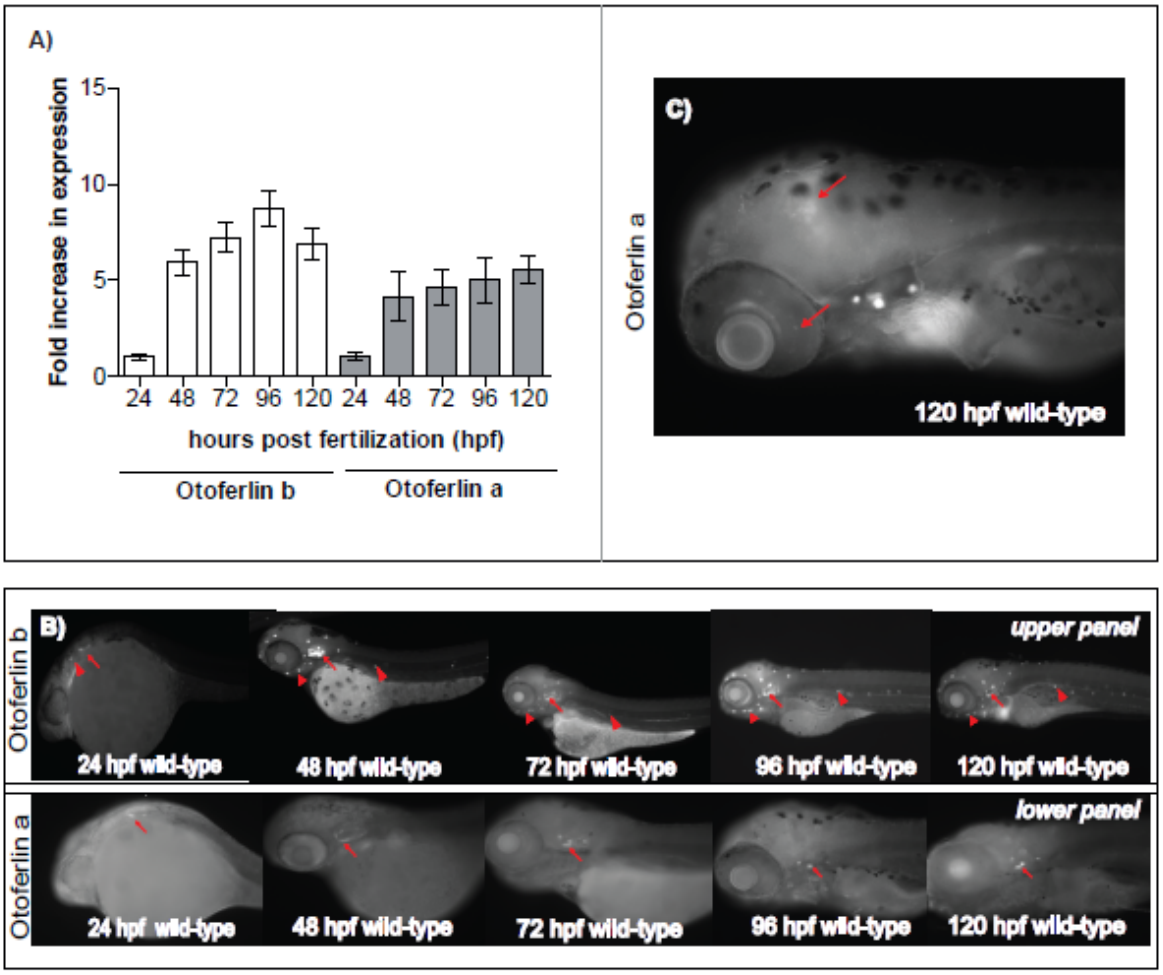

mRNA expression of otoferlin in developing zebrafish. **A)** Fold expression of otoferlin a and b transcripts at 24-120 hpf. Expression is normalized to 24 hpf. Error bars indicate 95% confidence interval of the sample mean (n=5). **B)** Whole-mount in situ hybridization images showing expression of otoferlin in 24-120 hpf wild-type zebrafish larvae. Upper panel – Expression of otoferlin b. Arrows indicate sensory patches in the inner ear. Arrowheads indicate anterior and posterior lateral line neuromasts; Lower panel – Expression of otoferlin a. Arrows indicate sensory patches in the inner ear. **C)** Expression of otoferlin a in the brain region and retina in a 120 hpf zebrafish larvae. Arrows indicate brain and retina.

Figure 2.3

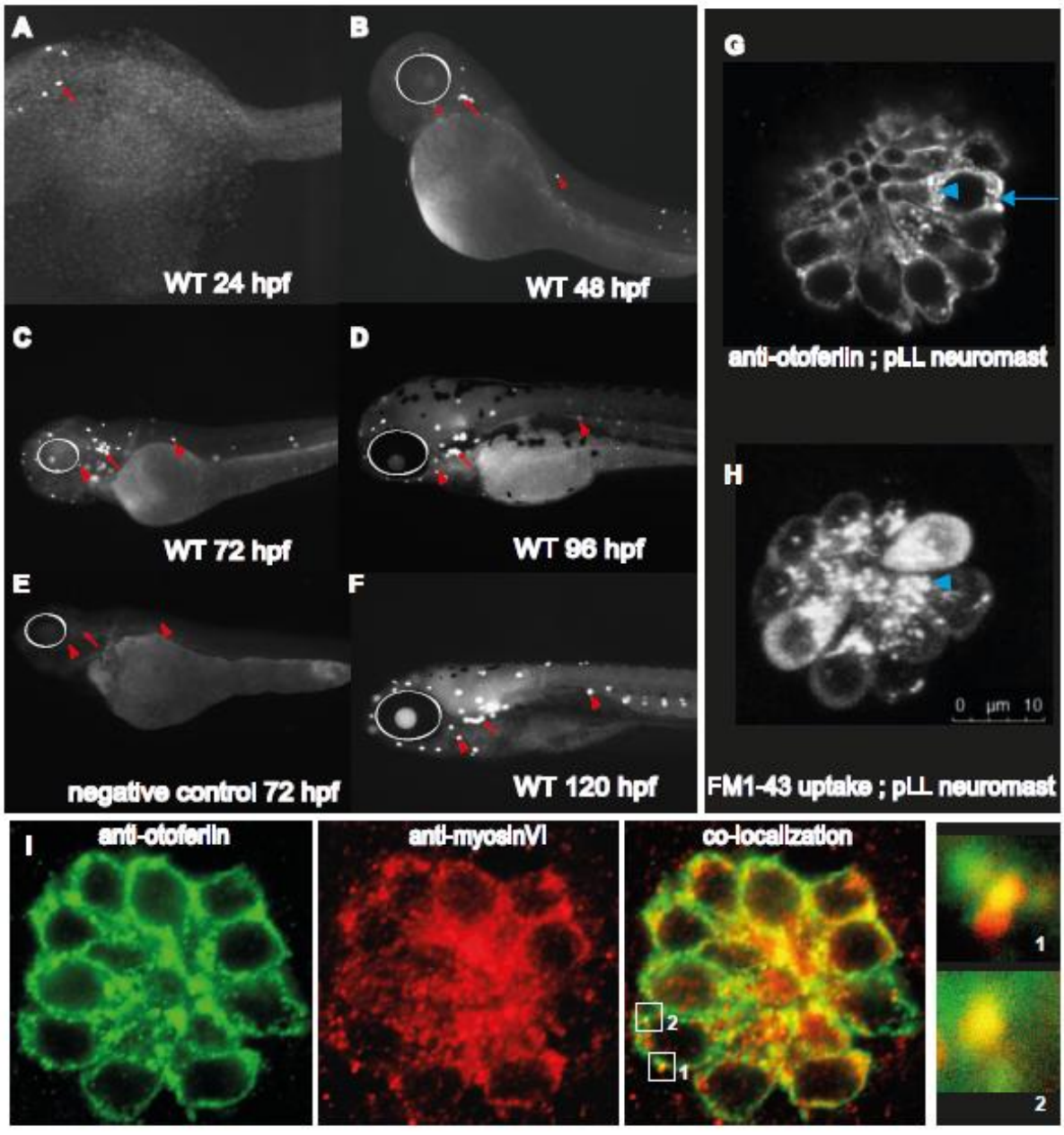

Otoferlin protein expression in developing zebrafish. (A-F) Whole-mount immunohistochemistry on wild-type larval zebrafish at indicated developmental time points (24-120 hpf). **E)** Negative control with no primary antibody in 72 hpf wild-type larvae. White circles indicate the position of the eye, arrows indicate sensory patches of

the ear, arrowheads denote anterior and lateral line neuromasts. **G)** Confocal image showing sub-cellular distribution of otoferlin in a 120 hpf hair cell neuromast cluster. Arrowhead indicates the supranuclear region of the hair cell, arrow indicates basolateral compartment of the hair cell (Scalebar 10um). **H)** Confocal image showing uptake of FM1-43 dye uptake in the apical end (arrowhead) of hair cells within a neuromast of the posterior lateral line. Dye incubation time – 3 minutes. **I)** Dual Immunofluorescence with wild-type 120 hpf zebrafish showing co-localization of otoferlin in the hair cells of the neuromast with another hair cell marker, myosinVI. White boxes 1 and 2 indicate regions of colocalization. Insets of regions 1 and 2 show otoferlin colocalizing with myosin VI.

Figure 2.4

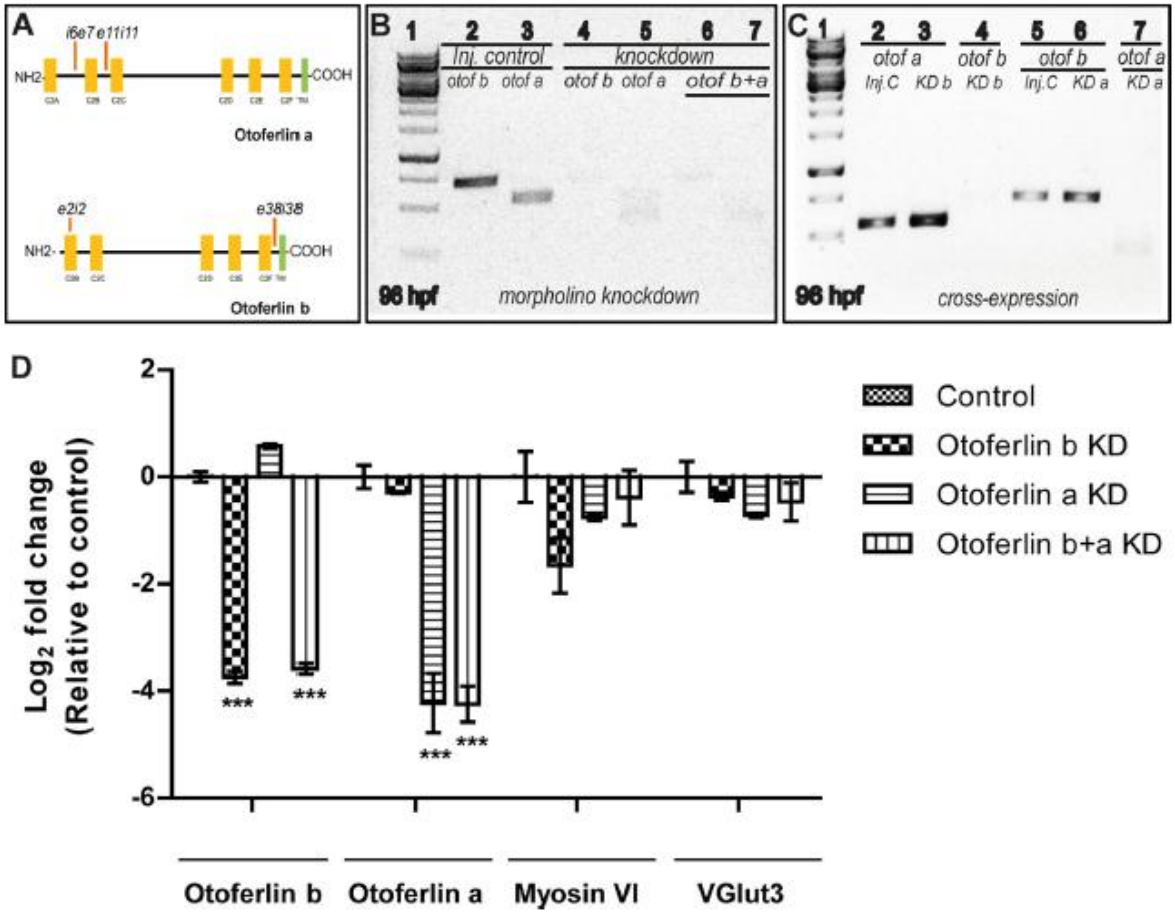

Morpholino knockdown of otoferlin in zebrafish larvae. A) Diagram of four splice-blocking morpholinos used in this study targeting otoferlin a and otoferlin b (e= exon; i= intron). **B)** RT-PCR gel image of otoferlin KD zebrafish larvae at 96 hpf, (lane 1) = molecular weight marker ; (lane 2) = negative control tested for otoferlin b; (lane 3) = negative control injected tested for otoferlin a; (lane 4)= otoferlin b KD tested for otoferlin b; (lane 5) = otoferlin a KD tested for otoferlin a; (lane 6) = otoferlin b+a double KD tested for otoferlin b; (lane 7) = otoferlin b+a double KD tested for otoferlin a. **C)** Cross expression studies with 96 hpf zebrafish larvae. RT-PCR gel image shows expression of: (lane 1)= molecular weight marker; (lane 2) = otoferlin a in control; (lane

3)= otoferlin a in otoferlin b KD; (lane 4) = otoferlin b in otoferlin b KD; (lane 5) = otoferlin b in control; (lane 6)= otoferlin b in otoferlin a KD; (lane 7) = otoferlin a in otoferlin a KD. (Inj. C – injected control, KD – Knockdown, otof a – otoferlin a, otof b – otoferlin b, otof b+a – otoferlin b+a) **D)** qPCR bar graph showing relative expression of otoferlin a, otoferlin b, myosinVI and VGlut3 genes in 96 hpf larval zebrafish across control, otoferlin a KD, otoferlin b KD and otoferlin b+a KD groups where each gene is normalized with respect to the corresponding controls. For the Myosin VI and Vglut3 genes, no statistical deviation in expression is observed among the different KD groups. Expression of otoferlin a is significantly reduced (p value <0.001) in the otoferlin a and otoferlin b+a KD groups, but not in the otoferlin b KD. Otoferlin b expression is significantly reduced in the otoferlin b and otoferlin b+a KD groups (p value <0.001), but not in the otoferlin a KD. The statistical significance is calculated through Bonferroni multiple comparisons in prism software. Error bars indicate 95% confidence interval of the sample mean (n=3).

Figure 2.5

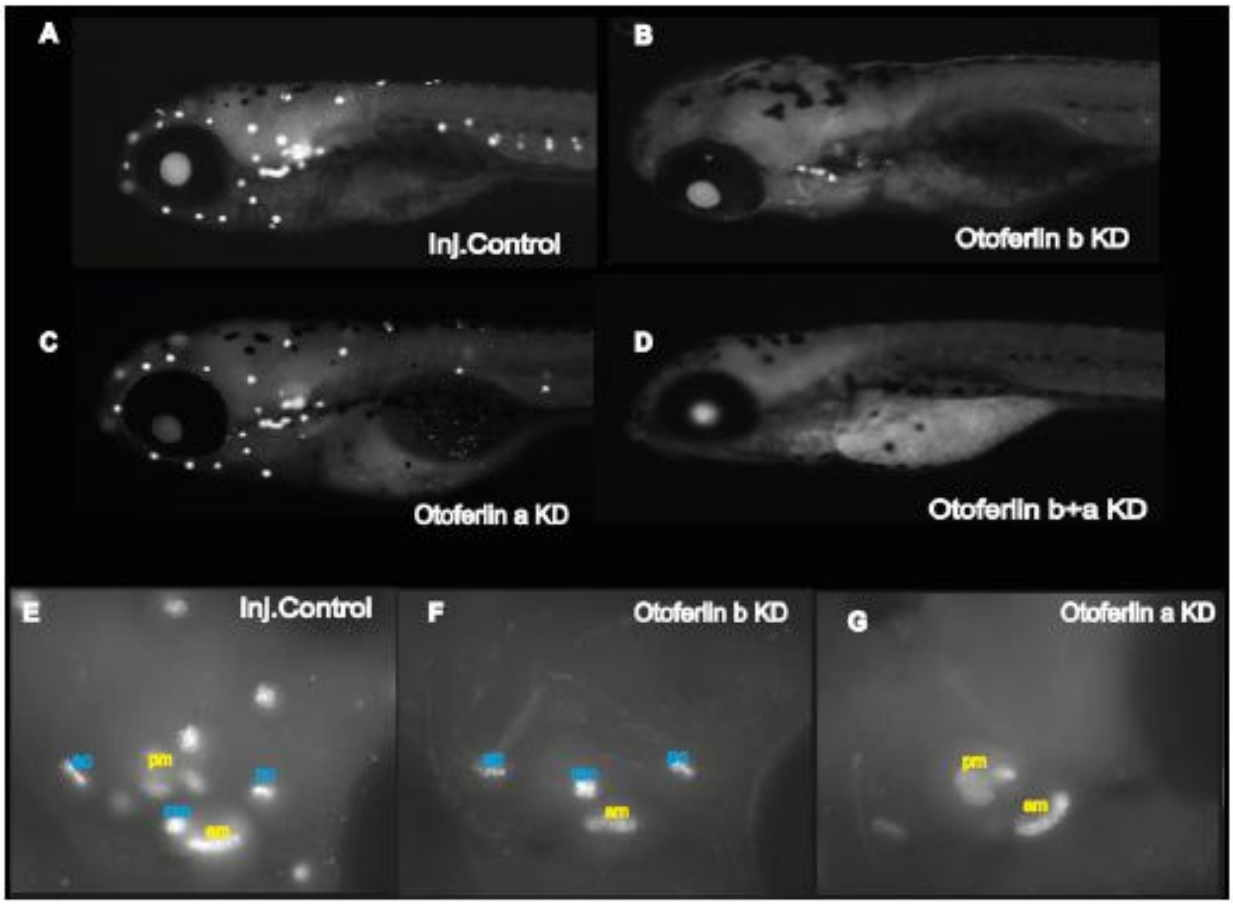

Whole mount immunohistochemistry with the HCS-1 anti-otoferlin antibody. A) 120 hpf larvae showing otoferlin expression in control injected, **B)** otoferlin b KD, **C)** otoferlin a KD, **D)** otoferlin b+a KD. Fluorescent MIP (maximum intensity projection) image of **E)** Injected Control, **F)** Otoferlin b KD, **G)** Otoferlin a KD, of 120 hpf larval otic region showing distinct distribution of otoferlin in the sensory patches of cristae and maculae (ac, anterior crista; mc, medial crista; pc, posterior crista; pm, posterior macula; am, anterior macula).

Figure 2.6

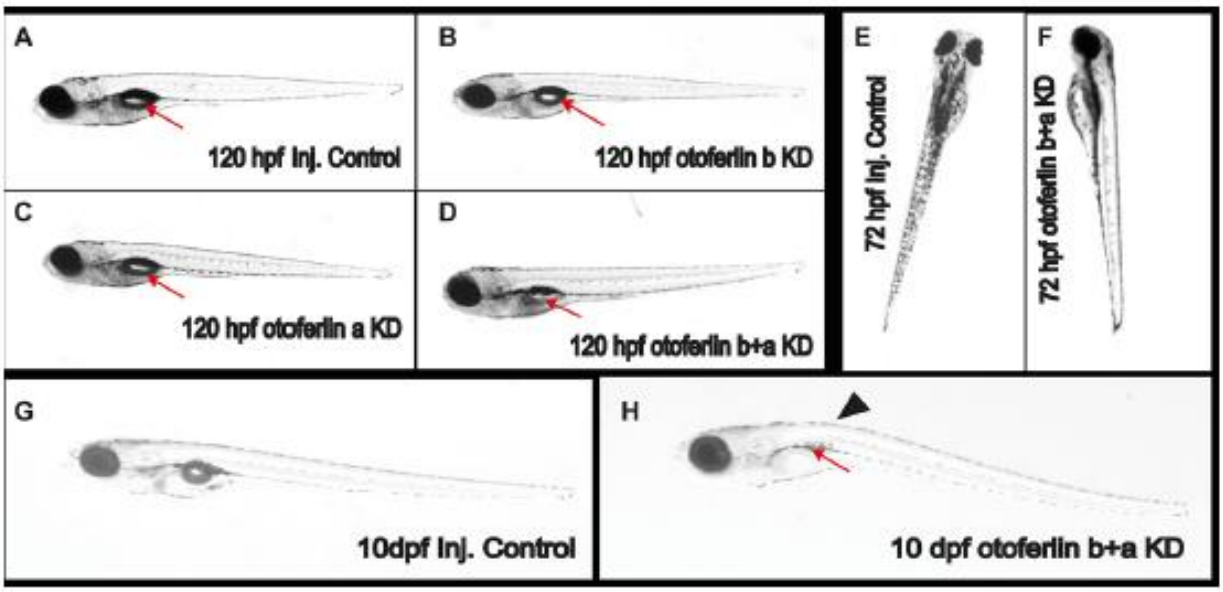

Observable phenotypes associated with the otoferlin KD 120 hpf larval zebrafish. **A)** Control injected, **B)** otoferlin b KD, **C)** otoferlin a KD, **D)** otoferlin b+a double KD (arrows denote the swim bladder). The otoferlin double KDs fail to develop an inflated swim bladder. **E)** 72 hpf control larvae maintains an upright posture, **F)** 72 hpf otoferlin b+a double KDs fail to maintain an upright posture **G)** 10-day old injected control larvae, **H)** 10-day old otoferlin b+a double KD zebrafish fail to inflate their swim bladders (arrow) and develops a curved spine (arrow-head).

Figure 2.7

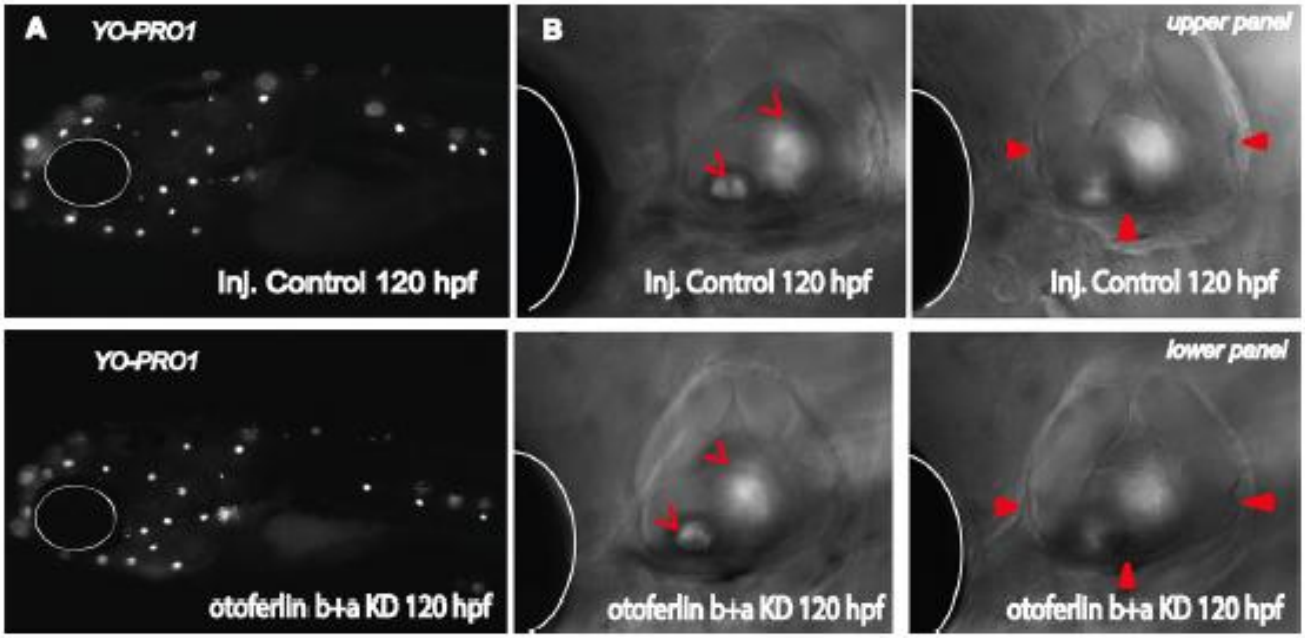

Otoferlin KD effect on structure and formation of lateral line, otic vesicle and semicircular canals. A) (upper panel) Yo-Pro1 uptake in injected control larval zebrafish at 120 hpf, (lower panel) Yo-Pro1 uptake in otoferlin b+a double KD larval zebrafish at 120 hpf **B)** (upper panel) Bright field images showing otic region in 120-hour old injected control and (lower panel) otoferlin b+a double KDs, open arrow heads points to the otoliths, filled arrow heads point to the semicircular canals, white circle and hemicircle indicates position of the eye.

Figure 2.8

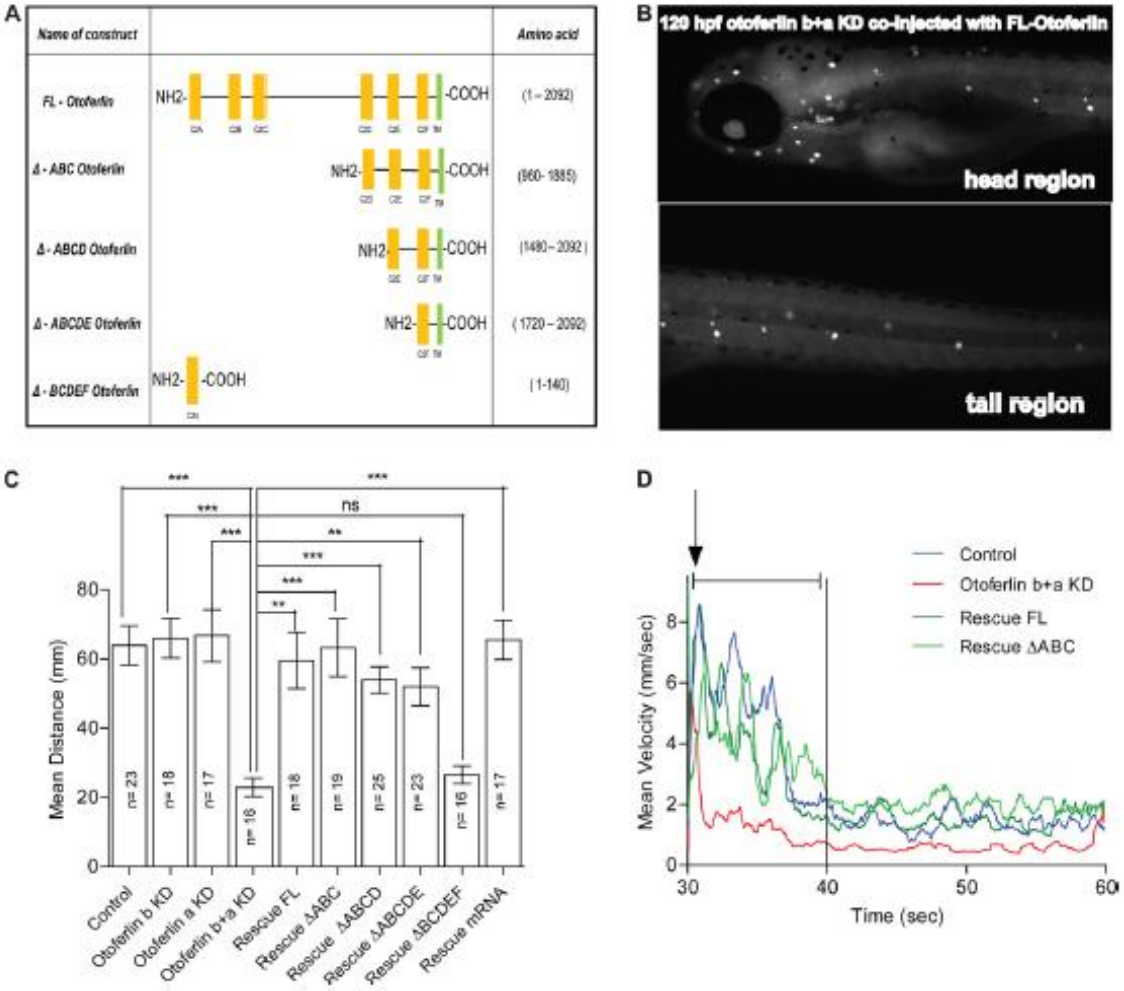

Rescue of zebrafish otoferlin knockdown with mouse otoferlin. A) Schematic of the truncated mouse otoferlin constructs used in this study. Amino acid numbers are indicated. **B)** Whole mount immunohistochemistry on 120 hpf larval zebrafish double morphants co-injected with the mouse full-length otoferlin construct under the hair cell specific promoter. Figure shows otoferlin expression only in the hair cells at 120 hpf. **C)** Otoferlin deficiency causes defects in startle escape response in 120 hpf larval

zebrafish. Plot of distance after startling for different groups. Control (n=23, mean distance 63.94 mm), Otoferlin b KD (n=18, mean distance = 66.03 mm), Otoferlin a KD (n = 17, mean distance = 66.79 mm), Otoferlin b+a KD (n = 16, mean distance = 22.92 mm), Rescue FL (n = 18, mean distance = 59.58 mm), Rescue ΔABC (n = 19, mean distance = 63.32 mm), Rescue ΔABCD (n = 25, mean distance = 53.94 mm), Rescue ΔABCDE (n = 23, mean distance = 52.00 mm), Rescue ΔBCDEF (n = 16, mean distance = 26.57 mm), Rescue mRNA (n = 17, mean distance = 65.55 mm),(Dunn's multiple comparison with standard 5% significance between otoferlin a+b KD and other groups, p-value<0.001). Error bars indicate 95% confidence interval of the sample mean. ns = not significant. **D)** Mean velocity (in mm/ sec) traces of different groups - Control (n = 23), Otoferlin b+a KD (n = 16), Rescue FL (n = 18), Rescue ΔABC (n = 19). The time point of startle is denoted with a vertical arrow, and the first 10 secs after startling is denoted with a capped line.

Figure 2.9

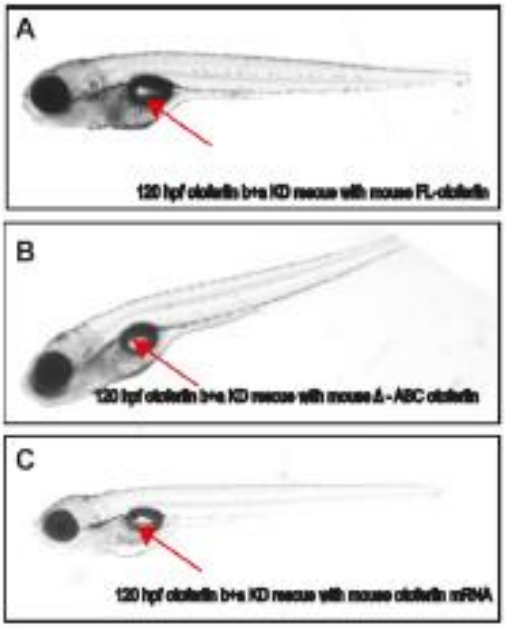

D

Otoferlin morphants co-injected with mouse rescue construct	Number of fish injected per group	% of injected larvae with inflated swim bladder
mRNA	120	22
FL-otoferlin	120	27
Δ-ABC	120	42
Δ-ABCD	150	16
Δ-ABCDE	110	20

Rescue of otoferlin KD swim bladder phenotype with mouse otoferlin constructs. **A)** Rescue of swim bladder defect in 120 hpf otoferlin b+a KDs with FL-otoferlin. **B)** Rescue of swim bladder defect in 120 hpf otoferlin b+a KDs with del-ABC construct. **C)** Rescue of swim bladder defect in 120-hpf old otoferlin b+a double KD zebrafish with otoferlin mRNA. Arrow indicates inflated swim bladder. **D)** Table showing percentage of fish rescued at 120 hpf co-injected with mouse otoferlin constructs including otoferlin mRNA. (FL = full length).

Figure 2.S1

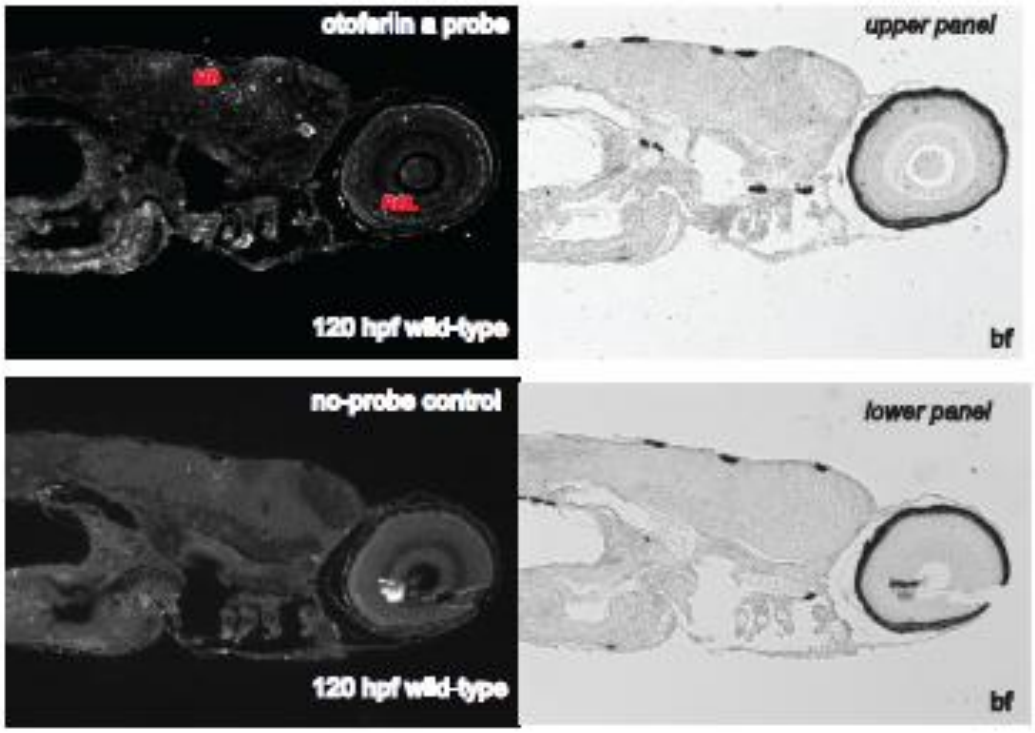

In situ **hybridization images of 120 hpf wild-type larval zebrafish paraffin sections** showing expression of otoferlin a in the mid-brain (MB) and retinal ganglion cell layer (RGL) . upper panel - otoferlin a probe and corresponding bright-field (bf) images. lower panel - no-probe control and corresponding bright-field (bf) images.

Figure 2.S2

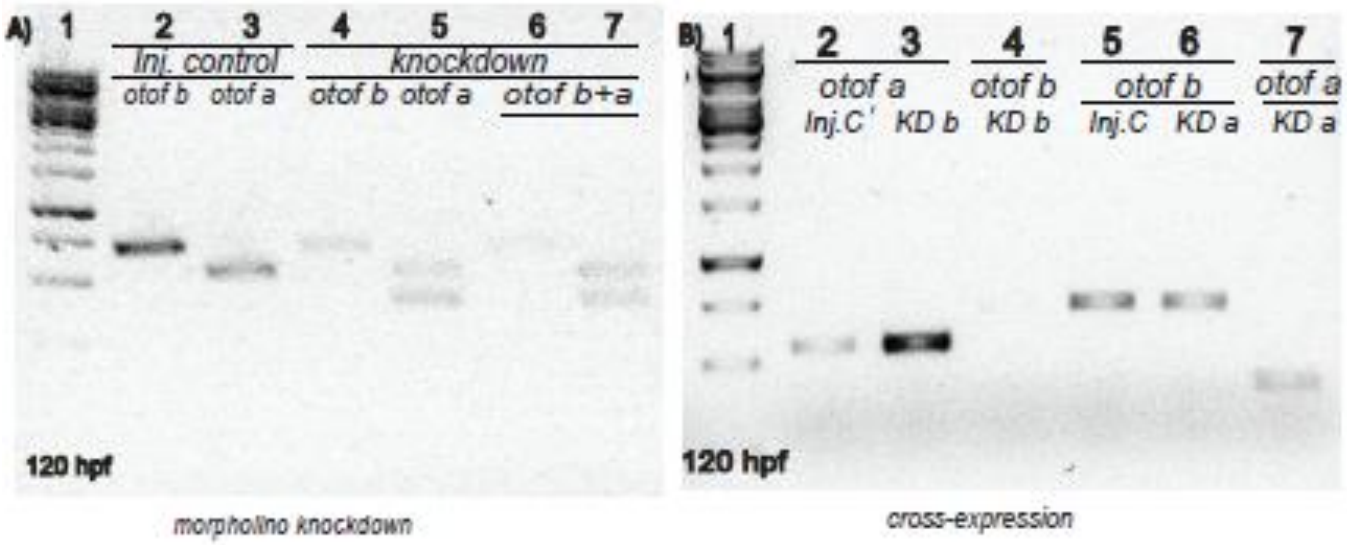

Morpholino knockdown of otoferlin in 120 hpf zebrafish larvae. A) RT-PCR gel image of otoferlin KD zebrafish larvae at 120 hpf, (lane 1) = molecular weight marker ; (lane 2) = negative control tested for otoferlin b; (lane 3) = negative control injected tested for otoferlin a; (lane 4)= otoferlin b KD tested for otoferlin b; (lane 5) = otoferlin a KD tested for otoferlin a; (lane 6) = otoferlin b+a double KD tested for otoferlin b; (lane 7) = otoferlin b+a double KD tested for otoferlin a. **B)** Cross expression studies with 120 hpf zebrafish larvae. RT-PCR gel image shows expression of: (lane 1)= molecular weight marker; (lane 2) = otoferlin a in control; (lane 3)= otoferlin a in otoferlin b KD; (lane 4) = otoferlin b in otoferlin b KD; (lane 5) = otoferlin b in control; (lane 6)= otoferlin b in otoferlin a KD; (lane 7) = otoferlin a in otoferlin a KD. (Inj. C – injected control, KD – Knockdown, otof a – otoferlin a, otof b – otoferlin b, otof b+a – otoferlin b+a)

Figure 2.S3

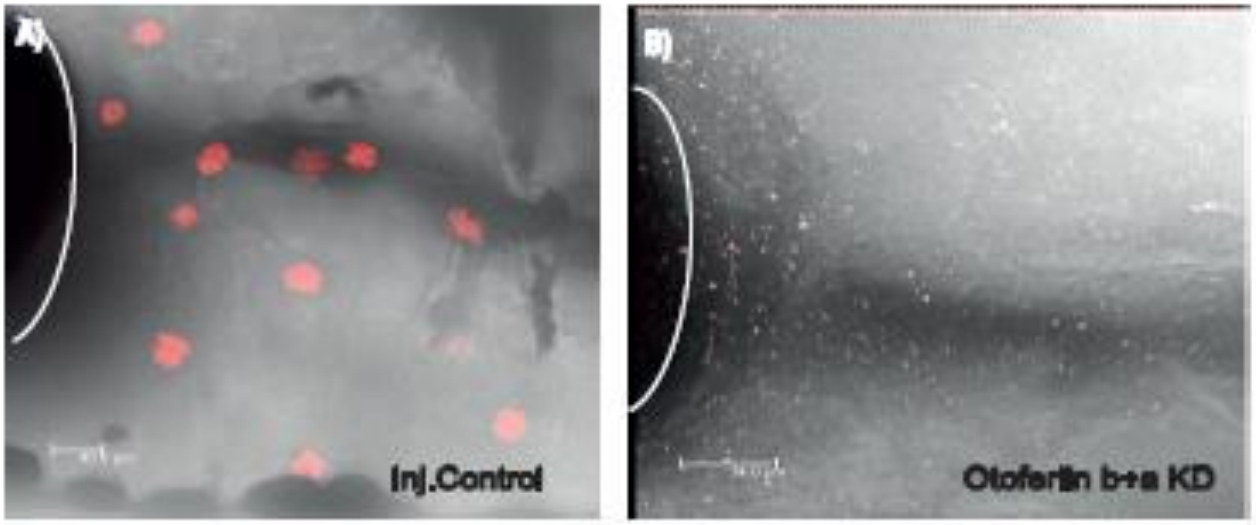

Compressed z-stack through the ear region showing otoferlin expression in 120 hpf injected control (A) larval zebrafish, and, otoferlin expression in double knockdown **(B)** 120 hpf larval fish (white hemicircles denotes the eye). Red clusters in Figure are otoferlin positively stained hair cell neuromasts.

Figure 2.S4

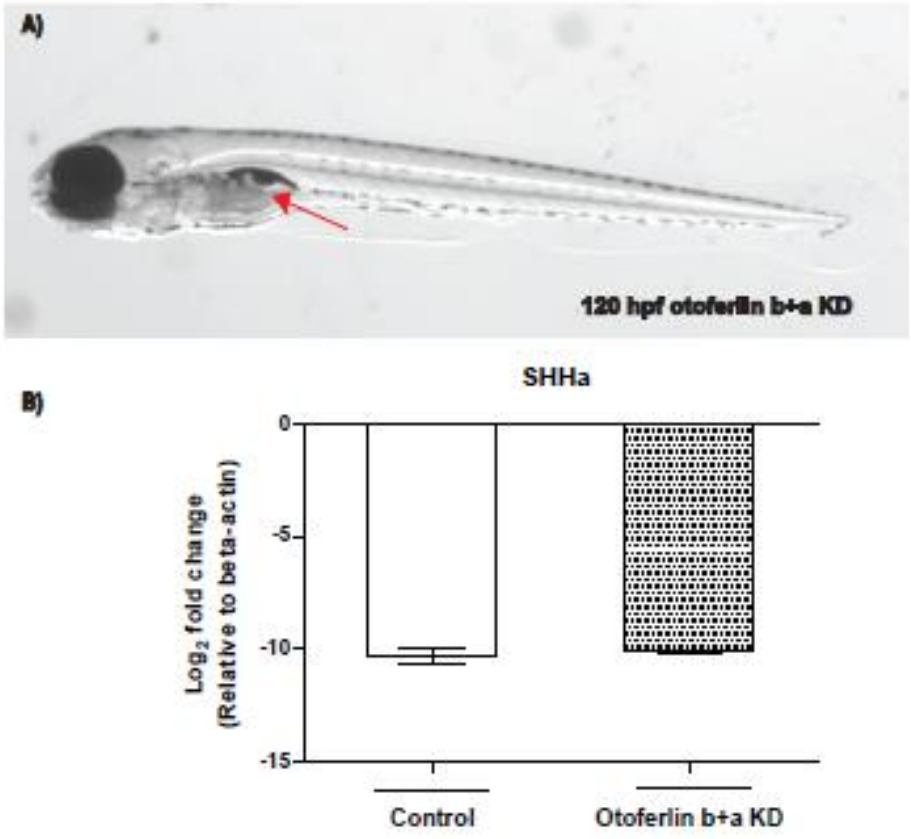

Phenotypic consistency with second set of morpholinos and qPCR showing expression of swim bladder marker A) Observable phenotypes associated with the otoferlin b+a KD in120 hpf larval zebrafish with second set of morpholinos (e11i11 - otoferlin a and e2i2- otoferlin b). Arrow indicates swim bladder. **B)** qPCR showing relative expression of shha in 72 hpf otoferlin control and double morphants normalized to beta-actin expression. Data shows no statistically significant differences in the expression of shha in control and double morphants. The statistical significance is calculated through Mann-Whitney test.

Figure 2.S5

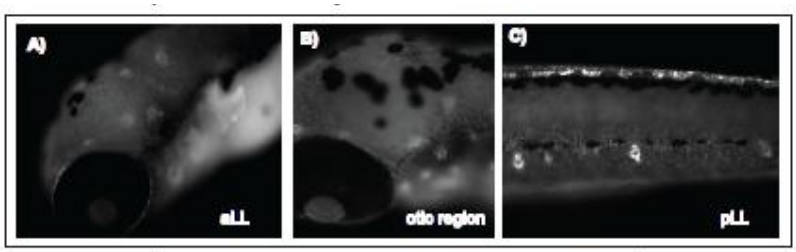

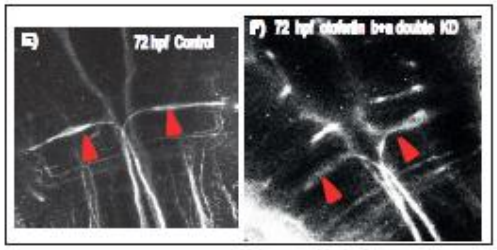

G)

Groups	Number of fish	Mean distance moved	sem
Control	23	63.84	5.69
Otoferlin a KD	18	66.03	5.73
Otoferlin b KD	17	66.79	7.53
Otoferlin b+a KD	16	22.92	2.65

Images showing hair cell specific expression of rescue construct and mauthner neurons; table with startle assay summary statistics (A-C) Whole-mount *in situ* hybridization on otoferlin double morphants co-injected with the full-length mouse otoferlin construct under the hair cell specific promoter at 96hpf. **A, B,** and **C** shows mRNA expression in the anterior lateral line (aLL) , posterior lateral line (pLL), and otic vesicle. **(E-F)** Confocal images of whole mount immunohistochemistry of 72 hpf larval zebrafish showing mauthner cells. **E)** Injected control, **F)** Otoferlin b+a double morphants. Arrowhead indicates the mauthner cells.**G)** Summary statistics of the startle between otoferlin morphants and control groups, sem - Std err of mean.

Figure 2.S6

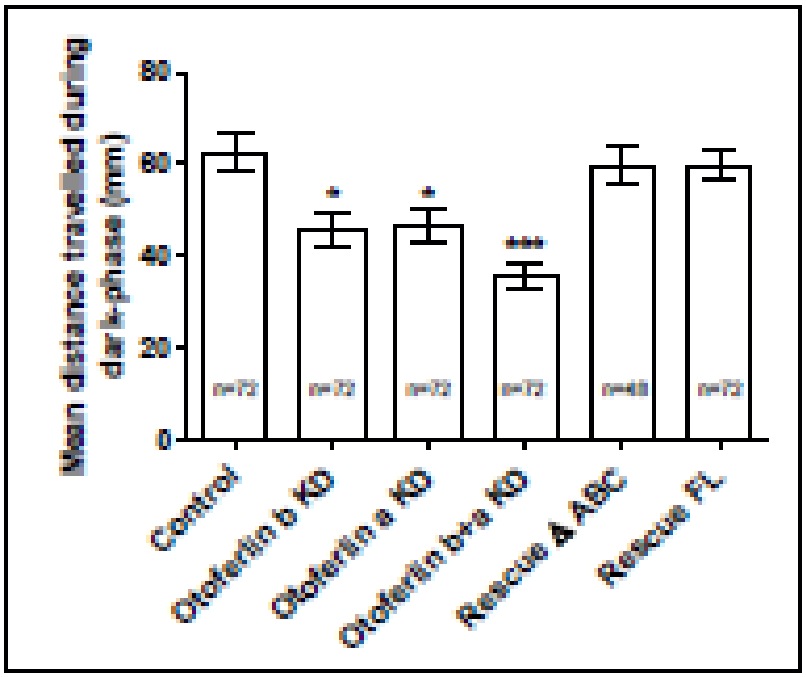

Dark-light behavioral assay : Distances travelled (in mm) during the dark-phase by larvae are shown. Mean distances moved in mm: Injected control (n=72) = 62.73, otoferlin b KD (n=72) = 45.67, otoferlin a KD (n=72) = 46.68, otoferlin b+a KD (n=72) = 35.61, Rescue FL (n=72) = 59.89, Rescue ΔABC (n=48) = 59.81. Dunn's multiple comparison test with standard 5% significance level shows significant difference between control and KD groups and no significant difference between control and rescue groups. Error bars indicate 95% confidence interval of the sample mean.

Figure 2.S7

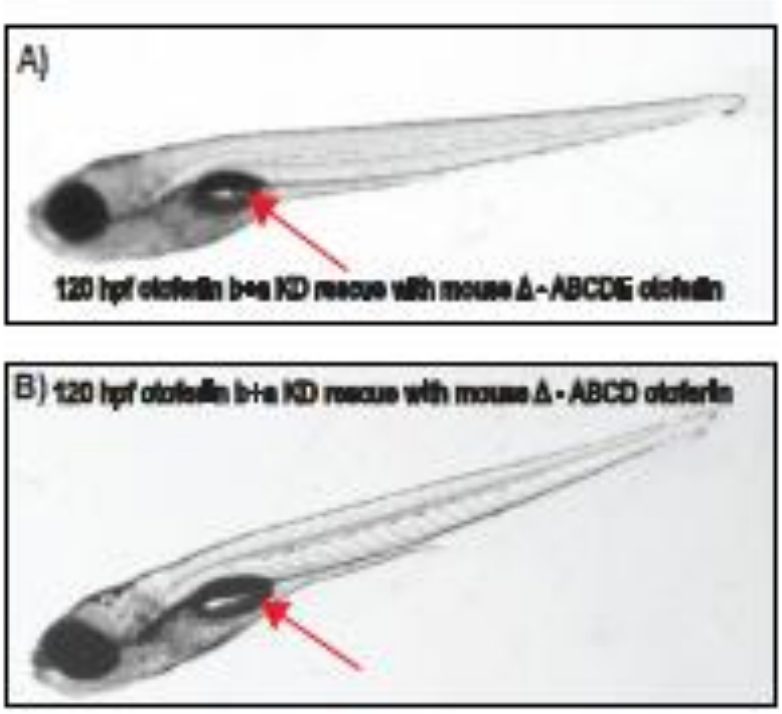

Rescue of zebrafish otoferlin KD with mouse otoferlin constructs. Rescue of swim bladder defect in 120 hpf otoferlin b+a KDs with mouse otoferlin, **A)** del-ABCDE, **B)** del-ABCD constructs. Arrow indicates inflated swim bladder.

Table 2.1

Table enlisting qRT-PCR primers:

Gene	**Primer sequence**
otoferlin b	GCAAAGACGGCAAAGCAGTGC (Forward); GCTTCCACTTTGCCTGTAATTTCTAGCTCATC (Reverse)
otoferlin a	GGACTGTTTACACACAACCTGAACATCAGT (Forward); CCCTCTATGTCATCCTCGTCTGCT (Reverse)
beta-actin	AAGCAGGAGTACGATGAGTC (Forward); TGGAGTCCTCAGATGCATTG (Reverse)
Myosin-6b	TGGCTCCCATCAGTCAAGTG (Forward) TTCTCGGTGTCATCCAAGCC (Reverse)
VGlut3	ATGTCTTCGTGATCGCCTCC (Forward) GTTTGCGGCCTGATGAGTTG (Reverse)
shha	ACCGAGACAAGAGCAAATACG(Forward) GTCCTTCACGGCCTTCTG (Reverse)

Table 2.2

Table enlisting ISH primers:

Gene	Primer sequence
otoferlin b	ATGGACTAAAGAAACAGACGGATGAGCATTTAG (Forward); TAATACGACTCACTATAGGG-TCAAACGCTGCAGAGAGAAGCTTCT (Reverse with T7-polymerase tag)
otoferlin a	GGACTGTTTACACACAACCTGAACATCAGT (Forward); TAATACGACTCACTATAGGG-CCCTCTATGTCATCCTCGTCTGCT (Reverse with T7-polymerase tag)
Mouse-otoferlin	TCCCCCAGGAAACCCAAGAAGTAC (Forward); TAATACGACTCACTATAGGG-GGGATCAGGTTCATTGCGAGCC (Reverse with T7-polymerase tag)

Table 2.3

Table enlisting primers for full-length and truncated mouse *otoferlin* constructs:

Gene	Primer sequence
Mouse *otoferlin full-length (FL)*	5'-GACCGCGGATGCATCATCACCATCACCATGGTATGGCCCTGATTGTTCACCTCAAG-3', 5'-CAGCGGCCGC*TCA*GGCCCCTAGGAGCTTC-3'
otoferlin ΔABC	5'-GACCGCGGATGCATCATCACCATCACCATGGTTCCTTTCCGCCCATCAGCCTAGTC-3', 5'-CAGCGGCCGC*TCA*GGCCCCTAGGAGCTTC-3'
Otoferlin ΔABCD	5’-CCG CGG ATG CCA AGC AAT GAC CCC ATC AAT GTG CTG GTC-3’ 5’ GCGGCCGC CTA GGC CCC TAG GAG CTT CTT GAC CAT GTA GCC TGG-3’
Otoferlin ΔABCDE	5’- CGA CCG CGG ATG CAC CAT CAC CAT CAC CAT GGC GCC TCC CCC AGG AAA CCC AAG AAG TAC GAG CTG-3’ 5’-GAT GCG GCC GCC TAG GCC CCT AGG AGC TTC TTG ACC ATG TAG CCT GG-3’
Otoferlin ΔBCDEF	5’- CGA CCG CGG ATG GCC CTG ATT GTT CAC CTC AAG ACT GTC TCA GAG-3’ 5’- GAT GCG GCC GCC TAC TGG AGG GAT TCA TCT CCC AGG AAG TCT CCA TC-3’

Table 2.4

Table enlisting the splice-blocking morpholino sequences targeting the *otoferlin a* and *b* gene:

Gene	Morpholino oligo sequences written from 5′ to 3′ and complementary to splice -junction target
otoferlin b	1) ACATTGTAAAACAGCACACCCAAGA (*e38i38*) 2) CATCTGCACACAAGAGCACAGAAGT (*e2i2*) - Morpholino 1 targets "Ensembl" splice variants: OTOF (1 of 2)-201 ENSDART00000041685, OTOF (1 of 2)-002 ENSDART00000149773, OTOF (1 of 2)-001 ENSDART00000149294 - Morpholino 2 targets "Ensembl" splice variants: OTOF (1 of 2)-201 ENSDART00000041685, OTOF (1 of 2)-002 ENSDART00000149773.
otoferlin a	1) TTTTTATGGTTACCGACCAGGTTGT (*e11i11*) 2) ATGAGATCATCTTTGGTCACCTCTT (*i6e7*) - Both morpholinos (1 and 2) target "Ensembl" splice variants: otof-001 ENSDART00000136255, otof-201 ENSDART00000008840.

Table 2.5

Table enlisting gene-specific primers for validating morpholino knockdown:

Gene	Primer sequence
otoferlin b	*e38i38-* CTCACCGAGGAAGCCAAAGA (Forward); TTGGTTGCAGACGAGATGGC (Reverse) *e2i2* – TTTACATACGCAGAGGATACGTCA (Forward); TTGTAGTAAGGGCAGTTGGTCG (Reverse)
otoferlin a	*i6e7* - GGATCGAAAAGCCATGCGTC (Forward); TAATACGACTCACTATAGGGTCTCCTTTTCCCACGACTGC (Reverse) *e11i11* – CTGGAACTTCACCTGGACGA (Forward); AACATGACGTCTGGAGGCAC (Reverse)

Chapter 3 - Loss of otoferlin alters the transcriptome profile and ribbon synapse architecture of sensory hair cells

Paroma Chatterjee, Aayushi Manchanda, Derik E. Haggard, Katie S. Kindt, Robert L. Tanguay, Colin P. Johnson.

Manuscript in preparation

3.1 Abstract

Auditory and vestibular sensory hair cells have adopted a unique architecture and gene expression profile to fulfill the requirements for hearing and balance. At the active zone of hair cells, the protein otoferlin plays an essential role in synaptic vesicle trafficking and has been linked to nonsyndromic hearing loss in humans. While required for hearing, the exact functions of otoferlin remain unclear, and the effects of loss of otoferlin on the hair cell and hearing pathway have yet to be fully characterized. Using a combination of immunofluorescence, transcriptome analysis, and calcium imaging, we find that in addition to reducing synaptic vesicle recycling, loss of otoferlin also leads to mistrafficking of synaptic vesicle proteins and larger but fewer synaptic ribbons, indicating that otoferlin contributes to ribbon synapse morphology. We also find that loss of otoferlin alters the expression levels of parvalbumin and s100, indicating that calcium handling is disrupted. Expression of neuronal genes linked to amino acid transport, axonal guidance, AMPA receptor trafficking, and neuronal growth were also abnormal, and suggesting that loss of otoferlin also affects the gene profile of surrounding neurons. We conclude that the mistrafficking of synaptic vesicle proteins and abnormal calcium handling in hair cells results in abnormal ribbon synapse sizes and distributions, which disrupt hair cell function. In turn, the dysfunction in the hair cells causes neurons to alter the level of expression for genes associated with axonal pathfinding and growth. Interestingly, we found that although a full-length (FL) otoferlin rescue construct with all the six C2 domains and transmembrane domains represses expression of neuromast and brain-specific transcripts in otoferlin-depleted larvae, a C2F-TM rescue construct with only the C2F and transmembrane domains fail to rescue expression of the same

transcripts. This indicates requirement of greater than one C2 domain of otoferlin in restoring expression levels of genes that are responsible for intricate cellular functions including calcium handling and axonal growth.

3.2 Introduction

Auditory and vestibular sensory hair cells transform mechanical forces into chemical signals for the purposes of hearing and balance (1-3). Unlike neurons, hair cells release neurotransmitter continuously and in a graded manner (4), and the presynaptic architecture has specialized to accommodate this requirement (5-11). Most prominent among these specializations is the ribbon synapse, which is composed of the protein ribeye and serves to tether synaptic vesicles proximal to the presynaptic membrane (4, 12-13). Another defining component of hair cell synapses is the expression of the hair cell marker otoferlin (7-9), which has been linked to DFNB9, a form of nonsyndromic hearing loss (14-15). Otoferlin binds calcium (16-18), and deletion of otoferlin results in a loss of neurotransmitter release (5, 7-9), suggesting a role in calcium sensitive synaptic vesicle priming and fusion (19). Unlike other synaptic proteins like VGlut3, otoferlin does not traffic exclusively to the ribbon synapse region but rather is distributed broadly in the cell body were it interacts with non-synaptic proteins (20-22). It remains to be determined however, whether loss of otoferlin significantly alters processes beyond synaptic vesicle exocytosis.

We find that in addition to the well characterized reduction in synaptic vesicle recycling, loss of otoferlin also results in mistrafficking of synaptic vesicle proteins and larger but fewer synaptic ribbons. In addition, analysis of the transcriptome profile of zebrafish

lacking otoferlin revealed altered expression levels of many genes associated with calcium handling, amino acid transport, axonal guidance, and neuronal growth. We conclude that loss of otoferlin both disrupts ribbon synapse architecture and disrupts the homeostatic gene expression profile of the hair cell.

3.3 Materials and Methods

Zebrafish lines and embryos

Tropical 5D strains of zebrafish (Danio rerio) were used for this study and reared according to Institutional Animal Care and Use Committee protocols at the Sinnhuber Aquatic Research Laboratory, Oregon State University. Adult 5D fish , were raised on a recirculating water system (28 + 1°C) with a 14:10 hour light-dark schedule. Spawning and embryo collection were followed as described (23).

Microinjections.

Morpholino depletion of otoferlin expression was conducted as described previously (24). Briefly, a pair of morpholinos (MOs) targeting exon/intron boundaries of *otoferlin a* and *otoferlin b* as well as a standard negative control were obtained from GeneTools, (Philomath, OR, USA) (24). Approximately 2nl of 0.6 mM of otoferlin a MO, 0.7 mM of otoferlin b MO and both MOs diluted with RNAse-free ultrapure distilled water and 3% phenol red were pressure-injected in WT embryos at one-cell stage as described in 24.

RNA extraction and sequencing

For transcriptomics, total RNA from pooled embryos of the microinjected control (WT), single morphant, and double morphant groups were extracted at 96 hours post fertilization (hpf) using Quick RNA miniprep kit, (Zymo Research, CA) according to the manufacturer’s protocol. RNA concentrations were measured with NanoDrop ND-1000

UV–vis spectrophotometer (Agilent Technologies, Palo Alto, CA) and RNA integrity was analyzed with Agilent 2100 Bioanalyzer (Agilent Technologies, Palo Alto, CA). Four independent biological replicates each of control, single and double morphant groups were prepared and submitted to the Center for Genome Research and Biocomputing (CGRB) , Oregon State University, OR, USA sequencing core for library prep and 150 bp paired-end sequencing on the Illumina HiSeq3000 . Sequencing reads were filtered and trimmed by running skewer on the mated fastq files based on quality score –q 30 –Q30.

RNA seq data analysis

Paired-end sequencing reads were aligned using TopHat (v2.1.1) to the Zv9.79 zebrafish genome, only mapping reads across known splice junctions with a corresponding mate pair (--no-novel-juncs and --no-mixed parameters, respectively) and having a mate pair inner distance of 0 ± 50 bp (25-26). 90-94% of the reads across all samples were successfully paired and mapped, with a mean of 22.6 million paired reads per sample. Differential expression analysis was performed with CuffDiff (v2.2.1) using the fragment bias detection and multiple read correction parameters (26-27). Sample visualization and QA/QC was performed using cummeRbund (v2.8.2) in the R statistical programming language. Multi-dimensional scaling analysis of the FPKM distribution identified an outlier in the *otoferlin a* morphant group . As a result, we repeated our differential expression analysis in CuffDiff with the outlier sample removed. P-values were adjusted with a false discovery rate (FDR) using the Benjamini-Hochberg procedure. Transcripts were considered significantly differentially expressed with a FDR corrected *p-value* ≤ 0.05 and a fold change of ≥ 1.5. Visualization of the double

morphant transcriptional profile was performed using a bi-hierarchically clustered heatmap with a custom R script. Fold-change values were calculated for each replicate by dividing the sample FPKM value by the average control FPKM value for each transcript. Sample and transcript clustering was performed using the agglomerative complete-linkage clustering algorithm based on a Euclidean distance matrix of the FPKM fold-changes.

Quantitative RT-PCR

Total RNA was extracted from control and otoferlin double morphant embryos collected at 96 hpf with RNAzol (Molecular Research Centre, OH, USA) and cDNA was synthesized using iScript cDNA synthesis kit (Bio-Rad, CA, USA). Primers for monitoring gene expression changes were designed from genomic sequences found in Ensembl and are listed under Table 3.1. Extracted RNA from four different biological replicate groups were used to validate expression changes. All qRT-PCR assays were performed in 20 µl reactions consisting of 10 µl Power SYBR Green PCR master mix (Applied Biosystems), 0.4 µl each primer, 7.2 µl H2O and 50 ng equivalents of cDNA on the StepOnePlus, Applied Biosystems machine. Relative fold change values in otoferlin double morphants compared to injected controls were calculated for genes of interest and normalized to *beta-actin*. Graphs were plotted and statistically analyzed with the Prism software version 5.0.

Whole-mount *In Situ* Hybridization.

In situ hybridization (ISH) was performed as described previously (28) with digoxygenin-labeled antisense RNA probes specific to zebrafish genes using wild-type (WT) zebrafish embryos collected at 48, 72 and 96 hpf. To synthesize the probes, gene-

specific primers (Table 3.2) with the T7-RNA polymerase promoter were designed for amplifying the probe templates, and cDNA was prepared from RNA isolated as described from whole zebrafish at 72 hpf (24). Embryos were labeled with Fast Red (29) stain. Stained embryos were imaged using the Keyence All-in-One Fluorescence Microscope, BZ-X700, (IL, USA).

Whole-mount Immunohistochemistry.

Control and morphant zebrafish embryos were collected at 96 hpf and fixed in 4% paraformaldehyde for 3-4 hours at 4° C After rinse, larvae were permeabilized with ice-cold acetone and blocked with PBS buffer containing 2% goat serum, 1% bovine serum albumin (BSA). Larvae were then incubated with primary antibodies diluted in PBS buffer containing 1% BSA for 2 hours at room temperature, followed by incubation with secondary antibodies coupled to Alexa Fluor 488, Alexa Fluor 555, Alexa Fluor 546 and Alexa Fluor 647 (Invitrogen), and mounted with ProLong Gold Antifade Reagent (Invitrogen) for confocal imaging. The following primary antibodies were used : Mouse monoclonal anti-otoferlin, Developmental Studies Hybridoma Bank, (Iowa, IA) (1:1000); Mouse monoclonal anti-ribeye, gift from Katie Kindt, National Institute of Health (NIH), (1:10,000); Mouse monoclonal K28/86 anti-MAGUK, NeuroMab, Antibodies Incorporated, (Davis, CA) (1:500) , anti-VGlut3 (from Teresa Nicolson, OHRC, Oregon Health and Science University, Portland, OR) (1:500) , mouse monoclonal anti-acetylated tubulin, Sigma Aldrich, (MO, USA) (1:4000).

Calcium imaging

Calcium imaging was performed as previously described in Kindt K.S. et al., (30) and Maeda R. et al., (31). Transgenic (Tg) *myo6b: R-GECO$_1$* zebrafish was used for the

experiment and generated as described in Maeda R. et al., (31). The *Tgmyo6b:R-GECO$_1$* fish are dim in the absence of calcium and bright when bound to calcium. The R-GECO$_1$ fluorescence change was visualized on a Zeiss Axio Examiner microscope fitted with an Orca ER CCD camera (Hamamatsu), a 63X, 1.0 N.A. Plan-Apochromat Zeiss water-immersion objective and the following filter sets: excitation, 535/50 565LP, and emission, 620/60 (Chroma). Two groups were tested for the calcium imaging experiment - control injected and otoferlin-depleted at 96 hpf. Briefly, the R-GECO1 transgenic zebrafish were anesthetized and attached to a Sylgard chamber and injected with bungarotoxin directly into the heart to suppress any movement during imaging. The larval preparation was bathed in an extracellular solution containing 140 mM Nacl, 2 mM KCl, 2 mM CaCl2, 1mM MgCl2, and 10 mM HEPES adjusted to pH 7.3 during imaging. The lateral line hair cells were stimulated using a fluid jet to deliver a square step stimulus, and data showing changes in calcium fluorescence were acquired and processed as previously described in Kindt K.S. et al., (30) and Maeda R. et al., (31). For determining the average calcium response of a single neuromast cluster, the response of each hair cell in a neuromast was measured and these individual responses were statistically analyzed.

Combined *In Situ* Hybridization and Immunofluorescence

A combined Fast Red in situ and immunofluorescence was performed as described previously (28-29). *In situ* hybridization (ISH) was performed as described previously (28) with digoxygenin-labeled antisense RNA probes specific to zebrafish genes (*s100s; rtn4rl2a; rtn4rl2b; pth2*) using control and otoferlin morphant zebrafish embryos collected at 96 hpf. Embryos were labeled with Fast Red (29) stain. Stained embryos

were washed in PBST (PBS with tween) before beginning the immunofluorescence. After rinse, larvae were blocked with PBS containing 2% goat serum, 1% bovine serum albumin (BSA) overnight at 4° C. Larvae were then incubated with primary antibodies diluted in PBS buffer containing 1% BSA for 2 hours at room temperature, followed by incubation with diluted secondary antibodies coupled to Alexa Fluor 488 (Invitrogen) flurophore. Larvae were washed with PBST, rinsed in water and mounted with ProLong Gold Antifade Reagent (Invitrogen) for confocal imaging. Please note that the control and knockdown larvae were run in same tube for a more controlled comparison of distribution of transcripts and synaptic protein.

Rescue quantitative RT-PCR.

The cDNA encoding mouse otoferlin was a gift from Christine Petit (Institut Pasteur, Paris, France). The p5E-pmyo6b vector used in cloning was a gift from Teresa Nicolson (Oregon Health and Science University, Portland, OR, USA). The p5E-pmyo6b vector contains the hair cell specific promoter for myosin VIb. Full length (FL) and C2F-TM domains of otoferlin were cloned as described previously in Chatterjee P. et al., (24). For the rescue, we used mouse full-length (FL) vector and C2F-TM constructs. These constructs were co-injected with the morpholinos. Larvae were screened as previously described in Chatterjee P. et al., (24) for rescue of the balance phenotype, acoustic startle response including rescue of un-inflated swim bladder for qRT-PCR analysis. For rescue, differentially expressed genes that match the temporal expression of otoferlin transcripts in larval zebrafish were selected.

Staining with vital dyes.

FM1-43FX dye (Life Technologies, NY, USA) labeling of neuromast hair cells was performed on live zebrafish at 120 hpf. Zebrafish larvae were immersed in 3 uM FM1-43FX dye in embryo medium and rinsed off after 6 minutes of incubation at room temperature. Both the control and KD zebrafish siblings were subjected to identical incubation conditions with the dye. The fish were washed several times with embryo medium and anaesthetized with 0.2 mg/ml tricaine solution for imaging. Stained embryos were imaged using the Keyence All-in-One Fluorescence Microscope, BZ-X700 (IL, USA).

mCLING (ATTO 488) , from Synaptic Systems (Germany) (32) was used to observe endocytosis in hair cells of zebrafish larvae. Larval zebrafish at 96 hpf were anaesthetized with tricaine and incubated in 1.7 µM of mCLING diluted in embryo medium for 6 minutes at room temperature to ensure adequate probe penetration. Both the control and KD zebrafish siblings were subjected to identical incubation conditions with the dye. The fish were washed with PBST for 5 minutes and fixed for 3-4 hours with 4% PFA at 4°C. Following fixation, fish were washed with PBST at room temperature, rinsed with water and mounted with ProLong Gold Antifade Reagent (Invitrogen) for confocal imaging.

Confocal image acquisition and analysis.

Whole-mount immunohistochemistry preparations were imaged with a confocal laser-scanning microscope Zeiss LSM 780 NLO fitted with a 63X oil-immersion objective and appropriate filters. Z-stack images of neuromasts were acquired using the lowest laser power possible to prevent photobleaching.

Maximal projections of Z-stacks of confocal images of zebrafish neuromast were created and analyzed using ImageJ software. Images containing ribeye or MAGUK immunolabeling were corrected for background; each image was analyzed using the analyze particle option, size 0.1-Infinity pixel^2 in each image for puncta count. Graphs were created and statistical analysis of the immunolabeled puncta was performed using Prism 5 (GraphPad Software).

3.4 Results

Results

Otoferlin depletion changes the basic architecture of the synaptic active zone

Zebrafish lateral line neuromast hair cells are structurally and morphologically similar to mammalian type II vestibular hair cells (33). Indeed, like mammalian hair cells, we found that zebrafish sensory hair cells possesssed apical stereociliary bundles (Figure 3.1A), otoferlin (Figure 3.1B) and afferent synapses at the basolateral region (Figure 3.1C), as determined by immunolabeling for acetylated tubulin, otoferlin, and the post-synaptic marker MAGUK. As shown in the composite image, otoferlin immunoreactivity is restricted to sensory hair cells and absent from the hair bundles and afferent neurons (Figure 3.1D). The basolateral region of hair cells are marked by pre-synaptic ribbons juxtaposed to post-synaptic densities during development, with multiple synaptic ribbons per cell (Figure 3.1E). These synaptic ribbons are electron-dense structures surrounded by multiple synaptic vesicles and are thought to play a role in synaptic transmission (34-36). Mutations in genes that directly contribute to stereocilia function, synaptic transmission, or maintenance of the pre-synaptic active zone have been linked to a ‘circler’ phenotype whereby larvae are defective in hearing and balance and fail to

develop an inflated swim bladder (37-43). Previously we have shown that the C2 domains of otoferlin both bind calcium and fuse liposomes (17) , and that depletion of otoferlin in zebrafish larvae results in a ‘circler’ phenotype 24, consistent with a role for the protein in membrane fusion and neurotransmitter release 7-8). However, otoferlin may have additional roles that extend beyond regulating exocytosis in sensory hair cells. For example, sensory hair cells in *deaf5/deaf5* otoferlin mutant mice display improper targeting of active zone components to the basolateral membrane, suggesting a role for otoferlin in the regulation of inner hair cell maturation and development (21). The effect of loss of otoferlin on synaptic ribbons and other components of the active zone are largely unknown however, as most studies have focused almost exclusively on defects in neurotransmitter release, and a complete understanding of the ‘circler’ phenotype in otoferlin deficient zebrafish has yet to be established.

To assess how the depletion of otoferlin might affect the ribbon synapse morphology in larval zebrafish, we examined immunolabeled lateral line neuromast hair cells in 96 hpf control and otoferlin-depleted zebrafish (Figure 3.2). At 96 hpf sensory hair cells of the lateral line are functionally mature with all the components necessary for effective mechanosensation and neurotransmission (33). Figure 3.2 shows the distribution of the pre-synaptic ribbon body immunolabeled with ribeye, and the afferent post-synaptic density immunolabeled with MAGUK. Relative to control, otoferlin-depleted lateral line hair cells show an atypical distribution of both ribeye and MAGUK (Figure 3.2A, 3.2B). Higher magnification images of the mutant neuromast (Figure 3.2C) reveal that ribeye puncta coalesce and form abnormally tight clusters at the pre-synapse compared to age-matched controls. MAGUK immunolabeling of otoferlin-depleted hair cells reveal an

abnormal dense loop-like pattern that closely traces ribeye clusters (Figure 3.2C). Ribeye staining colocalized with the enriched immunolabeled MAGUK (Figure 3.2C). Analyses of the average number of ribeye puncta per neuromast indicate fewer single puncta in otoferlin-depleted zebrafish compared to control (Figure 3.2D). We also found significantly less MAGUK single puncta in the otoferlin-depleted neuromasts compared to age-matched controls as well (Figure 3.2E). We did not notice any reduction in the number of hair cells per neuromast in the otoferlin-depleted larvae however, as determined by YO-PRO1.

Similar to the effects of otoferlin depletion, zebrafish CaV1.3a mutants also develop an abnormally enlarged pre-synaptic ribbon and post-synaptic density. This phenotype has been attributed to reduced calcium responses to mechanical deflection of stereocilia associated with loss of L-type voltage gated calcium channel activity (44). To determine if the phenotype linked to loss of otoferlin could be attributed to a reduced calcium response we measured calcium transients in control and otoferlin-depleted neuromasts using a transgenic line that expresses R-GECO$_1$ (red fluorescent protein- Genetically Encoded calcium indicators) in hair cells (31). R-GECO$_1$ is derived from GCaMP$_3$ and mApple, and allows detection of calcium influx in R-GECO$_1$ expressing hair cells via an increase in fluorescence when bound to calcium (45-46). When tested, robust calcium transients in hair cells expressing R-GECO$_1$ were observed in both control and otoferlin-depleted zebrafish in response to mechanical deflection of the hair bundles. No significant differences in the calcium response between control and otoferlin-depleted hair cells was detected (Figure 3.2F), indicating that otoferlin-depleted hair cells presumably have intact hair bundles and exhibit normal mechanosensation. Further, we

found that the average intracellular calcium rise was unaltered in response to reduction in otoferlin.

Another ribbon synapse component, VGlut3 has also been linked to the “circler” phenotype. VGlut3 is functionally conserved across species including mammals, and mice lacking VGlut3 are profoundly deaf due to absence of glutamate release (11). In our previous study (24) we demonstrated that VGlut3 transcript levels are unaffected in otoferlin-depleted zebrafish larvae. Given that otoferlin and VGlut3 co-localized to the hair cell ribbon synapse active zone (44, 9) we sought to determine the subcellular distribution of VGlut3 protein in otoferlin-depleted zebrafish hair cells. Immunolabeling of neuromast hair cells for VGlut3 revealed a diffuse and delocalized distribution in otoferlin-depleted hair cells, while VGlut3 in control neuromasts localized predominantly to the basolateral region of hair cells (Figure 3.2G). We then examined the combined expression and localization of the three essential synaptic components – VGlut3, ribeye and MAGUK in control and otoferlin-depleted zebrafish (Figure 3.2H). While VGlut3 was found to colocalize tightly around Ribeye containing ribbons in control hair cells (Figure 3.2H upper panels), abnormally diffuse VGlut3 depositions that poorly colocalized with Ribeye puncta were found in otoferlin-depleted hair cells (Figure 3.2H lower panels). We conclude that loss of otoferlin expression results in mistrafficking of VGlut3 and fewer but larger ribbon synapses.

Otoferlin-depleted hair cells display reduced synaptic vesicle cycling

To assess what effect depletion of otoferlin and the resulting abnormalities in ribeye and VGlut3 localization have on synaptic vesicle trafficking, we monitored vesicle cycling using two labels, mCLING and Fm1-43 dye. mCLING is a recently developed dye that

has been reported to be selectively uptaken and label recycling basolateral vesicles (32). Fm1-43 is a classical indicator used in the study of endocytosis and has been demonstrated to selectively label sensory hair cells of zebrafish although the dye may enter via apical mechanotransducer channels as well as synaptic vesicle cycling (47-48). We found that depleted neuromasts displayed severe reductions in mCLING probe uptake at the basolateral region of the cell compared to control, suggesting reduced or defective vesicle recycling at the presynaptic region (Figure 3.3 A, B). Similar results were obtained using the endocytotic vital dye Fm1-43FX, with otoferlin-depleted anterior and posterior lateral line neuromasts showing severe reductions in probe uptake compared to age-matched controls (Figure 3.3 C, D, E, F).

Otoferlin depletion alters the transcriptional profile in zebrafish

To better understand the transcriptome-wide effects of otoferlin depletion, we performed 150 bp RNA-sequencing on 96 hpf control or otoferlin-depleted zebrafish. Otoferlin depletion resulted in significant differential expression of 433 transcripts, of which 271 were decreased and 162 were increased (FDR adjusted P-value ≤ 0.05; fold change ≥ 1.5). Both otoferlin genes (*otoferlin a* and *otoferlin b*) were significantly decreased with log2 fold changes of -1.93 and -1.69, respectively, confirming the depletion of otoferlin in our transcriptome study. Figure 3.4 shows a heatmap of the transcriptional profiles of otoferlin-depleted and control zebrafish. There was a clear separation of the samples based on otoferlin status, suggesting robust transcriptional changes due to otoferlin depletion.

As we were interested in understanding downstream targets of otoferlin signaling, we examined the cluster of transcripts that were the most significantly decreased (Figure

3.4, right). Of the transcripts altered in the otoferlin-depleted larvae detected by RNAseq, we selected transcripts with the highest fold changes and validated the expression change by qRT-PCR. Analysis of the qRT-PCR results matched those of the RNAseq analysis for all transcripts tested (Figure 3.5). Of these transcripts, those of note were several which are expressed in the lateral line neuromast and otic region early in development (24, 49-51, 28, 52-54). These include several that play critical roles in morphogenesis and maturation of the lateral line and otic region (*pvalb3* - 52, *cldnb* - 53, *lama2* – 54-55, *rtn4rl2a/2b* – 56), and several that are proposed to play roles in maintenance of the mechanosensory cells of the lateral line via regulation of calcium-related signaling (*s100s* - 57, *pth2* – 58-59). Other transcripts that are significantly affected but are not found in the lateral line or otic region include *opsin*, *cacng*, several solute carrier membrane proteins (subtypes *6, 15, 22,* and *38*), and *CSAP*. *Opsin* regulates activity in photoreceptor cells, and expression follows a robust diurnal rhythm (60). *Cacng* regulates trafficking of AMPA receptors to the synaptic membrane in neurons (61). Of the SLC genes affected, SLC1*5* is responsible for proton-oligopeptide transport, *SLC22* responsible for organic cation/anion transport across membranes, *SLC38* responsible for sodium coupled neutral amino acid transport, and *SLC6* coupling transport of neurotransmitter to sodium and chloride gradients. CSAP affects neuronal development including development of reticulospinal neurons (62).

The qRT-PCR validated transcripts have been implicated in neuromast development and maintenance, and thus we next sought to characterize the temporal and spatial expression of some of these transcripts in the lateral line neuromast and otic region using *in situ* hybridization (Figure 3.6). Expression of *pth2* was found primarily in the otic

region at 48 hpf, 72 hpf and also 96 hpf and in the brain at 72 hpf (Figure 3.6A-C). Expression in the lateral line was not detected in Hogan B.M. et al., (58). By contrast, expression of *s100*s was detected in both neuromasts of the lateral line and otic regions at 72 hpf and 96 hpf (Figure 3.6D-E). Transient *s100s* expression was also detected in the brain at 96 hpf. The s100s expression pattern bore a high degree of resemblance to expression of otoferlin in the lateral line neruomast and otic region (Figure 3.6F). Figure 6G-I show localization of *rtn4rl2a* transcripts in the lateral line neuromasts and otic placode at 72 hpf and 96 hpf, with expression in the otic placode becoming greater at 96 hpf (Figure 3.6I) corresponding with maturation of the sensory cells in the otic region (33). R*tn4rl2b* transcripts were detected in the lateral line neuromasts and otic region at 72 hpf and 96 hpf, with expression in the otic placode becoming pronounced at 96 hpf (Figures 3.6J-L) corresponding with maturation of the sensory cells (33).

Characterizing the combined expression of lateral line and otic placode transcripts and ribbon synapse protein in otoferlin-depleted larvae

In principal, otoferlin depletion induced expression changes for *s100s, rtn4rl2a* and *rtn4rl2b* should correlate with the observed abnormal ribbon synapse morphology. We tested this by comparing dual immunolableing of ribeye and *in situ* hybridization of select transcripts in control and otoferlin-depleted zebrafish (Figure 3.7). When tested, we found that otoferlin-depleted hair cells display both reduced spatial labeling for *s100s* (Figures 3.7A-F) *, rtn4rl2b* (Figures 3.7G-L), and *rtn4rl2a* (Figures 3.7M-R) transcripts as well as abnormal clustering of the ribeye protein at the basolateral synapses (far right panels, Figure 3.7). Similar results were found when probing for ribeye and *pth2* in the otic region, however we note that mounting and imaging

inconsistencies precluded us from making any conclusions related to *in situ* hybridization for the *pth2* transcript level in the otic region of otoferlin-depleted zebrafish (Figure 3.S1). Overall these findings are in agreement with the conclusion that otoferlin-depleted sensory hair cells display both abnormal ribeye clustering and altered levels of *s100s*, *rtn4rl2a*, *rtn4rl2b* and *pth2* expression.

Exogenous otoferlin rescues the expression of transcripts in hair cells depleted of endogenous otoferlin

In our previous study (24) we demonstrated that co-injection of otoferlin-depleted embryos with a *p5E-pmyo6b* vector construct containing either full length or truncated versions of mouse otoferlin rescued gross phenotypic abnormalities in otoferlin morphants. If the observed changes in gene expression are indeed directly associated with loss of otoferlin, then co-injection of otoferlin morphants with exogenous otoferlin should restore expression of these genes. We therefore conducted qRT-PCR on the lateral line and otic placode transcripts *rtn4rl2a, rtn4rl2b, pth2 and s100s* with otoferlin morphants co-injected with a *p5E-pmyo6b* vector construct containing full length otoferlin (Rescue-FL construct) to determine if expression of exogenous otoferlin rescued repressed transcripts. Relative to otoferlin depletion, co-injected rescue zebrafish displayed increased levels of expression for all tested transcripts (Figure 3.8A). Overall these results support the conclusion that otoferlin is directly linked with gene expression levels associated with zebrafish neuromast development and embryogenesis. On the contrary, co-injection of otoferlin-depleted larvae with a truncated construct containing only the last C2 domain and the transmembrane domain (Rescue-C2F) failed to rescue the levels of the same transcripts (Figure 3.8B). This

indicates that even though other domains of otoferlin are not essential to rescue gross otoferlin-loss of functions (24), they may still be involved in affecting levels of transcripts that are necessary for more intricate cellular maintenance and functions.

3.5 Discussion

Sensory hair cell synapses differ from their neural counterparts both in their activity and molecular composition (63). Currently an outstanding challenge is in determining the molecular basis for the formation of hair cell ribbon synapses and the interdependence of the molecular components for information encoding. We examined the essential ribbon synapse protein otoferlin to understand how the loss of a hair cell specific protein effects the sensory cells and the organism as a whole.

Otoferlin-depleted hair cells have fewer but larger synaptic ribbons as well as mistrafficked VGlut3 **(Figure 3.2A-C and 3.2G-H).** Both studies on VGLut3 knockout mice and loss of function mutants in zebrafish have concluded that VGlut3 function is not required for normal synaptic ribbon formation 43-44). It is therefore unlikely that the observed mislocalization of VGlut3 release is the cause of the observed ribbon abnormalities. While no strong link between VGlut3 and ribbon synapse formation has been found, dependence for calcium influx for ribbon formation and maintenance has been documented (44). Mutations in CaV1.3 or acute blocking of L-type calcium channels have been reported to lead to an increase in the size and number of double ribbons (44). While calcium influx through CaV1.3 appears to be required for proper ribbon morphology, our R-GECO$_1$ imaging measurements did not reveal any calcium influx deficiencies, suggesting normal CaV1.3 activity **(Figure 3.2F).** However analysis of the RNAseq data revealed that loss of otoferlin results in lower levels of the EF-hand

proteins parvalbumin 3 and s100s, which act as calcium homeostasis and buffering proteins **(Figures 3.4 and 3.5)** (64, 52, 50, 57). We therefore speculate that downstream targets of calcium influx, including otoferlin, parvalbumin, and s100 account for the calcium sensitivity of the synaptic ribbon. We note that we found that parathyroid hormone pth2, which is also associated with calcium signaling, was downregulated in otoferlin-depleted hair cells as well **(Figures 3.4 and 3.5)** (58-59).

Analysis of RNAseq data also indicate that loss of otoferlin changes the expression pattern of Nogo-A *(rtn4rl2a, 2b*) and CSAP (**Figures 3.4 and 3.5**), genes associated with neuronal growth and wiring. Nogo-A belongs to the neurite outgrowth inhibitory family of signaling proteins (65), and CSAP (centriole and spindle–associated protein). Abnormal levels of CSAP have been linked to reductions in the density of Mauthner interneurons (62), which reside downstream of VIIIth nerve afferents and play essential roles in hearing and startle reflex in zebrafish (66). We speculate that the reduced number of transcripts in neuromasts may represent an attempt to compensate for loss of signaling between the hair cell and afferent neuron. Since expression of these genes are essential for neural development and circuit formation, these results provide a possible explanation for why restoration of expression of otoferlin upon loss of morpholino potency does not restore hearing and balance in zebrafish. The abnormal expression of neuronal genes may also provide a molecular basis for a recent study that reported a considerable reduction of auditory nerve and ventral cochlear nuclei size in otoferlin knockout mice (67). Altered transcript levels of neurotransmitter membrane transporters and Cacng, which regulates trafficking of AMPA receptor trafficking, were

also detected and support a role for otoferlin in modulating neural synaptic strength and maintenance **(Figure 3.5)** (61).

3.6 Acknowledgements: This work was supported by funds from Oregon State University and NIH NIDCD K99/R00, NIH NIDCD RO1, Medical Research Foundation (MRF) award. We thank Prof. Teresa Nicolson for providing us with the *p5E- pmyo6b* vector and the anti-VGlut3 antibody, Prof. Christine Petit for providing us with mouse otoferlin cDNA, Carrie Barton for help with fish maintenance and embryo collection, Gloria Garcia for help with *in situ* hybridization, Christopher Sullivan for help with RNA seq data analysis, Rachael Kuintzle for providing suggestion on transcriptome data analysis, Jane LaDu for help with imaging and general lab stuff, Ananda S. Roy for help with statistics.

3.7 References

1. **Hudspeth AJ.** 1997. How hearing happens. Neuron **19:**947-950.

2. **Hudspeth AJ.** 2000. Hearing and deafness. Neurobiology of disease **7:**511-514.

3. **Hudspeth AJ.** 1985. The cellular basis of hearing: the biophysics of hair cells. Science **230:**745-752.

4. **Khimich D, Nouvian R, Pujol R, Tom Dieck S, Egner A, Gundelfinger ED, Moser T.** 2005. Hair cell synaptic ribbons are essential for synchronous auditory signalling. Nature **434:**889-894.

5. **Beurg M, Michalski N, Safieddine S, Bouleau Y, Schneggenburger R, Chapman ER, Petit C, Dulon D.** 2010. Control of exocytosis by synaptotagmins and otoferlin in auditory hair cells. The Journal of neuroscience : the official journal of the Society for Neuroscience **30:**13281-13290.

6. **Brandt A, Khimich D, Moser T.** 2005. Few CaV1.3 channels regulate the exocytosis of a synaptic vesicle at the hair cell ribbon synapse. The Journal of neuroscience : the official journal of the Society for Neuroscience **25:**11577-11585.

7. **Dulon D, Safieddine S, Jones SM, Petit C.** 2009. Otoferlin is critical for a highly sensitive and linear calcium-dependent exocytosis at vestibular hair cell ribbon synapses. The Journal of neuroscience **29:**10474-10487.

8. **Roux I, Safieddine S, Nouvian R, Grati M, Simmler MC, Bahloul A, Perfettini I, Le Gall M, Rostaing P, Hamard G, Triller A, Avan P, Moser T, Petit C.** 2006. Otoferlin, defective in a human deafness form, is essential for exocytosis at the auditory ribbon synapse. Cell **127:**277-289.

9. **Pangrsic T, Lasarow L, Reuter K, Takago H, Schwander M, Riedel D, Frank T, Tarantino LM, Bailey JS, Strenzke N, Brose N, Muller U, Reisinger E, Moser T.** 2010. Hearing requires otoferlin-dependent efficient replenishment of synaptic vesicles in hair cells. Nature neuroscience **13:**869-876.

10. **Ruel J, Emery S, Nouvian R, Bersot T, Amilhon B, Van Rybroek JM, Rebillard G, Lenoir M, Eybalin M, Delprat B, Sivakumaran TA, Giros B, El Mestikawy S, Moser T, Smith RJ, Lesperance MM, Puel JL.** 2008. Impairment of SLC17A8 encoding vesicular glutamate transporter-3, VGLUT3, underlies nonsyndromic deafness DFNA25 and inner hair cell dysfunction in null mice. American journal of human genetics **83:**278-292.

11. **Seal RP, Akil O, Yi E, Weber CM, Grant L, Yoo J, Clause A, Kandler K, Noebels JL, Glowatzki E, Lustig LR, Edwards RH.** 2008. Sensorineural deafness and seizures in mice lacking vesicular glutamate transporter 3. Neuron **57:**263-275.

12. **Zenisek D, Davila V, Wan L, Almers W.** 2003. Imaging calcium entry sites and ribbon structures in two presynaptic cells. The Journal of neuroscience **23:**2538-2548.

13. **Sheets L, Hagen MW, Nicolson T.** 2014. Characterization of Ribeye subunits in zebrafish hair cells reveals that exogenous Ribeye B-domain and CtBP1 localize to the basal ends of synaptic ribbons. PloS one **9:**e107256.

14. **Yasunaga S, Grati M, Cohen-Salmon M, El-Amraoui A, Mustapha M, Salem N, El-Zir E, Loiselet J, Petit C.** 1999. A mutation in OTOF, encoding otoferlin, a FER-1-like protein, causes DFNB9, a nonsyndromic form of deafness. Nature genetics **21:**363-369.

15. **Yasunaga S, Grati M, Chardenoux S, Smith TN, Friedman TB, Lalwani AK, Wilcox ER, Petit C.** 2000. OTOF encodes multiple long and short isoforms: genetic evidence that the long ones underlie recessive deafness DFNB9. American journal of human genetics **67:**591-600.

16. **Johnson CP, Chapman ER.** 2010. Otoferlin is a calcium sensor that directly regulates SNARE-mediated membrane fusion. The Journal of cell biology **191:**187-197.

17. **Padmanarayana M, Hams N, Speight LC, Petersson EJ, Mehl RA, Johnson CP.** 2014. Characterization of the lipid binding properties of Otoferlin reveals specific interactions between PI(4,5)P2 and the C2C and C2F domains. Biochemistry **53:**5023-5033.

18. **Ramakrishnan NA, Drescher MJ, Drescher DG.** 2009. Direct interaction of otoferlin with syntaxin 1A, SNAP-25, and the L-type voltage-gated calcium channel Cav1.3. The Journal of biological chemistry **284:**1364-1372.

19. **Vogl C, Cooper BH, Neef J, Wojcik SM, Reim K, Reisinger E, Brose N, Rhee JS, Moser T, Wichmann C.** 2015. Unconventional molecular regulation of synaptic vesicle replenishment in cochlear inner hair cells. Journal of cell science **128:**638-644.

20. **Duncker SV, Franz C, Kuhn S, Schulte U, Campanelli D, Brandt N, Hirt B, Fakler B, Blin N, Ruth P, Engel J, Marcotti W, Zimmermann U, Knipper M.** 2013. Otoferlin couples to clathrin-mediated endocytosis in mature cochlear inner hair cells. The Journal of neuroscience **33:**9508-9519.

21. **Heidrych P, Zimmermann U, Kuhn S, Franz C, Engel J, Duncker SV, Hirt B, Pusch CM, Ruth P, Pfister M, Marcotti W, Blin N, Knipper M.** 2009. Otoferlin interacts with myosin VI: implications for maintenance of the basolateral synaptic structure of the inner hair cell. Human molecular genetics **18:**2779-2790.

22. **Schug N, Braig C, Zimmermann U, Engel J, Winter H, Ruth P, Blin N, Pfister M, Kalbacher H, Knipper M.** 2006. Differential expression of otoferlin in brain, vestibular system, immature and mature cochlea of the rat. The European journal of neuroscience **24:**3372-3380.

23. **Westerfield M**. 2000. The zebrafish book. A guide for the laboratory use of zebrafish (Danio rerio). 4th ed., Univ. of Oregon Press, Eugene.

24. **Chatterjee P, Padmanarayana M, Abdullah N, Holman CL, LaDu J, Tanguay RL, Johnson CP.** 2015. Otoferlin deficiency in zebrafish results in defects in balance and hearing: rescue of the balance and hearing phenotype with full-length and truncated forms of mouse otoferlin. Molecular and cellular biology **35:**1043-1054.

25. **Trapnell C, Pachter L, Salzberg SL.** 2009. TopHat: discovering splice junctions with RNA-Seq. Bioinformatics **25:**1105-1111.

26. **Trapnell C, Hendrickson DG, Sauvageau M, Goff L, Rinn JL, Pachter L.** 2013. Differential analysis of gene regulation at transcript resolution with RNA-seq. Nature biotechnology **31:**46-53.

27. **Roberts A, Trapnell C, Donaghey J, Rinn JL, Pachter L.** 2011. Improving RNA-Seq expression estimates by correcting for fragment bias. Genome biology **12:**R22.

28. **Thisse C, Thisse B.** 2008. High-resolution in situ hybridization to whole-mount zebrafish embryos. Nature protocols **3:**59-69.

29. **Novak AE, Ribera AB.** 2003. Immunocytochemistry as a tool for zebrafish developmental neurobiology. Methods in cell science **25:**79-83.

30. **Kindt KS, Finch G, Nicolson T.** 2012. Kinocilia mediate mechanosensitivity in developing zebrafish hair cells. Developmental cell **23:**329-341.

31. **Maeda R, Kindt KS, Mo W, Morgan CP, Erickson T, Zhao H, Clemens-Grisham R, Barr-Gillespie PG, Nicolson T.** 2014. Tip-link protein protocadherin 15 interacts with transmembrane channel-like proteins TMC1 and TMC2. Proceedings of the National Academy of Sciences of the United States of America **111:**12907-12912.

32. **Revelo NH, Kamin D, Truckenbrodt S, Wong AB, Reuter-Jessen K, Reisinger E, Moser T, Rizzoli SO.** 2014. A new probe for super-resolution imaging of membranes elucidates trafficking pathways. The Journal of cell biology **205:**591-606.

33. **Nicolson T.** 2005. The genetics of hearing and balance in zebrafish. Annual review of genetics **39:**9-22.

34. **Matthews G, Fuchs P.** 2010. The diverse roles of ribbon synapses in sensory neurotransmission. Nature reviews. Neuroscience **11:**812-822.

35. **Moser T, Brandt A, Lysakowski A.** 2006. Hair cell ribbon synapses. Cell and tissue research **326:**347-359.

36. **Nouvian R, Beutner D, Parsons TD, Moser T.** 2006. Structure and function of the hair cell ribbon synapse. The Journal of membrane biology **209:**153-165.

37. **Ernest S, Rauch GJ, Haffter P, Geisler R, Petit C, Nicolson T.** 2000. Mariner is defective in myosin VIIA: a zebrafish model for human hereditary deafness. Human molecular genetics **9:**2189-2196.

38. **Sollner C, Rauch GJ, Siemens J, Geisler R, Schuster SC, Muller U, Nicolson T.** 2004. Mutations in cadherin 23 affect tip links in zebrafish sensory hair cells. Nature **428:**955-959.

39. **Kappler JA, Starr CJ, Chan DK, Kollmar R, Hudspeth AJ.** 2004. A nonsense mutation in the gene encoding a zebrafish myosin VI isoform causes defects in hair-cell mechanotransduction. Proceedings of the National Academy of Sciences of the United States of America **101:**13056-13061.

40. **Clemens Grisham R, Kindt K, Finger-Baier K, Schmid B, Nicolson T.** 2013. Mutations in ap1b1 cause mistargeting of the Na(+)/K(+)-ATPase pump in sensory hair cells. PloS one **8:**e60866.

41. **Seiler C, Ben-David O, Sidi S, Hendrich O, Rusch A, Burnside B, Avraham KB, Nicolson T.** 2004. Myosin VI is required for structural integrity of the apical surface of sensory hair cells in zebrafish. Developmental biology **272:**328-338.

42. **Sidi S, Busch-Nentwich E, Friedrich R, Schoenberger U, Nicolson T.** 2004. gemini encodes a zebrafish L-type calcium channel that localizes at sensory hair cell ribbon synapses. The Journal of neuroscience **24:**4213-4223.

43. **Obholzer N, Wolfson S, Trapani JG, Mo W, Nechiporuk A, Busch-Nentwich E, Seiler C, Sidi S, Sollner C, Duncan RN, Boehland A, Nicolson T.** 2008. Vesicular glutamate transporter 3 is required for synaptic transmission in zebrafish hair cells. The Journal of neuroscience **28:**2110-2118.

44. **Sheets L, Kindt KS, Nicolson T.** 2012. Presynaptic CaV1.3 channels regulate synaptic ribbon size and are required for synaptic maintenance in sensory hair cells. The Journal of neuroscience **32:**17273-17286.

45. **Tewson P, Westenberg M, Zhao Y, Campbell RE, Quinn AM, Hughes TE.** 2012. Simultaneous detection of Ca2+ and diacylglycerol signaling in living cells. PloS one **7:**e42791.

46. **Zhao Y, Araki S, Wu J, Teramoto T, Chang YF, Nakano M, Abdelfattah AS, Fujiwara M, Ishihara T, Nagai T, Campbell RE.** 2011. An expanded palette of genetically encoded Ca(2)(+) indicators. Science **333:**1888-1891.

47. **Seiler C, Nicolson T.** 1999. Defective calmodulin-dependent rapid apical endocytosis in zebrafish sensory hair cell mutants. Journal of neurobiology **41:**424-434.

48. **Gale JE, Marcotti W, Kennedy HJ, Kros CJ, Richardson GP.** 2001. FM1-43 dye behaves as a permeant blocker of the hair-cell mechanotransducer channel. The Journal of neuroscience : the official journal of the Society for Neuroscience **21:**7013-7025.

49. **Erickson T, Nicolson T.** 2015. Identification of sensory hair-cell transcripts by thiouracil-tagging in zebrafish. BMC genomics **16:**842.

50. **Kraemer AM, Saraiva LR, Korsching SI.** 2008. Structural and functional diversification in the teleost S100 family of calcium-binding proteins. BMC evolutionary biology **8:**48.

51. **Han HW, Chou CM, Chu CY, Cheng CH, Yang CH, Hung CC, Hwang PP, Lee SJ, Liao YF, Huang CJ.** 2014. The Nogo-C2/Nogo receptor complex regulates the morphogenesis of zebrafish lateral line primordium through modulating the expression of dkk1b, a Wnt signal inhibitor. PloS one **9:**e86345.

52. **Hsiao CD, Tsai WY, Tsai HJ.** 2002. Isolation and expression of two zebrafish homologues of parvalbumin genes related to chicken CPV3 and mammalian oncomodulin. Mechanisms of development **119 Suppl 1:**S161-166.

53. **Froehlicher M, Liedtke A, Groh K, Lopez-Schier H, Neuhauss SC, Segner H, Eggen RI.** 2009. Estrogen receptor subtype beta2 is involved in neuromast

development in zebrafish (Danio rerio) larvae. Developmental biology **330:**32-43.

54. Sztal T, Berger S, Currie PD, Hall TE. 2011. Characterization of the laminin gene family and evolution in zebrafish. Developmental dynamics **240:**422-431.

55. Petersen SC, Luo R, Liebscher I, Giera S, Jeong SJ, Mogha A, Ghidinelli M, Feltri ML, Schoneberg T, Piao X, Monk KR. 2015. The adhesion GPCR GPR126 has distinct, domain-dependent functions in Schwann cell development mediated by interaction with laminin-211. Neuron **85:**755-769.

56. Han HW, Chou CM, Chu CY, Cheng CH, Yang CH, Hung CC, Hwang PP, Lee SJ, Liao YF, Huang CJ. 2014. The Nogo-C2/Nogo receptor complex regulates the morphogenesis of zebrafish lateral line primordium through modulating the expression of dkk1b, a Wnt signal inhibitor. PloS one **9:**e86345.

57. Germana A, Paruta S, Germana GP, Ochoa-Erena FJ, Montalbano G, Cobo J, Vega JA. 2007. Differential distribution of S100 protein and calretinin in mechanosensory and chemosensory cells of adult zebrafish (Danio rerio). Brain research **1162:**48-55.

58. Hogan BM, Danks JA, Layton JE, Hall NE, Heath JK, Lieschke GJ. 2005. Duplicate zebrafish pth genes are expressed along the lateral line and in the central nervous system during embryogenesis. Endocrinology **146:**547-551.

59. Bhattacharya P, Yan YL, Postlethwait J, Rubin DA. 2011. Evolution of the vertebrate pth2 (tip39) gene family and the regulation of PTH type 2 receptor (pth2r) and its endogenous ligand pth2 by hedgehog signaling in zebrafish development. The Journal of endocrinology **211:**187-200.

60. Matos-Cruz V, Blasic J, Nickle B, Robinson PR, Hattar S, Halpern ME. 2011. Unexpected diversity and photoperiod dependence of the zebrafish melanopsin system. PloS one **6:**e25111.

61. Price MG, Davis CF, Deng F, Burgess DL. 2005. The alpha-amino-3-hydroxyl-5-methyl-4-isoxazolepropionate receptor trafficking regulator "stargazin" is related to the claudin family of proteins by Its ability to mediate cell-cell adhesion. The Journal of biological chemistry **280:**19711-19720.

62. Backer CB, Gutzman JH, Pearson CG, Cheeseman IM. 2012. CSAP localizes to polyglutamylated microtubules and promotes proper cilia function and zebrafish development. Mol Biol Cell **23:**2122-2130.

63. **Pangrsic T, Reisinger E, Moser T.** 2012. Otoferlin: a multi-C2 domain protein essential for hearing. Trends in neurosciences **35:**671-680.

64. **Pack AK, Slepecky NB.** 1995. Cytoskeletal and calcium-binding proteins in the mammalian organ of Corti: cell type-specific proteins displaying longitudinal and radial gradients. Hearing research **91:**119-135.

65. **Sepe M, Lignitto L, Porpora M, Delle Donne R, Rinaldi L, Belgianni G, Colucci G, Cuomo O, Viggiano D, Scorziello A, Garbi C, Annunziato L, Feliciello A.** 2014. Proteolytic control of neurite outgrowth inhibitor NOGO-A by the cAMP/PKA pathway. Proceedings of the National Academy of Sciences of the United States of America **111:**15729-15734.

66. **Burgess HA, Granato M.** 2007. Sensorimotor gating in larval zebrafish. The Journal of neuroscience **27:**4984-4994.

67. **Wright S, Hwang Y, Oertel D.** 2014. Synaptic transmission between end bulbs of Held and bushy cells in the cochlear nucleus of mice with a mutation in Otoferlin. Journal of neurophysiology **112:**3173-3188.

Figure 3.1

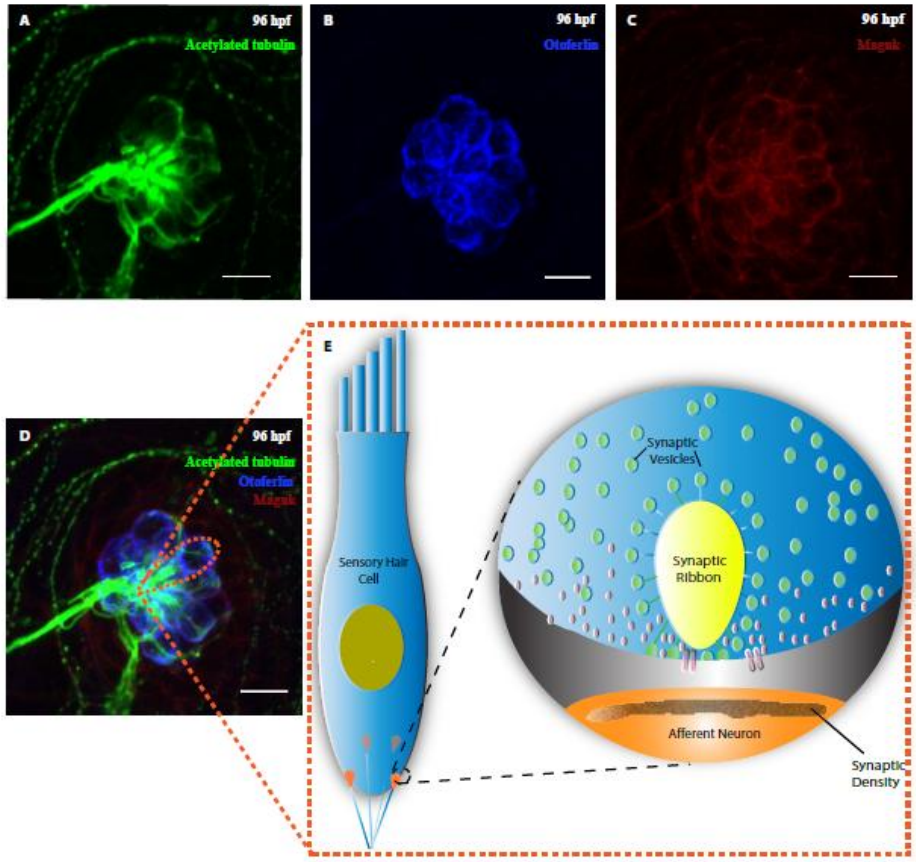

Images illustrating the anatomical and molecular structure of a sensory hair cell from larval zebrafish posterior lateral line neuromast. **(A-D)** Representative maximum confocal z-projection immunofluorescence images of neuromast hair cells in 96 hpf wild type zebrafish larvae. **(A)** Acetylated tubulin (green) labeling the apical end of the hair cells and the abutting afferent neurons. **(B)** Anti-HCS1 (blue) labeling showing diffused otoferlin distribution in the hair cells of the neuromast. **(C)** MAGUK (red) labeling the post synaptic density. **(D)** Composite image for A-C labeling. Orange dotted line shows an individual hair cell in the neuromast cluster **(E)** Schematic of an individual lateral line hair cell with the apical stereocilia and basolateral afferent

neurons. Dotted black circle indicates the area between the sensory hair cell pre (blue) and post synapse (orange). A closer look at the cross-section of the dotted area shows the molecular structure of the active zone of a hair cell synapse as indicated by the presence of a presynaptic ribbon body (yellow), synaptic vesicles (green), calcium channels and calcium ions at the active zone (purple) and the post-synaptic density (brown).

Figure 3.2

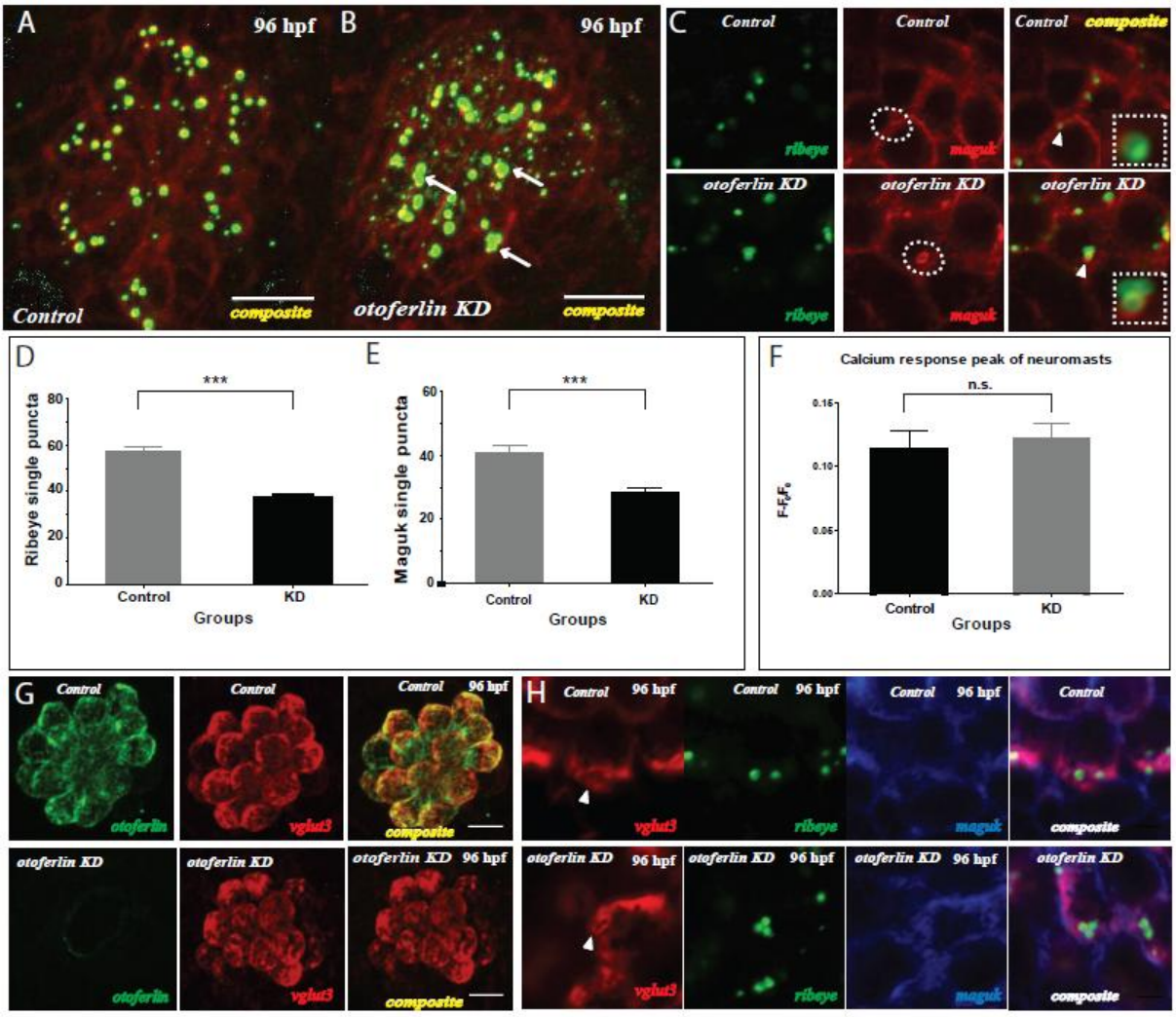

Effects of otoferlin depletion on synaptic morphology and calcium response in posterior lateral line neuromasts of 96 hpf zebrafish larvae. (A-C) Representative confocal z-projection images showing distribution of ribeye (green) and MAGUK (red) in neuromast hair cells, **(A)** Composite image of ribeye and MAGUK punctae per neuromast in control and **(B)** otoferlin-depleted larvae. White arrow indicates tight clustering of multiple ribeye punctae in the otoferlin-depleted neuromast. **(C)** High magnification image of the ribeye and MAGUK puncta including a composite in control

neuromast (upper panel); lower panel shows high magnification image of ribeye and MAGUK puncta in morphant neuromast. White dotted circles in upper and lower panels indicates a difference in the formation of the post synapse between control and morphnats White arrowhead indicates juxtaposition of the ribeye and MAGUK punctae. **(D)** Average number of single ribeye puncta per neuromast in control (grey bar, number of neuromasts = 20) and otoferlin-depleted larvae (black bar, number of neuromasts = 24) and **(E)** Average number of single MAGUK puncta per neuromast in control (grey bar, number of neuromasts = 20) and otoferlin-depleted larvae (black bar, number of neuromasts = 24). (Wilcoxon's test, *p-value < 0.0001 (for Ribeye) and p-value <0.0001 (for MAGUK),* Error bars indicate s.e.m.). **(F)** Average calcium response per neuromast in control and otoferlin-depletedlarvae. Number of neuromast for control = 10, number of neuromast for KD = 8 (Wilcoxon's test, p-value = 0.6). Error bars indicate s.e.m. **(G)** VGlut3 distribution in control and otoferlin-depleted larvae. Representative confocal z-projections of otoferlin (green), vglut3 (red) and composite (yellow) immunolabel in control neuromast hair cells (*upper panel*) and otoferlin-depleted neuromast hair cells (*lower panel*). **(H)** Representative confocal image of the distribution of vglut3 (red), ribeye (green) and MAGUK (blue) immunolabel in control (upper panel) and otoferlin-depleted(lower panel) larvae. White arrowhead indicates the distribution of vglut3 in control and morphant larvae.

Figure 3.3

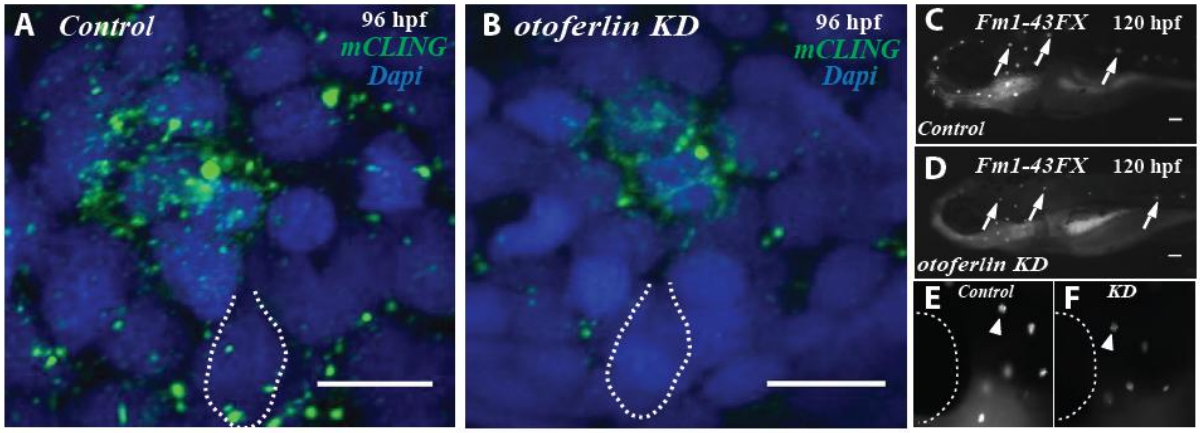

Depletion of otoferlin results in reduced hair cell vesicle cycling. (A-B) Representative confocal z-projections showing mCLING dye uptake after 6 minutes of incubation at room temperature (RT) in control **(A)** and otoferlin-depleted **(B)** larvae at 96 hpf. Dotted area outlines a representative single hair cell of the neuromast. **(C-D)** Uptake of Fm1-43FX dye in control **(C)** and otoferlin-depleted **(D)** larvae at 120 hpf after 6 minutes of incubation at RT. Arrows indicate dye uptake in anterior and posterior lateral line neuromasts **(E-F)** Representative high magnification images of Fm1-43FX dye uptake in control **(E)** and otoferlin-depleted **(F)** larvae at 120 hpf, dotted line indicates the eye region. Arrowheads indicates uptake of the dye in a single neuromast cluster.

Figure 3.4

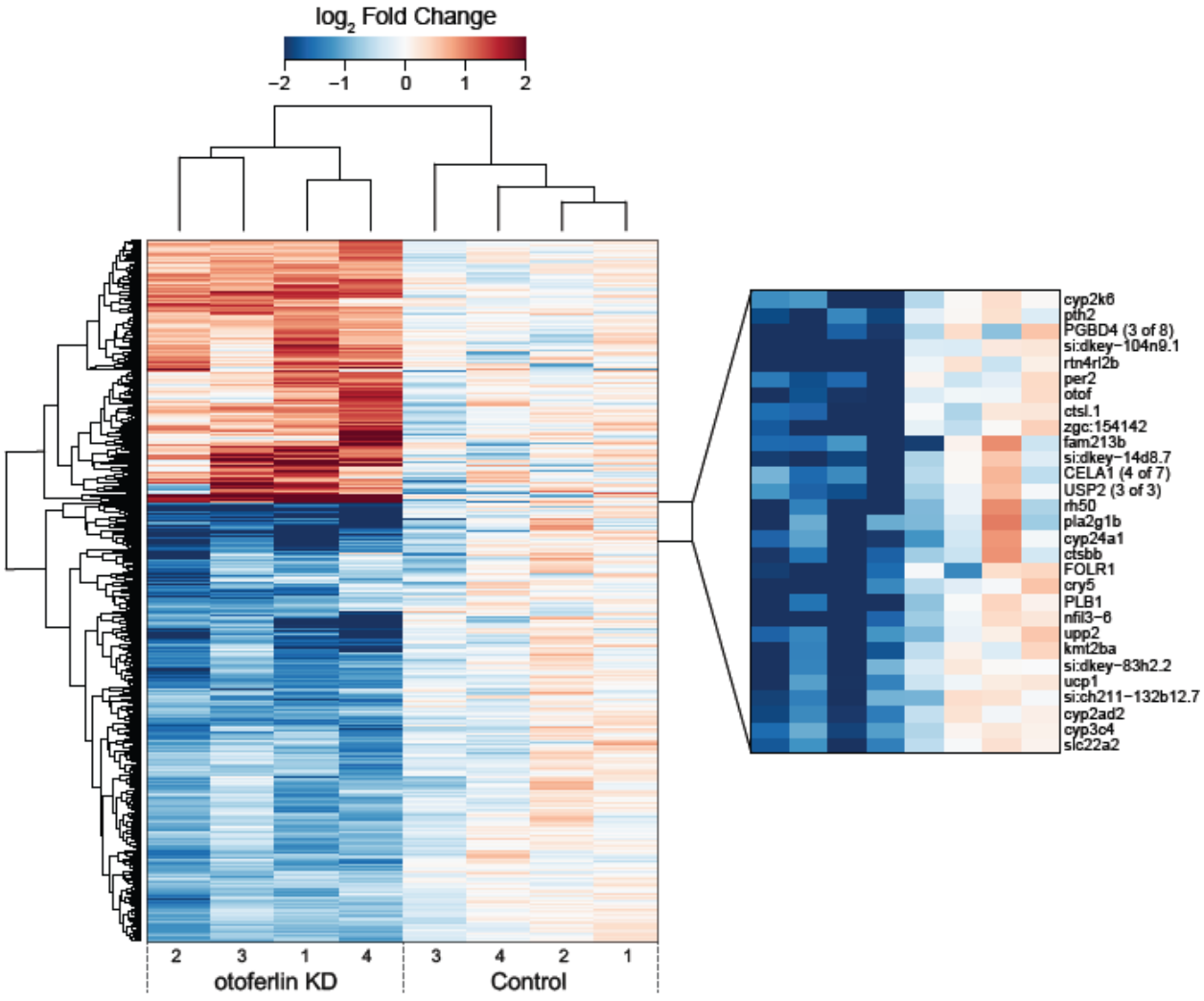

Bi-hierarchically clustered heatmap – Heatmap of the 433 significantly differentially expressed transcripts in otoferlin-depleted larvae (FDR adjusted P-value ≤ 0.05; fold change ≥ 1.5). The inset on the right highlights the cluster of the most highly decreased transcripts.

Figure 3.5

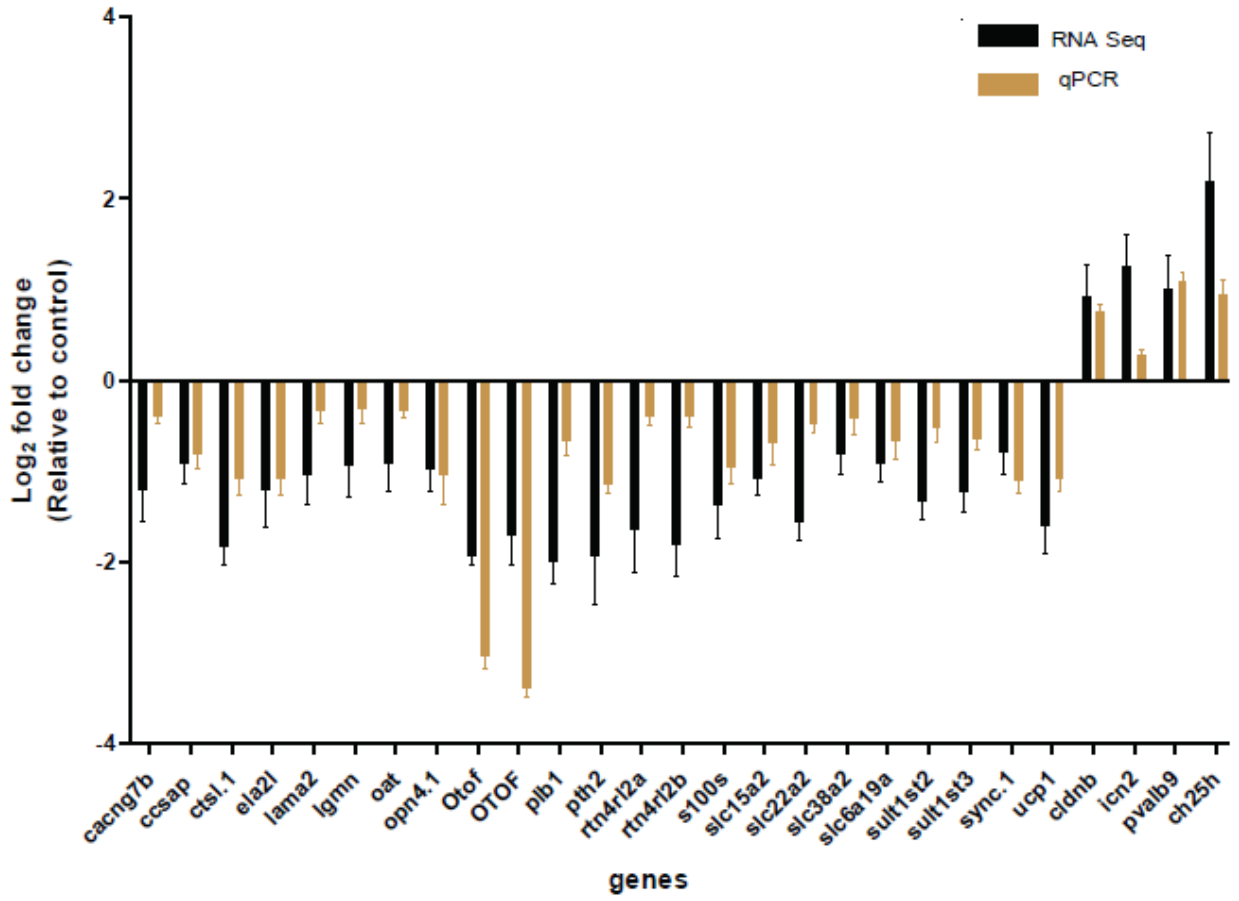

Comparison of RNA sequencing and qRT–PCR for differentially expressed genes in otoferlin-depleted larvae. Black bar graphs represents relative mRNA expression changes of the upregulated and downregulated genes derived from transcriptomic analysis (number of biological replicates = 4, each replicate consists of 15 pooled embryos). **Brown bars** represent qRT– PCR data of mRNA expression changes of genes in larval otoferlin mutant zebrafish at 96 hpf (number of biological replicates = 4, each replicate consists of 30 pooled embryos). Each gene is normalized with respect to the corresponding controls. qRT–PCR, ΔΔCt values were calculated by comparing ΔCt

values (normalized to beta-actin) to the mean ΔCt for each gene. Data were analyzed by Wilcoxon's test with standard 5% significance level. Error bars are s.e.m. *Abbreviations – cacng7*: *Calcium Voltage-Gated Channel Auxiliary Subunit Gamma 7, ccsap: Centriole, Cilia and Spindle Associated Protein, ctsl.1: CathepsinL.1, ela2l: Elastase 2, lama2: Laminin α2, lgmn: Legumain, oat: Ornithine Aminotransferase, opn4.1*: *Opsin4.1, Otof: Otoferlin a, OTOF: Otoferlin b, plb1: Phospholipase B1, pth2: Parathyroid Hormone 2, rtn4rl2a: Reticulon 4 Receptor like 2a, rtn4rl2b: Reticulon 4 Receptor like 2b, s100s: S100 Calcium Binding Protein S, slc15a2: Solute Carrier Family 15 (oligopeptide transporter) Member 2, slc22a2: Solute Carrier Family 22 (organic cation transporter), Member 2, slc38a2: Solute Carrier Family 38, Member 2, slc6a19a: Solute Carrier Family 6 (neutral amino acid transporter), Member 19a, sult1st2: Sulfotransferase Family 1, Cytosolic Sulfotransferase 2, sult1st3: Sulfotransferase Family 1, Cytosolic Sulfotransferase 3, sync.1: Syncoilin, Intermediate Filament 1, UCP1: Uncoupling Protein 1, cldnb: Claudin b, icn2: Ictacalcin 2, pvalb9: Parvalbumin 9, ch25h: cholesterol 25-hydroxylase*

Figure 3.6

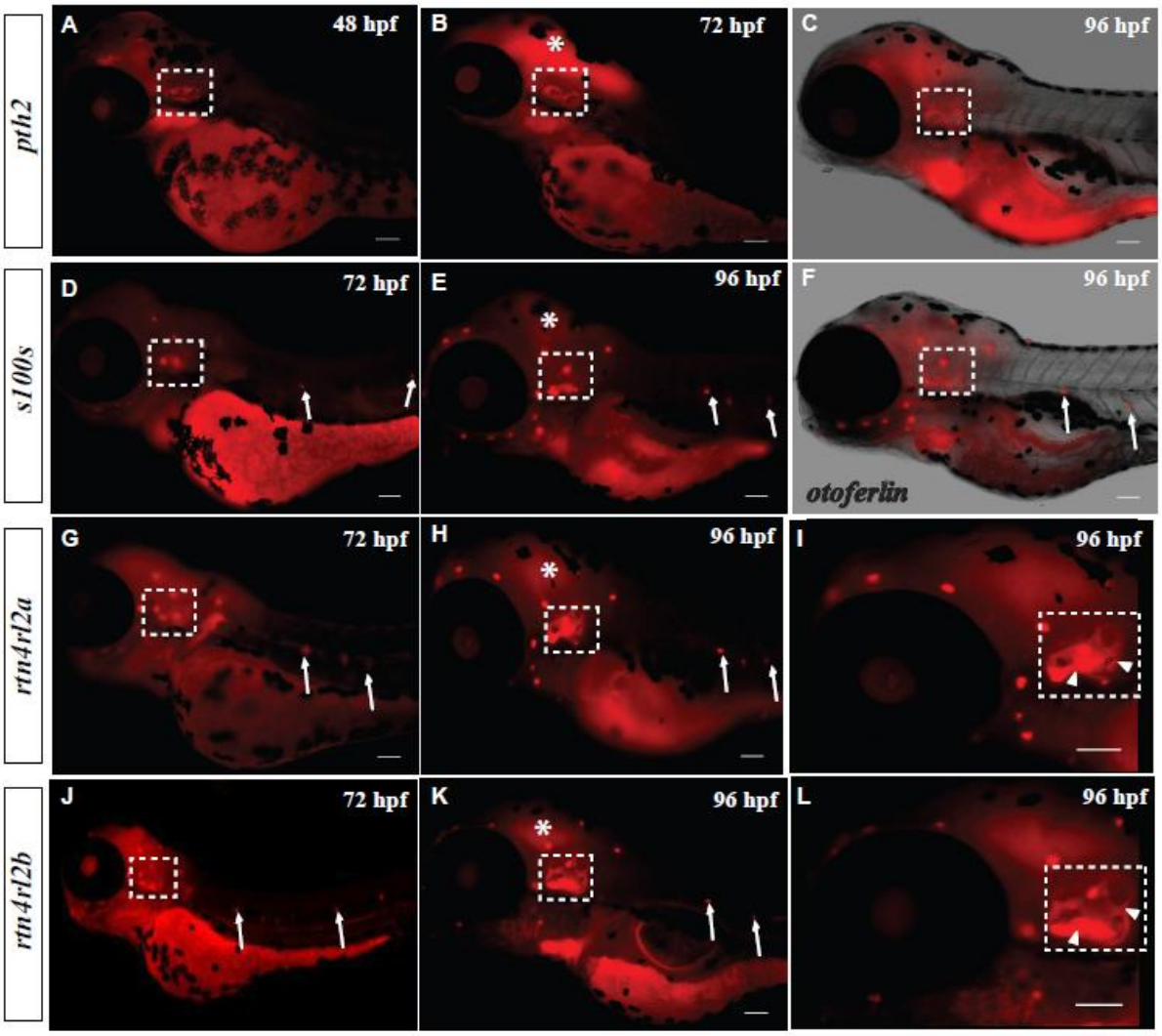

Representative fast red *in situ* hybridization images showing spatial expression of neuromast and otic region specific transcripts in developing zebrafish. (A-C) *pth2* expression at 48 hpf **(A)**, 72 hpf **(B)** and 96 hpf **(C)** larval zebrafish. **(D-E)** *s100s* expression at 72 hpf **(D)** and 96 hpf **(E)** larval zebrafish. **(F)** *otoferlin* expression at 96 hpf larval zebrafish. **(G-I)** *rtn4rl2a* expression at 72 hpf **(G)** and 96 hpf **(H)** larval zebrafish, **(I)** High magnification images showing *rtn4rl2a* expression in the semicircular canal folds of the otic region indicated by arrowheads. **(J-K)** *rtn4rl2b* expression at 72

hpf **(J)** and 96 hpf **(K)** larval zebrafish. **(L)** Specific localization of *rtn4rl2b* transcripts to the semicircular canal folds of the otic region indicated by arrowheads. Dotted box indicates otic region. Arrows indicate the lateral line neuromasts. Asterisk indicates expression in the brain.

Figure 3.7

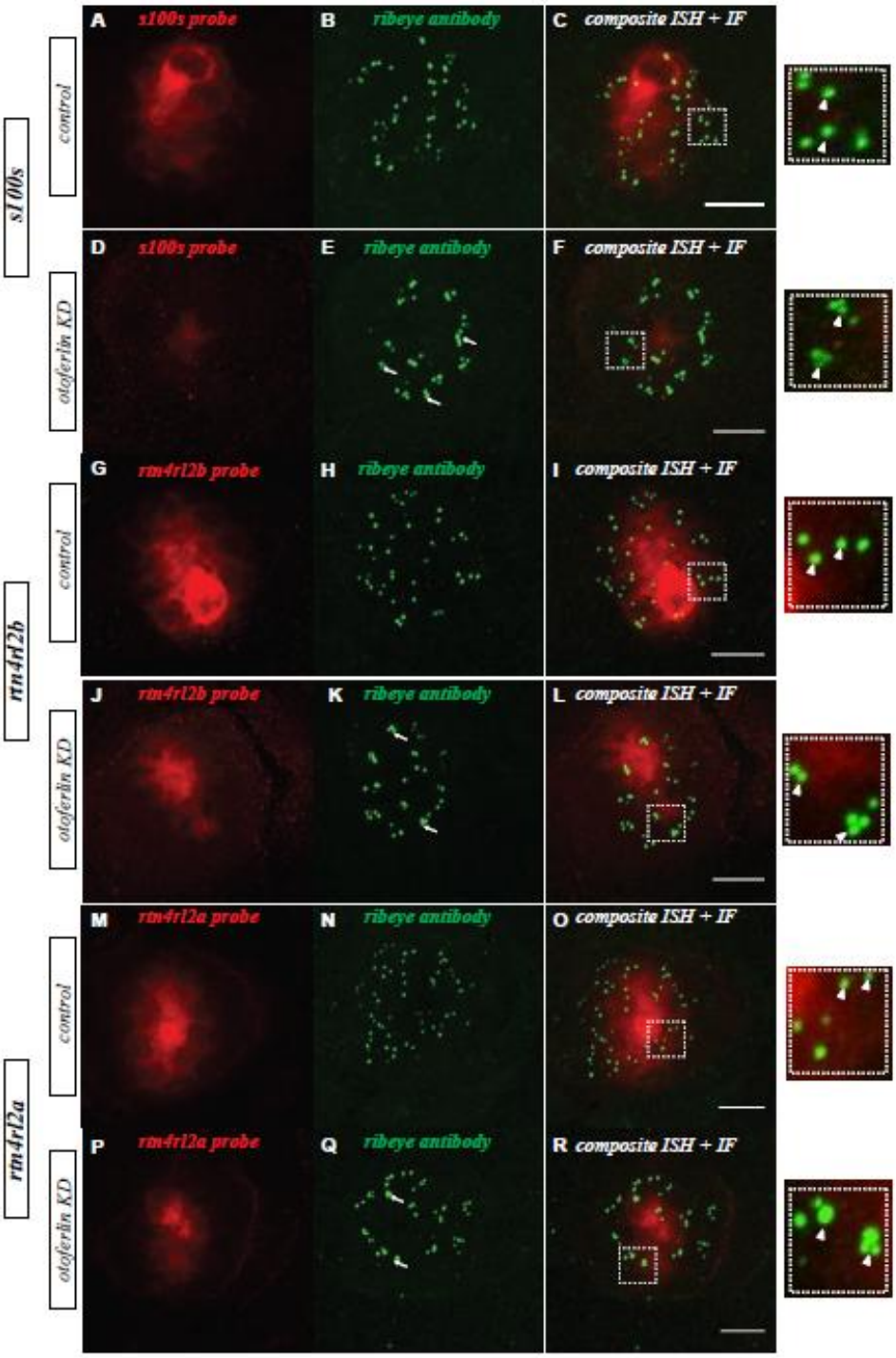

Combined *in situ* hybridization and immunofluorescence images showing reduced gene expression and ribeye clustering in 96 hpf otoferlin-depleted

zebrafish. (A-C) Representative confocal z-projections of *s100s in situ* probe (red) **(A)**, ribeye immunolabel (green) **(B)** and a composite image **(C)** of a control lateral line neuromast. The dotted box is a high magnification image showing single ribeye puncta distribution in the control. **(D-F)** Representative confocal z-projections of *s100s in situ* probe (red) **(D)**, ribeye immunolabel (green) **(E)** and composite image **(F)** of a otoferlin-depleted lateral line neuromast. The dotted box is a high magnification image showing clustered ribeye distribution in the morphant. **(G-I)** Representative confocal z-projections of *rtn4rl2b in situ* probe (red) **(G)**, ribeye immunolabel (green) **(H)** and a composite image **(I)** of a control lateral line neuromast. The dotted box is a high magnification image showing single ribeye puncta distribution in the control. **(J-L)** Representative confocal z-projections of *rtn4rl2b in situ* probe (red) **(J)**, ribeye immunolabel (green) **(K)** and a composite image **(L)** of a otoferlin-depleted lateral line neuromast. The dotted box is a high magnification image showing clustered ribeye distribution in the KD. **(M-O)** Representative confocal z-projections of *s100s in situ* probe (red) **(M)**, ribeye immunolabel (green) **(N)** and a composite image **(O)** of a control lateral line neuromast. The dotted box in the far right panel is a high magnification image showing single ribeye puncta distribution in the control. **(P-R)** Representative confocal z-projections of *rtn4rl2b in situ* probe (red) **(P)**, ribeye immunolabel (green) **(Q)** and a composite image **(R)** of a otoferlin-depleted lateral line neuromast. The dotted box is a high magnification image showing clustered ribeye distribution in the KD.

Figure 3.8

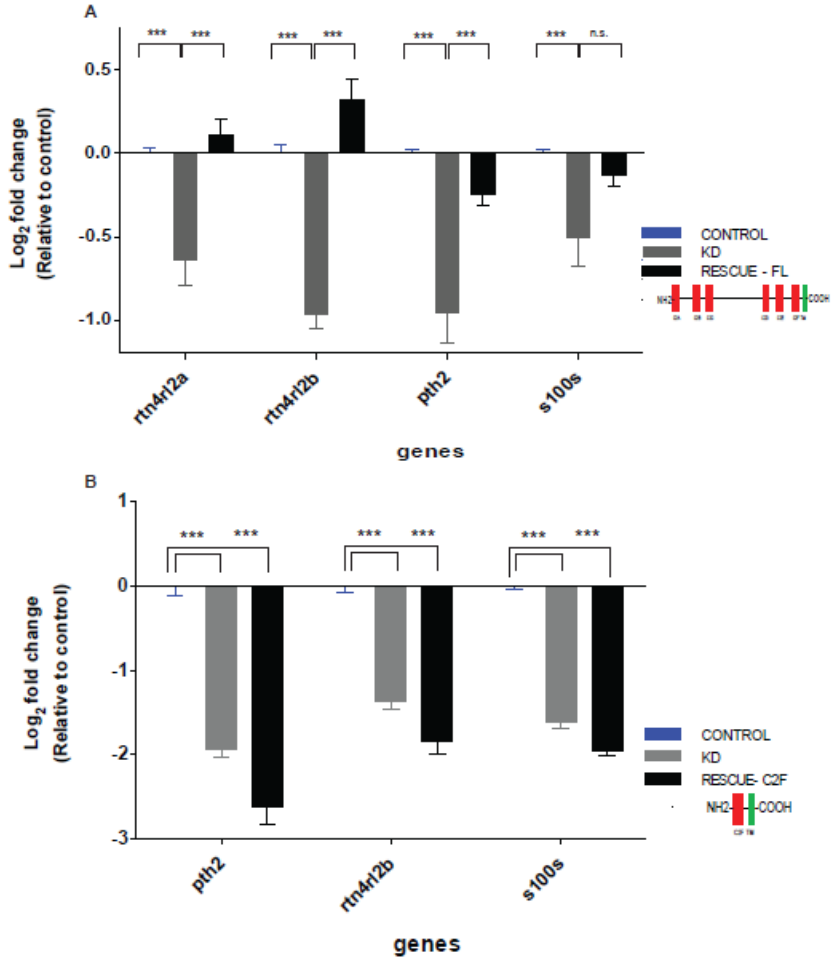

Rescue of repressed transcripts in otoferlin-depleted larvae. Bar graphs represent relative mRNA expression changes of transcripts in otoferlin-depleted larvae at 96 hpf (grey bars) and rescue of the transcripts (black bars) in morphants coinjected with rescue constructs RESCUE-FL or full length otoferlin rescue contruct, or RESCUE-C2F with the last C2 domain and transmembrane domain consctruct; number of biological replicates = 4, each replicate consists of 30 pooled embryos. Each gene is normalized with respect to the corresponding controls (blue bars). ΔΔCt values were calculated by comparing ΔCt values (normalized to beta-actin) to the mean ΔCt for each gene. Data

were analyzed by Wilcoxon's test. **(A)** For *pth2*, *rtn4rl2a* and *rtn4rl2b* groups both otoferlin-depleted and rescue samples (RESCUE-FL) showed statistically significant changes in expression (p-value < 0.05). For *s100s* significant repression in expression for the KD were found (p-value < 0.05), and there was partial restoration of repressed transcripts in the rescue larvae (p-value = 0.3). Error bars are s.e.m. **(B)** For *pth2*, *rtn4rl2a rtn4rl2b* and *s100s* groups otoferlin-depleted samples showed statistically significant changes in expression (p-value < 0.05). However, RESCUE-C2F construct does not significantly rescue *pth2*, *rtn4rl2a* and *rtn4rl2b and s100s* transcripts.

Figure 3.S1

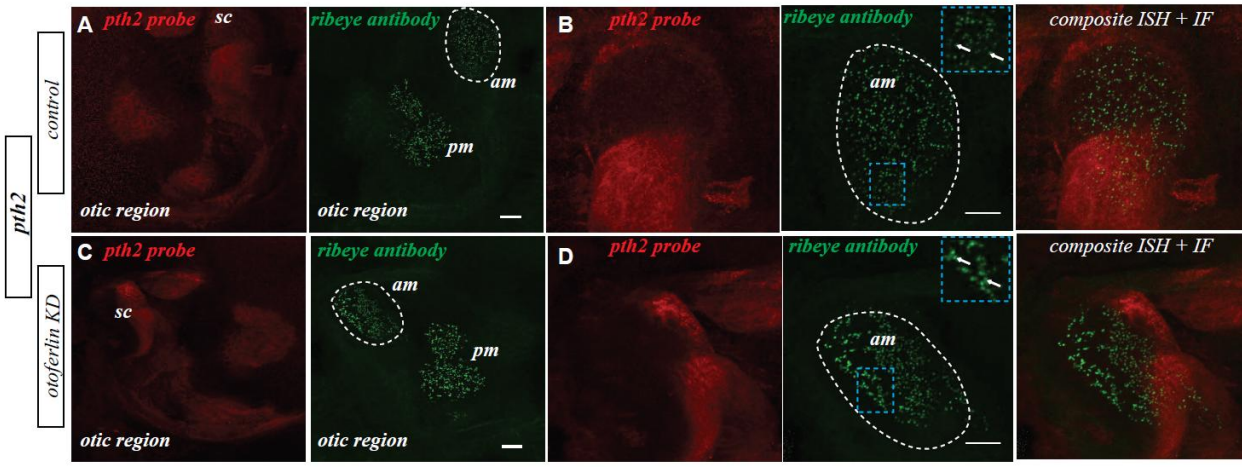

Combined *in situ* hybridization (ISH) and immunofluorescence (IF) images showing *pth2* gene expression and ribeye clustering in 96 hpf otoferlin-depleted zebrafish. (A) Representative confocal z-projections of *pth2 in situ* probe (red), ribeye immunolabel (green). Dotted circle represents the anterior macula (*am*) , **(B)** Enlargement of the dotted circle from (A) showing distribution of the pth2 probe and the ribeye immunolabel in the *am*. Dotted box is a high magnification image and arrow shows the single ribeye puncta in the control *am* region. **(C)** Representative confocal z-projections of *pth2 in situ* probe (red), ribeye immunolabel (green). Dotted circle represents the *am*, **(D)** Enlargement of the dotted circle showing distribution of the pth2 probe and the ribeye immunolabel in the *am*. Dotted box is a high magnification image and arrow shows the single ribeye puncta in the otoferlin-depleted *am* region. *pm* – posterior macula, *sc* – semicircular canal.

Table 3.1 - Primer list of genes for qRT- PCR

Gene ID	Gene Name	Forward primer sequence	Reverse primer sequence
ENSDARG00000070624	*cacng7b*	CCA GCG ACA TCT CCA TCC AAC T	GCA GCT GGT ATC CAG TTC CTG A
ENSDARG00000036773	*s100s*	GGA GAA CTG AGG GAA CTT CTG AC	CCG TCG TTA TTG GAG TCC AGA
ENSDARG00000045886	*slc38a2*	CCT GTC AGA TCA TCA CTT GGG	GGT GTT GGC CAT AGC ATA AGA C
ENSDARG00000018621	*slc6a19a*	GCT GAT CGC TGT GGT TTA CGT	GCT GAT CTG CCA GAA AAT GTT GGG
ENSDARG00000030530	*slc22a2*	CTC TTG CTT TTG TGG CTG G	GCT GTT GAC TCT GCT GAG GGT TT
ENSDARG00000007553	*opn4.1*	CCA TCA CTC TTC ATG GAG AGG	GGC ACA TGG AGC AAC TTG TAG T
ENSDARG00000099390	*lama2*	GGG TGG CCC GAA TAA AGA CAA	CGT CCT TGT GTT TCC ACT C
ENSDARG00000096445	*PLB1*	CCA GTT GAT GAG ATC TCT GTG TGC C	GGT CAC TTG ACA GTC CAC GCC AAA
ENSDARG00000025325	*CCSAP (1 of 2)*	CCA AGC GCC ATC TGT TTA CCT T	CGC TTG GTC ACC ATA TTG ACT TGT CG
ENSDARG00000056765	*ela2l*	GGC TTC CCA CTT TCC CTC CTA TT	GGT ACC AGT TGC TTC CAC TT
ENSDARG00000090469	*sync.1*	GGTCTGATTGCTCTTCTCCTGGTGG	GCT GCT GTG CTC AAA CAT CT
ENSDARG00000003902	*ctsl.1*	CCC CAT ATC TGT TGC CAT AGA TGC	GCC AGA ACA CCG TGA TCT A
ENSDARG00000023151	*ucp1*	CCT ACA GGC AGA TCT TCC AGC TT	CGT GAT GTT CGG CAG AGT T
ENSDARG00000018361	*sult1st3*	GGA CTT CAA GAT CTC GCC CTT	GCG GAA CTT GAC AGT GGT GTT
ENSDARG00000041540	*sult1st2*	CCACTCTCCCTGTCATGGACTTCAA	GCC ACA GTG AAG TGA TTT CTC C
ENSDARG00000045190	*ch25h*	CCT GCC TGC TTC TGT TTG ACT T	GCA CCT TAT GGA AAG TCC GGT A
ENSDARG00000071601	*pvalb9*	GCT GTC AAA GAC TGC CAA G	GCT CAG CCT CCT CGA TAA ATC CA
ENSDARG00000022951	*pth2*	CCA CAC ACT GGA AAC AAA GAG C	CGA GGA GGC AAG GAT AAA GCC AT
ENSDARG00000039150	*lgmn*	CGG TCC GAA TGA TCA TGT GT	GGT ATC CAT CAG GTC GTC AAC A
ENSDARG00000078425	*oat*	GCC TTC TAC AAC GAC ATC CTG	GGC CTC ATA TTT AGG GAT GCC CTT
ENSDARG00000037495	*rtn4rl2b*	CCA GCG TGT CTT CTT GCA GAA	GCA CCT GCT TCG ATC CAT GTG AT
ENSDARG00000052012	*rtn4rl2a*	GCA GAA CAA CCG CAT TAC TGA ACT G	CGC AAC TCA CTG AAT GCA C
ENSDARG00000032010	*slc15a2*	GGTGCGTGTCTGCAAATGTATC	CCCTGCACACCATTTTAATCTCC
ENSDARG00000009544	*cldnb*	CCA TGT GGA AAG TCA CAG CCT T	CCA GCC ATC GAC AGC ATG ATT
ENSDARG00000055514	*icn2*	CCC AGA AAG CAA TGG CTA TGC TCA	GCC ATC AGC ATT TGC ATC CAG A
ENSDARG00000030832	*Otof*	GGACTGTTTACACACAACCTGAACATCAGT	CCCTCTATGTCATCCTCGTCTGCT
ENSDARG00000020581	*OTOF*	GAG GAC GAT GAC ATT TTC ACT GGA G	CGA TTC AGG TCC AAT TCG ATC GCA C
ENSDARG00000037870	*Beta-Actin*	AAGCAGGAGTACGATGAGTC	TGGAGTCCTCAGATGCATTG

Table 3.2 - Primer list of genes for *in situ* hybridization.

Transcript ID	Gene name	Primer	Sequence
ENSDART00000142955	*s100s*	Forward primer	GTG TGA TGT GAT GTC CAA AGA GCC AAG CAC CAA C
		T7-with reverse complement	TAATACGACTCACTATAGGG-CTA CTC TTT CTT CTC GTC TCC ACC G
ENSDART00000033691	*pth2*	Forward primer	GTA ACT TGC CTG CAA TTG GTC AAG AAG ACT CC
		T7-with reverse complement	TAATACGACTCACTATAGGG-CCA TTG CTG TCA ACA GCT TAC TCT TCT CTC TAA ACG C
ENSDART00000054598	*rtn4rl2b*	Forward primer	GAT CGA CTG CTT CTG CAT GAC AAC CGC ATT CG
		T7-with reverse complement	TAA TAC GAC TCA CTA TAG GG- TAA GGC AGC CTC CTC TGC TGT GAG AT
ENSDART00000073736	*rtn4rl2a*	Forward primer	AAC TGC CCG CAC CGG TGT GTG TGT TAT C
		T7-with reverse complement	TAA TAC GAC TCA CTA TAG GG-ATC AGG TCG GCG AAG AGA TCA TCC TG
ENSDARG00000020581	*Otoferlin*	Forward primer	ATGGACTAAAGAAACAGACGGATGAGCATTTAG
		T7-with reverse complement	TAATACGACTCACTATAGGG-TCAAACGCTGCAGAGAGAAGCTTCT

Chapter 4 – General conclusions and future directions

Paroma Chatterjee and Colin P. Johnson

4.1 General Conclusions and Future Directions

Otoferlin is a DFNB9 gene that was identified almost two decades ago and mutations in otoferlin are known to cause non-syndromic hearing loss in children (1,2). Otoferlin is expressed mostly in cochlear hair cells, vestibular hair cells and brain (3,4). In the sensory hair cells of the cochlea, otoferlin is diffusedly distributed in the supranuclear region and also localized to the presynaptic terminal. Given its structural and biochemical similarities with the conventional neuronal calcium sensor synaptotagmin 1, (2) and also due to localization at the presynaptic terminal, it was proposed that otoferlin acts as a calcium sensor and is required for exocytosis at hair cell synapses (3,4). Infact, some studies have demonstrated that otoferlin deficient sensory and vestibular hair cells exhibit dramatically reduced calcium dependent exocytotic responses (3, 5, 6). Even though synaptotagmin 1 is suggested to be the structural and biochemical equivalent of otoferlin, expression of synaptotagmin 1 in cochlear hair cells of otoferlin mutants does not rescue neurotransmitter release, indicating that otoferlin and synaptotagmin are not functionally equivalent (7). The initial description of a role for otoferlin was in calcium-triggered exocytosis, more recent research has identified novel functions for this protein in endocytosis (8, 9) and hair cell maturation (10). Furthermore, other studies have demonstrated that exocytosis can proceed unaffected in immature hair cells lacking otoferlin, thus questioning the indispensible role of this protein in calcium triggered exocytosis (11). Moreover, studies on otoferlin-depleted neuronal cells have found that this protein helps in regulation of GABAergic activity (12) and also regulates the size of auditory neurons (13). With all these roles for the protein emerging, it is becoming increasingly important to characterize contributions of the protein by

focusing on aspects that extends beyond exocytosis. However, otoferlin research is currently limited by the availability of an easy-to-use and genetically tractable animal model whose hair cells are easy to access. With this goal in mind we, for the first time, used zebrafish as a model organism to study otoferlin (14). Zebrafish is genetically easily manipulable and has the lateral line organ system containing clusters of easily accessible hair cells called neuromasts. We found that otoferlin is conserved in zebrafish and expressed early in development (Figures 2.1 and 2.2). However, due to the genome-wide duplication event in zebrafish, zebrafish otoferlin is paralogous (Figure 2.1). There is a shorter gene which lacks the C2A N-terminal domain but possess the other five C2 domains including the transmembrane domain. We named this gene *otoferlin b*. The other gene with all the C2 domains and the transmembrane domain was called *otoferlin a* (Figure 2.1). Otoferlin a mRNA and protein is strictly expressed in the otic region and otoferlin b is expressed at both the otic region and neuromast hair cells (Figures 2.2 and 2.5). However, in the otic region the otoferlin genes found are in separate sensory patches of hair cells (Figure 2.5). Cross expression studies show no down or up regulation of one gene when we knock down the other (Figure 2.4). Zebrafish depleted of one gene did not show any gross phenotypic hearing or balance abnormalities (Figures 2.6 and 2.8). However, zebrafish depleted of both, fall under category of zebrafish motility mutants, known as circler mutants (15). These fish exhibit defective swimming behavior and fail to develop an inflated swim bladder. Moreover they show a severely reduced startle response, which is based on a behavioral assay that monitors the response of zebrafish to a loud auditory stimulus. This reiterates that otoferlin is conserved across species including zebrafish. Otoferlin-depleted zebrafish

also exhibit balance defects and develop a curved spine which enhances the circular phenotype (Figures 2.6 and 2.8). Some of the other genes that show a similar circler phenotype are myosin VI (16) and VGlut3 (17). The phenotypic abnormalities associated with otoferlin depletion can be rescued with truncated versions of mouse otoferlin indicating the possibility of trans-species rescue and also giving us a sense of otoferlin domains sufficient to rescue gross functions (Figure 2.8). A closer look at the sensory hair cells of otoferlin-depleted zebrafish neuromasts reveals an atypical synaptic architecture compared to control siblings. The presynaptic ribbon body forms tightly coalesced bundles that induce the deposition of abnormally dense post-synaptic deposits. The synaptic vesicles are diffused and delocalized. There is a significantly reduced number of single pre-synaptic ribbon punctae and post-synaptic density (Figure 3.2). However, hair cell mechanosensation is intact as determined by calcium imaging (Figure 3.2). Transcriptomic analysis of otoferlin-depleted larvae identified several significantly affected transcripts (Figures 3.4 and 3.5) some of which are very specific to the neuromast and otic region (14, 18, 19, 20, 21, 22, 23, 24). Most of these transcripts are responsible for calcium handling and homeostasis (25, 26, 27), neuronal development, including formation of the mauthner circuit that mediates the startle reflex (28), morphogenesis and maturation of the lateral line and otic region (22, 23, 29, 20); and trafficking of post synaptic receptors in neurons (30). Some of these transcripts can be rescued by coinjection of otoferlin morphants with the mouse rescue constructs, which indicates a direct correlation between otoferlin levels and the effected transcripts (Figure 3.8). These data suggest that loss of otoferlin disrupts the synaptic architecture and also affects expression of other genes that mediate the process of hair cell

development, maturation and maintenance. Future studies will focus on finding detailed molecular relations between effected transcripts and otoferlin.

Now that we've successfully established zebrafish as a facile model organism to study otoferlin, this has opened new horizons in the field of otoferlin research. Additionally this has bridged the gap between the lack of a genetically tractable animal model with accessible sensory cells and otofelin research. Future research goals will focus on generating stable zebrafish *otoferlin a* and *otoferlin b* mutants, and characterizing the effects of individual and double knockout using super-resolution and electron microscopic techniques and also using the knockout zebrafish for high throughput micro-RNA analysis. Another goal is to generate otoferlin point mutants, to phenocopy human pathogenic otoferlin mutations. Also, we want to develop methods to generate rescue constructs with a reporter gene to specifically look at neuromast hair cell expressing the construct and perform electrophysiology studies on the rescued hair cells.

4.2 References

1) **Yasunaga S, Grati M, Cohen-Salmon M, El-Amraoui A, Mustapha M, Salem N, El-Zir E, Loiselet J, Petit C.** 1999. A mutation in OTOF, encoding otoferlin, a FER-1-like protein, causes DFNB9, a nonsyndromic form of deafness. Nature genetics **21:**363-369.

2) **Yasunaga S, Grati M, Chardenoux S, Smith TN, Friedman TB, Lalwani AK, Wilcox ER, Petit C.** 2000. OTOF encodes multiple long and short isoforms: genetic evidence that the long ones underlie recessive deafness DFNB9. American journal of human genetics **67:**591-600.

3) **Roux I, Safieddine S, Nouvian R, Grati M, Simmler MC, Bahloul A, Perfettini I, Le Gall M, Rostaing P, Hamard G, Triller A, Avan P, Moser T, Petit C.** 2006. Otoferlin, defective in a human deafness form, is essential for exocytosis at the auditory ribbon synapse. Cell **127:**277-289.

4) **Schug N, Braig C, Zimmermann U, Engel J, Winter H, Ruth P, Blin N, Pfister M, Kalbacher H, Knipper M.** 2006. Differential expression of otoferlin in brain, vestibular system, immature and mature cochlea of the rat. The European journal of neuroscience **24:**3372-3380.

5) **Dulon D, Safieddine S, Jones SM, Petit C.** 2009. Otoferlin is critical for a highly sensitive and linear calcium-dependent exocytosis at vestibular hair cell ribbon synapses. The Journal of neuroscience : the official journal of the Society for Neuroscience **29:**10474-10487.

6) **Pangrsic T, Lasarow L, Reuter K, Takago H, Schwander M, Riedel D, Frank T, Tarantino LM, Bailey JS, Strenzke N, Brose N, Muller U, Reisinger E, Moser T.** 2010. Hearing requires otoferlin-dependent efficient replenishment of synaptic vesicles in hair cells. Nature neuroscience **13:**869-876.

7) **Reisinger E, Bresee C, Neef J, Nair R, Reuter K, Bulankina A, Nouvian R, Koch M, Buckers J, Kastrup L, Roux I, Petit C, Hell SW, Brose N, Rhee JS, Kugler S, Brigande JV, Moser T.** 2011. Probing the functional equivalence of otoferlin and synaptotagmin 1 in exocytosis. The Journal of neuroscience : the official journal of the Society for Neuroscience **31:**4886-4895.

8) **Duncker SV, Franz C, Kuhn S, Schulte U, Campanelli D, Brandt N, Hirt B, Fakler B, Blin N, Ruth P, Engel J, Marcotti W, Zimmermann U, Knipper M.** 2013. Otoferlin couples to clathrin-mediated endocytosis in mature cochlear inner hair cells. The Journal of neuroscience : the official journal of the Society for Neuroscience **33:**9508-9519.

9) **Jung S, Maritzen T, Wichmann C, Jing Z, Neef A, Revelo NH, Al-Moyed H, Meese S, Wojcik SM, Panou I, Bulut H, Schu P, Ficner R, Reisinger E,**

Rizzoli SO, Neef J, Strenzke N, Haucke V, Moser T. 2015. Disruption of adaptor protein 2mu (AP-2mu) in cochlear hair cells impairs vesicle reloading of synaptic release sites and hearing. The EMBO journal **34:**2686-2702.

10) **Heidrych P, Zimmermann U, Kuhn S, Franz C, Engel J, Duncker SV, Hirt B, Pusch CM, Ruth P, Pfister M, Marcotti W, Blin N, Knipper M.** 2009. Otoferlin interacts with myosin VI: implications for maintenance of the basolateral synaptic structure of the inner hair cell. Human molecular genetics **18:**2779-2790.

11) **Brandt N, Kuhn S, Munkner S, Braig C, Winter H, Blin N, Vonthein R, Knipper M, Engel J.** 2007. Thyroid hormone deficiency affects postnatal spiking activity and expression of Ca2+ and K+ channels in rodent inner hair cells. The Journal of neuroscience : the official journal of the Society for Neuroscience **27:**3174-3186.

12) **Wu W, Rahman MN, Guo J, Roy N, Xue L, Cahill CM, Zhang S, Jia Z.** 2015. Function coupling of otoferlin with GAD65 acts to modulate GABAergic activity. Journal of molecular cell biology **7:**168-179.

13) **Wright S, Hwang Y, Oertel D.** 2014. Synaptic transmission between end bulbs of Held and bushy cells in the cochlear nucleus of mice with a mutation in Otoferlin. Journal of neurophysiology **112:**3173-3188.

14) **Chatterjee P, Padmanarayana M, Abdullah N, Holman CL, LaDu J, Tanguay RL, Johnson CP.** 2015. Otoferlin deficiency in zebrafish results in defects in balance and hearing: rescue of the balance and hearing phenotype with full-length and truncated forms of mouse otoferlin. Molecular and cellular biology **35:**1043-1054.

15) **Nicolson T, Rusch A, Friedrich RW, Granato M, Ruppersberg JP, Nusslein-Volhard C.** 1998. Genetic analysis of vertebrate sensory hair cell mechanosensation: the zebrafish circler mutants. Neuron **20:**271-283.

16) **Kappler JA, Starr CJ, Chan DK, Kollmar R, Hudspeth AJ.** 2004. A nonsense mutation in the gene encoding a zebrafish myosin VI isoform causes defects in hair-cell mechanotransduction. Proceedings of the National Academy of Sciences of the United States of America **101:**13056-13061.

17) **Obholzer N, Wolfson S, Trapani JG, Mo W, Nechiporuk A, Busch-Nentwich E, Seiler C, Sidi S, Sollner C, Duncan RN, Boehland A, Nicolson T.** 2008. Vesicular glutamate transporter 3 is required for synaptic transmission in zebrafish hair cells. The Journal of neuroscience : the official journal of the Society for Neuroscience **28:**2110-2118.

18) **Erickson T, Nicolson T.** 2015. Identification of sensory hair-cell transcripts by thiouracil-tagging in zebrafish. BMC genomics **16:**842.

19) **Kraemer AM, Saraiva LR, Korsching SI.** 2008. Structural and functional diversification in the teleost S100 family of calcium-binding proteins. BMC evolutionary biology **8:**48.

20) **Han HW, Chou CM, Chu CY, Cheng CH, Yang CH, Hung CC, Hwang PP, Lee SJ, Liao YF, Huang CJ.** 2014. The Nogo-C2/Nogo receptor complex regulates the morphogenesis of zebrafish lateral line primordium through modulating the expression of dkk1b, a Wnt signal inhibitor. PloS one **9:**e86345.

21) **Thisse C, Thisse B.** 2008. High-resolution in situ hybridization to whole-mount zebrafish embryos. Nature protocols **3:**59-69.

22) **Hsiao CD, Tsai WY, Tsai HJ.** 2002. Isolation and expression of two zebrafish homologues of parvalbumin genes related to chicken CPV3 and mammalian oncomodulin. Mechanisms of development **119 Suppl 1:**S161-166.

23) **Froehlicher M, Liedtke A, Groh K, Lopez-Schier H, Neuhauss SC, Segner H, Eggen RI.** 2009. Estrogen receptor subtype beta2 is involved in neuromast development in zebrafish (Danio rerio) larvae. Developmental biology **330:**32-43.

24) **Sztal T, Berger S, Currie PD, Hall TE.** 2011. Characterization of the laminin gene family and evolution in zebrafish. Developmental dynamics : an official publication of the American Association of Anatomists **240:**422-431.

25) **Germana A, Paruta S, Germana GP, Ochoa-Erena FJ, Montalbano G, Cobo J, Vega JA.** 2007. Differential distribution of S100 protein and calretinin in mechanosensory and chemosensory cells of adult zebrafish (Danio rerio). Brain research **1162:**48-55.

26) **Hogan BM, Danks JA, Layton JE, Hall NE, Heath JK, Lieschke GJ.** 2005. Duplicate zebrafish pth genes are expressed along the lateral line and in the central nervous system during embryogenesis. Endocrinology **146:**547-551.

27) **Bhattacharya P, Yan YL, Postlethwait J, Rubin DA.** 2011. Evolution of the vertebrate pth2 (tip39) gene family and the regulation of PTH type 2 receptor (pth2r) and its endogenous ligand pth2 by hedgehog signaling in zebrafish development. The Journal of endocrinology **211:**187-200.

28) **Backer CB, Gutzman JH, Pearson CG, Cheeseman IM.** 2012. CSAP localizes to polyglutamylated microtubules and promotes proper cilia function and zebrafish development. Mol Biol Cell **23:**2122-2130.

29) **Petersen SC, Luo R, Liebscher I, Giera S, Jeong SJ, Mogha A, Ghidinelli M, Feltri ML, Schoneberg T, Piao X, Monk KR.** 2015. The adhesion GPCR

GPR126 has distinct, domain-dependent functions in Schwann cell development mediated by interaction with laminin-211. Neuron **85:**755-769.

30) **Price MG, Davis CF, Deng F, Burgess DL.** 2005. The alpha-amino-3-hydroxyl-5-methyl-4-isoxazolepropionate receptor trafficking regulator "stargazin" is related to the claudin family of proteins by Its ability to mediate cell-cell adhesion. The Journal of biological chemistry **280:**19711-19720.

Bibliography

Abdullah N, Padmanarayana M, Marty NJ, Johnson CP. 2014. Quantitation of the calcium and membrane binding properties of the C2 domains of dysferlin. Biophysical journal **106:**382-389.

ACMG Genetics evaluation guidelines for the etiologic diagnosis of congenital hearing loss. Genetic Evaluation of Congenital Hearing Loss Expert Panel: ACMG statement. Genet Med.2002;4:162–171

Backer CB, Gutzman JH, Pearson CG, Cheeseman IM. 2012. CSAP localizes to polyglutamylated microtubules and promotes proper cilia function and zebrafish development. Mol Biol Cell **23:**2122-2130.

Baldwin CT, Weiss S, Farrer LA, De Stefano AL, Adair R, Franklyn B, Kidd KK, Korostishevsky M, Bonne-Tamir B. 1995. Linkage of congenital, recessive deafness (DFNB4) to chromosome 7q31 and evidence for genetic heterogeneity in the Middle Eastern Druze population. Human molecular genetics **4:**1637-1642.

Beurg M, Michalski N, Safieddine S, Bouleau Y, Schneggenburger R, Chapman ER, Petit C, Dulon D. 2010. Control of exocytosis by synaptotagmins and otoferlin in auditory hair cells. The Journal of neuroscience **30:**13281-13290.

Beurg M, Safieddine S, Roux I, Bouleau Y, Petit C, Dulon D. 2008. Calcium- and otoferlin-dependent exocytosis by immature outer hair cells. The Journal of neuroscience **28:**1798-1803.

Bhattacharya P, Yan YL, Postlethwait J, Rubin DA. 2011. Evolution of the vertebrate pth2 (tip39) gene family and the regulation of PTH type 2 receptor (pth2r) and its endogenous ligand pth2 by hedgehog signaling in zebrafish development. The Journal of endocrinology **211:**187-200.

Brandt A, Khimich D, Moser T. 2005. Few CaV1.3 channels regulate the exocytosis of a synaptic vesicle at the hair cell ribbon synapse. The Journal of neuroscience **25:**11577-11585.

Brandt N, Kuhn S, Munkner S, Braig C, Winter H, Blin N, Vonthein R, Knipper M, Engel J. 2007. Thyroid hormone deficiency affects postnatal spiking activity and expression of Ca2+ and K+ channels in rodent inner hair cells. The Journal of neuroscience **27:**3174-3186.

Burgess HA, Granato M. 2007. Sensorimotor gating in larval zebrafish. The Journal of neuroscience **27:**4984-4994.

Chatterjee P, Padmanarayana M, Abdullah N, Holman CL, LaDu J, Tanguay RL, Johnson CP. 2015. Otoferlin deficiency in zebrafish results in defects in balance

and hearing: rescue of the balance and hearing phenotype with full-length and truncated forms of mouse otoferlin. Molecular and cellular biology **35:**1043-1054.

Clemens Grisham R, Kindt K, Finger-Baier K, Schmid B, Nicolson T. 2013. Mutations in ap1b1 cause mistargeting of the Na(+)/K(+)-ATPase pump in sensory hair cells. PloS one **8:**e60866.

Cone-Wesson B, Vohr BR, Sininger YS, Widen JE, Folsom RC, Gorga MP, Norton SJ. 2000. Identification of neonatal hearing impairment: infants with hearing loss. Ear and hearing **21:**488-507.

Dulon D, Safieddine S, Jones SM, Petit C. 2009. Otoferlin is critical for a highly sensitive and linear calcium-dependent exocytosis at vestibular hair cell ribbon synapses. The Journal of neuroscience **29:**10474-10487.

Duncker SV, Franz C, Kuhn S, Schulte U, Campanelli D, Brandt N, Hirt B, Fakler B, Blin N, Ruth P, Engel J, Marcotti W, Zimmermann U, Knipper M. 2013. Otoferlin couples to clathrin-mediated endocytosis in mature cochlear inner hair cells. The Journal of neuroscience **33:**9508-9519.

Erickson T, Nicolson T. 2015. Identification of sensory hair-cell transcripts by thiouracil-tagging in zebrafish. BMC genomics **16:**842.

Ernest S, Rauch GJ, Haffter P, Geisler R, Petit C, Nicolson T. 2000. Mariner is defective in myosin VIIA: a zebrafish model for human hereditary deafness. Human molecular genetics **9:**2189-2196.

Faber DS, Fetcho JR, Korn H. 1989. Neuronal networks underlying the escape response in goldfish. General implications for motor control. Annals of the New York Academy of Sciences **563:**11-33.

Friedman TB, Griffith AJ. 2003. Human nonsyndromic sensorineural deafness. Annual review of genomics and human genetics **4:**341-402.

Friedman TB, Liang Y, Weber JL, Hinnant JT, Barber TD, Winata S, Arhya IN, Asher JH, Jr. 1995. A gene for congenital, recessive deafness DFNB3 maps to the pericentromeric region of chromosome 17. Nature genetics **9:**86-91.

Froehlicher M, Liedtke A, Groh K, Lopez-Schier H, Neuhauss SC, Segner H, Eggen RI. 2009. Estrogen receptor subtype beta2 is involved in neuromast development in zebrafish (Danio rerio) larvae. Developmental biology **330:**32-43.

Fuchs PA. 2005. Time and intensity coding at the hair cell's ribbon synapse. J Physiol-London **566:**7-12.

Fukushima K, Ramesh A, Srisailapathy CR, Ni L, Chen A, O'Neill M, Van Camp G, Coucke P, Smith SD, Kenyon JB, et al. 1995. Consanguineous nuclear families used to identify a new locus for recessive non-syndromic hearing loss on 14q. Human molecular genetics **4:**1643-1648.

Gale JE, Marcotti W, Kennedy HJ, Kros CJ, Richardson GP. 2001. FM1-43 dye behaves as a permeant blocker of the hair-cell mechanotransducer channel. The Journal of neuroscience **21:**7013-7025.

Geppert M, Goda Y, Stevens CF, Sudhof TC. 1997. The small GTP-binding protein Rab3A regulates a late step in synaptic vesicle fusion. Nature **387:**810-814.

Germana A, Paruta S, Germana GP, Ochoa-Erena FJ, Montalbano G, Cobo J, Vega JA. 2007. Differential distribution of S100 protein and calretinin in mechanosensory and chemosensory cells of adult zebrafish (Danio rerio). Brain research **1162:**48-55.

Goodyear RJ, Legan PK, Christiansen JR, Xia B, Korchagina J, Gale JE, Warchol ME, Corwin JT, Richardson GP. 2010. Identification of the hair cell soma-1 antigen, HCS-1, as otoferlin. Journal of the Association for Research in Otolaryngology : JARO **11:**573-586.

Griesinger CB, Richards CD, Ashmore JF. 2002. Fm1-43 reveals membrane recycling in adult inner hair cells of the mammalian cochlea. The Journal of neuroscience : **22:**3939-3952.

Guilford P, Ayadi H, Blanchard S, Chaib H, Le Paslier D, Weissenbach J, Drira M, Petit C. 1994. A human gene responsible for neurosensory, non-syndromic recessive deafness is a candidate homologue of the mouse sh-1 gene. Human molecular genetics **3:**989-993.

Guilford P, Ben Arab S, Blanchard S, Levilliers J, Weissenbach J, Belkahia A, Petit C. 1994. A non-syndrome form of neurosensory, recessive deafness maps to the pericentromeric region of chromosome 13q. Nature genetics **6:**24-28.

Han HW, Chou CM, Chu CY, Cheng CH, Yang CH, Hung CC, Hwang PP, Lee SJ, Liao YF, Huang CJ. 2014. The Nogo-C2/Nogo receptor complex regulates the morphogenesis of zebrafish lateral line primordium through modulating the expression of dkk1b, a Wnt signal inhibitor. PloS one **9:**e86345.

He S, Yang J. 2011. Maturation of neurotransmission in the developing rat cochlea: immunohistochemical evidence from differential expression of synaptophysin and synaptobrevin 2. European journal of histochemistry : EJH **55:**e2.

Heidrych P, Zimmermann U, Kuhn S, Franz C, Engel J, Duncker SV, Hirt B, Pusch CM, Ruth P, Pfister M, Marcotti W, Blin N, Knipper M. 2009. Otoferlin interacts

with myosin VI: implications for maintenance of the basolateral synaptic structure of the inner hair cell. Human molecular genetics **18:**2779-2790.

Helfmann S, Neumann P, Tittmann K, Moser T, Ficner R, Reisinger E. 2011. The crystal structure of the C(2)A domain of otoferlin reveals an unconventional top loop region. Journal of molecular biology **406:**479-490.

Hogan BM, Danks JA, Layton JE, Hall NE, Heath JK, Lieschke GJ. 2005. Duplicate zebrafish pth genes are expressed along the lateral line and in the central nervous system during embryogenesis. Endocrinology **146:**547-551.

Howe K, Clark MD, Torroja CF, Torrance J, Berthelot C, Muffato M, Collins JE, Humphray S, McLaren K, Matthews L, McLaren S, Sealy I, Caccamo M, Churcher C, Scott C, Barrett JC, Koch R, Rauch GJ, White S, Chow W, Kilian B, Quintais LT, Guerra-Assuncao JA, Zhou Y, Gu Y, Yen J, Vogel JH, Eyre T, Redmond S, Banerjee R, Chi J, Fu B, Langley E, Maguire SF, Laird GK, Lloyd D, Kenyon E, Donaldson S, Sehra H, Almeida-King J, Loveland J, Trevanion S, Jones M, Quail M, Willey D, Hunt A, Burton J, Sims S, McLay K, Plumb B, Davis J, Clee C, Oliver K, Clark R, Riddle C, Elliot D, Threadgold G, Harden G, Ware D, Mortimore B, Kerry G, Heath P, Phillimore B, Tracey A, Corby N, Dunn M, Johnson C, Wood J, Clark S, Pelan S, Griffiths G, Smith M, Glithero R, Howden P, Barker N, Stevens C, Harley J, Holt K, Panagiotidis G, Lovell J, Beasley H, Henderson C, Gordon D, Auger K, Wright D, Collins J, Raisen C, Dyer L, Leung K, Robertson L, Ambridge K, Leongamornlert D, McGuire S, Gilderthorp R, Griffiths C, Manthravadi D, Nichol S, Barker G, Whitehead S, Kay M, Brown J, Murnane C, Gray E, Humphries M, Sycamore N, Barker D, Saunders D, Wallis J, Babbage A, Hammond S, Mashreghi-Mohammadi M, Barr L, Martin S, Wray P, Ellington A, Matthews N, Ellwood M, Woodmansey R, Clark G, Cooper J, Tromans A, Grafham D, Skuce C, Pandian R, Andrews R, Harrison E, Kimberley A, Garnett J, Fosker N, Hall R, Garner P, Kelly D, Bird C, Palmer S, Gehring I, Berger A, Dooley CM, Ersan-Urun Z, Eser C, Geiger H, Geisler M, Karotki L, Kirn A, Konantz J, Konantz M, Oberlander M, Rudolph-Geiger S, Teucke M, Osoegawa K, Zhu B, Rapp A, Widaa S, Langford C, Yang F, Carter NP, Harrow J, Ning Z, Herrero J, Searle SM, Enright A, Geisler R, Plasterk RH, Lee C, Westerfield M, de Jong PJ, Zon LI, Postlethwait JH, Nusslein-Volhard C, Hubbard TJ, Roest Crollius H, Rogers J, Stemple DL, Begum S, Lloyd C, Lanz C, Raddatz G, Schuster SC. 2013. The zebrafish reference genome sequence and its relationship to the human genome. Nature **496:**498-503.

Hsiao CD, Tsai WY, Tsai HJ. 2002. Isolation and expression of two zebrafish homologues of parvalbumin genes related to chicken CPV3 and mammalian oncomodulin. Mechanisms of development **119 Suppl 1:**S161-166.

Hudspeth AJ. 1985. The cellular basis of hearing: the biophysics of hair cells. Science **230:**745-752.

Hudspeth AJ. 1997. How hearing happens. Neuron **19:**947-950.

Hudspeth AJ. 2000. Hearing and deafness. Neurobiology of disease **7:**511-514.

Javelle M, Marco CF, Timmermans M. 2011. In situ hybridization for the precise localization of transcripts in plants. Journal of visualized experiments : JoVE**:**e3328.

Jimenez JL, Bashir R. 2007. In silico functional and structural characterisation of ferlin proteins by mapping disease-causing mutations and evolutionary information onto three-dimensional models of their C2 domains. Journal of the neurological sciences **260:**114-123.

Johnson CP, Chapman ER. 2010. Otoferlin is a calcium sensor that directly regulates SNARE-mediated membrane fusion. The Journal of cell biology **191:**187-197.

Jung S, Maritzen T, Wichmann C, Jing Z, Neef A, Revelo NH, Al-Moyed H, Meese S, Wojcik SM, Panou I, Bulut H, Schu P, Ficner R, Reisinger E, Rizzoli SO, Neef J, Strenzke N, Haucke V, Moser T. 2015. Disruption of adaptor protein 2mu (AP-2mu) in cochlear hair cells impairs vesicle reloading of synaptic release sites and hearing. The EMBO journal **34:**2686-2702.

Kappler JA, Starr CJ, Chan DK, Kollmar R, Hudspeth AJ. 2004. A nonsense mutation in the gene encoding a zebrafish myosin VI isoform causes defects in hair-cell mechanotransduction. Proceedings of the National Academy of Sciences of the United States of America **101:**13056-13061.

Kelsell DP, Dunlop J, Stevens HP, Lench NJ, Liang JN, Parry G, Mueller RF, Leigh IM. 1997. Connexin 26 mutations in hereditary non-syndromic sensorineural deafness. Nature **387:**80-83.

Khan Z, Carey J, Park HJ, Lehar M, Lasker D, Jinnah HA. 2004. Abnormal motor behavior and vestibular dysfunction in the stargazer mouse mutant. Neuroscience **127:**785-796.

Khimich D, Nouvian R, Pujol R, Tom Dieck S, Egner A, Gundelfinger ED, Moser T. 2005. Hair cell synaptic ribbons are essential for synchronous auditory signalling. Nature **434:**889-894.

Kimmel CB, Ballard WW, Kimmel SR, Ullmann B, Schilling TF. 1995. Stages of embryonic development of the zebrafish. Developmental dynamics : an official publication of the American Association of Anatomists **203:**253-310.

Kindt KS, Finch G, Nicolson T. 2012. Kinocilia mediate mechanosensitivity in developing zebrafish hair cells. Developmental cell **23:**329-341.

Kraemer AM, Saraiva LR, Korsching SI. 2008. Structural and functional diversification in the teleost S100 family of calcium-binding proteins. BMC evolutionary biology **8:**48.

Kushwaha N, Harwood SC, Wilson AM, Berger M, Tecott LH, Roth BL, Albert PR. 2006. Molecular determinants in the second intracellular loop of the 5-hydroxytryptamine-1A receptor for G-protein coupling. Molecular pharmacology **69:**1518-1526.

Leibovici M, Safieddine S, Petit C. 2008. Mouse models for human hereditary deafness. Current topics in developmental biology **84:**385-429.

LeMasurier M, Gillespie PG. 2005. Hair-cell mechanotransduction and cochlear amplification. Neuron **48:**403-415.

Lindema S, Gernet M, Bennay M, Koch M, Loscher W. 2008. Comparative analysis of anxiety-like behaviors and sensorimotor functions in two rat mutants, ci2 and ci3, with lateralized rotational behavior. Physiology & behavior **93:**417-426.

Liu J, Aoki M, Illa I, Wu C, Fardeau M, Angelini C, Serrano C, Urtizberea JA, Hentati F, Hamida MB, Bohlega S, Culper EJ, Amato AA, Bossie K, Oeltjen J, Bejaoui K, McKenna-Yasek D, Hosler BA, Schurr E, Arahata K, de Jong PJ, Brown RH, Jr. 1998. Dysferlin, a novel skeletal muscle gene, is mutated in Miyoshi myopathy and limb girdle muscular dystrophy. Nature genetics **20:**31-36.

Longo-Guess C, Gagnon LH, Bergstrom DE, Johnson KR. 2007. A missense mutation in the conserved C2B domain of otoferlin causes deafness in a new mouse model of DFNB9. Hearing research **234:**21-28.

Maeda R, Kindt KS, Mo W, Morgan CP, Erickson T, Zhao H, Clemens-Grisham R, Barr-Gillespie PG, Nicolson T. 2014. Tip-link protein protocadherin 15 interacts with transmembrane channel-like proteins TMC1 and TMC2. Proceedings of the National Academy of Sciences of the United States of America **111:**12907-12912.

Marty NJ, Holman CL, Abdullah N, Johnson CP. 2013. The C2 domains of otoferlin, dysferlin, and myoferlin alter the packing of lipid bilayers. Biochemistry **52:**5585-5592.

Marres HA. Congenital abnormalities of the inner ear. Ludman H, Wright T Bath, editors. Arnold & Oxford University Press; Diseases of the Ear.1998:288–296.

Mason JA, **Herrmann KR**. Universal infant hearing screening by automated auditory brainstem response measurement. Pediatrics. 1998;101:221–228

Matos-Cruz V, Blasic J, Nickle B, Robinson PR, Hattar S, Halpern ME. 2011. Unexpected diversity and photoperiod dependence of the zebrafish melanopsin system. PloS one **6:**e25111.

Matsunaga T, Mutai H, Kunishima S, Namba K, Morimoto N, Shinjo Y, Arimoto Y, Kataoka Y, Shintani T, Morita N, Sugiuchi T, Masuda S, Nakano A, Taiji H, Kaga K. 2012. A prevalent founder mutation and genotype-phenotype correlations of OTOF in Japanese patients with auditory neuropathy. Clinical genetics **82:**425-432.

Matthews G, Fuchs P. 2010. The diverse roles of ribbon synapses in sensory neurotransmission. Nature reviews. Neuroscience **11:**812-822.

Mcmahon HT, Missler M, Li C, Sudhof TC. 1995. Complexins - Cytosolic Proteins That Regulate Snap Receptor Function. Cell **83:**111-119.

Migliosi V, Modamio-Hoybjor S, Moreno-Pelayo MA, Rodriguez-Ballesteros M, Villamar M, Telleria D, Menendez I, Moreno F, Del Castillo I. 2002. Q829X, a novel mutation in the gene encoding otoferlin (OTOF), is frequently found in Spanish patients with prelingual non-syndromic hearing loss. Journal of medical genetics **39:**502-506.

Monroe JD, Rajadinakaran G, Smith ME. 2015. Sensory hair cell death and regeneration in fishes. Frontiers in cellular neuroscience **9:**131.

Moser T, Brandt A, Lysakowski A. 2006. Hair cell ribbon synapses. Cell and tissue research **326:**347-359.

Nicolson T. 2005. The genetics of hearing and balance in zebrafish. Annual review of genetics **39:**9-22.

Nicolson T, Rusch A, Friedrich RW, Granato M, Ruppersberg JP, Nusslein-Volhard C. 1998. Genetic analysis of vertebrate sensory hair cell mechanosensation: the zebrafish circler mutants. Neuron **20:**271-283.

Nouvian R, Beutner D, Parsons TD, Moser T. 2006. Structure and function of the hair cell ribbon synapse. The Journal of membrane biology **209:**153-165.

Nouvian R, Neef J, Bulankina AV, Reisinger E, Pangrsic T, Frank T, Sikorra S, Brose N, Binz T, Moser T. 2011. Exocytosis at the hair cell ribbon synapse apparently operates without neuronal SNARE proteins. Nature neuroscience **14:**411-413.

Novak AE, Ribera AB. 2003. Immunocytochemistry as a tool for zebrafish developmental neurobiology. Methods in cell science **25:**79-83.

Obholzer N, Wolfson S, Trapani JG, Mo W, Nechiporuk A, Busch-Nentwich E, Seiler C, Sidi S, Sollner C, Duncan RN, Boehland A, Nicolson T. 2008. Vesicular glutamate transporter 3 is required for synaptic transmission in zebrafish hair cells. The Journal of neuroscience **28:**2110-2118.

Pack AK, Slepecky NB. 1995. Cytoskeletal and calcium-binding proteins in the mammalian organ of Corti: cell type-specific proteins displaying longitudinal and radial gradients. Hearing research **91:**119-135.

Padmanarayana M, Hams N, Speight LC, Petersson EJ, Mehl RA, Johnson CP. 2014. Characterization of the lipid binding properties of Otoferlin reveals specific interactions between PI(4,5)P2 and the C2C and C2F domains. Biochemistry **53:**5023-5033.

Pangrsic T, Lasarow L, Reuter K, Takago H, Schwander M, Riedel D, Frank T, Tarantino LM, Bailey JS, Strenzke N, Brose N, Muller U, Reisinger E, Moser T. 2010. Hearing requires otoferlin-dependent efficient replenishment of synaptic vesicles in hair cells. Nature neuroscience **13:**869-876.

Pangrsic T, Reisinger E, Moser T. 2012. Otoferlin: a multi-C2 domain protein essential for hearing. Trends in neurosciences **35:**671-680.

Parving A. The need for universal neonatal hearing screening: some aspects of epidemiology and identification. Acta Paediatr Suppl. 1999;88:69–72.

Petersen SC, Luo R, Liebscher I, Giera S, Jeong SJ, Mogha A, Ghidinelli M, Feltri ML, Schoneberg T, Piao X, Monk KR. 2015. The adhesion GPCR GPR126 has distinct, domain-dependent functions in Schwann cell development mediated by interaction with laminin-211. Neuron **85:**755-769.

Petit C, Levilliers J, Hardelin JP. 2001. Molecular genetics of hearing loss. Annual review of genetics **35:**589-646.

Petit C, Levilliers J, Marlin S, Hardelin J-P. Hereditary hearing loss. Scriver CR, Beaudet AL, Sly WS, Valle D, editors. New York: McGraw-Hill;2001:6281–6328

Price MG, Davis CF, Deng F, Burgess DL. 2005. The alpha-amino-3-hydroxyl-5-methyl-4-isoxazolepropionate receptor trafficking regulator "stargazin" is related to the claudin family of proteins by Its ability to mediate cell-cell adhesion. The Journal of biological chemistry **280:**19711-19720.

Ramakrishnan NA, Drescher MJ, Morley BJ, Kelley PM, Drescher DG. 2014. Calcium Regulates Molecular Interactions of Otoferlin with SNARE Proteins Required for Hair Cell Exocytosis. The Journal of biological chemistry.

Reim K, Mansour M, Varoqueaux F, McMahon HT, Sudhof TC, Brose N, Rosenmund C. 2001. Complexins regulate a late step in Ca2+-dependent neurotransmitter release. Cell **104:**71-81.

Reim K, Wegmeyer H, Brandstatter JH, Xue MS, Rosenmund C, Dresbach T, Hofmann K, Brose N. 2005. Structurally and functionally unique complexins at retinal ribbon synapses. Journal of Cell Biology **169:**669-680.

Reisinger E, Bresee C, Neef J, Nair R, Reuter K, Bulankina A, Nouvian R, Koch M, Buckers J, Kastrup L, Roux I, Petit C, Hell SW, Brose N, Rhee JS, Kugler S, Brigande JV, Moser T. 2011. Probing the functional equivalence of otoferlin and synaptotagmin 1 in exocytosis. The Journal of neuroscience **31:**4886-4895.

Revelo NH, Kamin D, Truckenbrodt S, Wong AB, Reuter-Jessen K, Reisinger E, Moser T, Rizzoli SO. 2014. A new probe for super-resolution imaging of membranes elucidates trafficking pathways. The Journal of cell biology **205:**591-606.

Rizo J, Sudhof TC. 1998. C2-domains, structure and function of a universal Ca2+-binding domain. The Journal of biological chemistry **273:**15879-15882.

Roberts A, Trapnell C, Donaghey J, Rinn JL, Pachter L. 2011. Improving RNA-Seq expression estimates by correcting for fragment bias. Genome biology **12:**R22.

Rodriguez-Ballesteros M, Reynoso R, Olarte M, Villamar M, Morera C, Santarelli R, Arslan E, Meda C, Curet C, Volter C, Sainz-Quevedo M, Castorina P, Ambrosetti U, Berrettini S, Frei K, Tedin S, Smith J, Cruz Tapia M, Cavalle L, Gelvez N, Primignani P, Gomez-Rosas E, Martin M, Moreno-Pelayo MA, Tamayo M, Moreno-Barral J, Moreno F, del Castillo I. 2008. A multicenter study on the prevalence and spectrum of mutations in the otoferlin gene (OTOF) in subjects with nonsyndromic hearing impairment and auditory neuropathy. Human mutation **29:**823-831.

Roux I, Hosie S, Johnson SL, Bahloul A, Cayet N, Nouaille S, Kros CJ, Petit C, Safieddine S. 2009. Myosin VI is required for the proper maturation and function of inner hair cell ribbon synapses. Human molecular genetics **18:**4615-4628.

Roux I, Safieddine S, Nouvian R, Grati M, Simmler MC, Bahloul A, Perfettini I, Le Gall M, Rostaing P, Hamard G, Triller A, Avan P, Moser T, Petit C. 2006. Otoferlin, defective in a human deafness form, is essential for exocytosis at the auditory ribbon synapse. Cell **127:**277-289.

Ruel J, Emery S, Nouvian R, Bersot T, Amilhon B, Van Rybroek JM, Rebillard G, Lenoir M, Eybalin M, Delprat B, Sivakumaran TA, Giros B, El Mestikawy S, Moser T, Smith RJ, Lesperance MM, Puel JL. 2008. Impairment of SLC17A8 encoding vesicular glutamate transporter-3, VGLUT3, underlies nonsyndromic deafness DFNA25 and inner hair cell dysfunction in null mice. American journal of human genetics **83:**278-292.

Sabaliauskas NA, Foutz CA, Mest JR, Budgeon LR, Sidor AT, Gershenson JA, Joshi SB, Cheng KC. 2006. High-throughput zebrafish histology. Methods **39:**246-254.

Safieddine S, El-Amraoui A, Petit C. 2012. The auditory hair cell ribbon synapse: from assembly to function. Annual review of neuroscience **35:**509-528.

Safieddine S, Wenthold RJ. 1999. SNARE complex at the ribbon synapses of cochlear hair cells: analysis of synaptic vesicle- and synaptic membrane-associated proteins. The European journal of neuroscience **11:**803-812.

Schoch S, Castillo PE, Jo T, Mukherjee K, Geppert M, Wang Y, Schmitz F, Malenka RC, Sudhof TC. 2002. RIM1alpha forms a protein scaffold for regulating neurotransmitter release at the active zone. Nature **415:**321-326.

Schug N, Braig C, Zimmermann U, Engel J, Winter H, Ruth P, Blin N, Pfister M, Kalbacher H, Knipper M. 2006. Differential expression of otoferlin in brain, vestibular system, immature and mature cochlea of the rat. The European journal of neuroscience **24:**3372-3380.

Schwander M, Sczaniecka A, Grillet N, Bailey JS, Avenarius M, Najmabadi H, Steffy BM, Federe GC, Lagler EA, Banan R, Hice R, Grabowski-Boase L, Keithley EM, Ryan AF, Housley GD, Wiltshire T, Smith RJH, Tarantino LM, Muller U. 2007. A forward genetics screen in mice identifies recessive deafness traits and reveals that pejvakin is essential for outer hair cell function. Journal of Neuroscience **27:**2163-2175.

Seal RP, Akil O, Yi E, Weber CM, Grant L, Yoo J, Clause A, Kandler K, Noebels JL, Glowatzki E, Lustig LR, Edwards RH. 2008. Sensorineural deafness and seizures in mice lacking vesicular glutamate transporter 3. Neuron **57:**263-275.

Seiler C, Ben-David O, Sidi S, Hendrich O, Rusch A, Burnside B, Avraham KB, Nicolson T. 2004. Myosin VI is required for structural integrity of the apical surface of sensory hair cells in zebrafish. Developmental biology **272:**328-338.

Seiler C, Nicolson T. 1999. Defective calmodulin-dependent rapid apical endocytosis in zebrafish sensory hair cell mutants. Journal of neurobiology **41:**424-434.

Sepe M, Lignitto L, Porpora M, Delle Donne R, Rinaldi L, Belgianni G, Colucci G, Cuomo O, Viggiano D, Scorziello A, Garbi C, Annunziato L, Feliciello A. 2014. Proteolytic control of neurite outgrowth inhibitor NOGO-A by the cAMP/PKA pathway. Proceedings of the National Academy of Sciences of the United States of America **111:**15729-15734.

Sheets L, Hagen MW, Nicolson T. 2014. Characterization of Ribeye subunits in zebrafish hair cells reveals that exogenous Ribeye B-domain and CtBP1 localize to the basal ends of synaptic ribbons. PloS one **9:**e107256.

Sheets L, Kindt KS, Nicolson T. 2012. Presynaptic CaV1.3 channels regulate synaptic ribbon size and are required for synaptic maintenance in sensory hair cells. The Journal of neuroscience **32:**17273-17286.

Sheets L, Trapani JG, Mo W, Obholzer N, Nicolson T. 2011. Ribeye is required for presynaptic Ca(V)1.3a channel localization and afferent innervation of sensory hair cells. Development **138:**1309-1319.

Sidi S, Busch-Nentwich E, Friedrich R, Schoenberger U, Nicolson T. 2004. gemini encodes a zebrafish L-type calcium channel that localizes at sensory hair cell ribbon synapses. The Journal of neuroscience **24:**4213-4223.

Sollner C, Rauch GJ, Siemens J, Geisler R, Schuster SC, Muller U, Nicolson T. 2004. Mutations in cadherin 23 affect tip links in zebrafish sensory hair cells. Nature **428:**955-959.

Starr A, Sininger YS, Pratt H. 2000. The varieties of auditory neuropathy. Journal of basic and clinical physiology and pharmacology **11:**215-230.

Strenzke N, Chakrabarti R, Al-Moyed H, Muller A, Hoch G, Pangrsic T, Yamanbaeva G, Lenz C, Pan KT, Auge E, Geiss-Friedlander R, Urlaub H, Brose N, Wichmann C, Reisinger E. 2016. Hair cell synaptic dysfunction, auditory fatigue and thermal sensitivity in otoferlin Ile515Thr mutants. The EMBO journal.

Strenzke N, Chanda S, Kopp-Scheinpflug C, Khimich D, Reim K, Bulankina AV, Neef A, Wolf F, Brose N, Xu-Friedman MA, Moser T. 2009. Complexin-I Is Required for High-Fidelity Transmission at the Endbulb of Held Auditory Synapse. Journal of Neuroscience **29:**7991-8004.

Sztal T, Berger S, Currie PD, Hall TE. 2011. Characterization of the laminin gene family and evolution in zebrafish. Developmental dynamics **240:**422-431.

Tekin M, Akcayoz D, Incesulu A. 2005. A novel missense mutation in a C2 domain of OTOF results in autosomal recessive auditory neuropathy. American journal of medical genetics. Part A **138:**6-10.

Tewson P, Westenberg M, Zhao Y, Campbell RE, Quinn AM, Hughes TE. 2012. Simultaneous detection of Ca2+ and diacylglycerol signaling in living cells. PloS one **7:**e42791.

Therrien C, Di Fulvio S, Pickles S, Sinnreich M. 2009. Characterization of lipid binding specificities of dysferlin C2 domains reveals novel interactions with phosphoinositides. Biochemistry **48:**2377-2384.

Thisse C, Thisse B. 2008. High-resolution in situ hybridization to whole-mount zebrafish embryos. Nature protocols **3:**59-69.

Trapnell C, Hendrickson DG, Sauvageau M, Goff L, Rinn JL, Pachter L. 2013. Differential analysis of gene regulation at transcript resolution with RNA-seq. Nature biotechnology **31:**46-53.

Trapnell C, Pachter L, Salzberg SL. 2009. TopHat: discovering splice junctions with RNA-Seq. Bioinformatics **25:**1105-1111.

Uthaiah RC, Hudspeth AJ. 2010. Molecular anatomy of the hair cell's ribbon synapse. The Journal of neuroscience **30:**12387-12399.

Valiyaveettil M, Alamneh Y, Miller SA, Hammamieh R, Wang Y, Arun P, Wei Y, Oguntayo S, Nambiar MP. 2012. Preliminary studies on differential expression of auditory functional genes in the brain after repeated blast exposures. Journal of rehabilitation research and development **49:**1153-1162.

Varga R, Avenarius MR, Kelley PM, Keats BJ, Berlin CI, Hood LJ, Morlet TG, Brashears SM, Starr A, Cohn ES, Smith RJ, Kimberling WJ. 2006. OTOF mutations revealed by genetic analysis of hearing loss families including a potential temperature sensitive auditory neuropathy allele. Journal of medical genetics **43:**576-581.

Varga R, Kelley PM, Keats BJ, Starr A, Leal SM, Cohn E, Kimberling WJ. 2003. Non-syndromic recessive auditory neuropathy is the result of mutations in the otoferlin (OTOF) gene. Journal of medical genetics **40:**45-50.

Vincent PF, Bouleau Y, Safieddine S, Petit C, Dulon D. 2014. Exocytotic machineries of vestibular type I and cochlear ribbon synapses display similar intrinsic otoferlin-dependent Ca2+ sensitivity but a different coupling to Ca2+ channels. The Journal of neuroscience **34:**10853-10869.

Vogl C, Cooper BH, Neef J, Wojcik SM, Reim K, Reisinger E, Brose N, Rhee JS, Moser T, Wichmann C. 2015. Unconventional molecular regulation of synaptic vesicle replenishment in cochlear inner hair cells. Journal of cell science **128:**638-644.

Waterman RE, Bell DH. 1984. Epithelial fusion during early semicircular canal formation in the embryonic zebrafish, Brachydanio rerio. The Anatomical record **210:**101-114.

Westerfield M. 2000. The zebrafish book. A guide for the laboratory use of zebrafish (Danio rerio). 4th ed., Univ. of Oregon Press, Eugene.

Whitfield TT. 2002. Zebrafish as a model for hearing and deafness. Journal of neurobiology **53:**157-171.

Winata CL, Korzh S, Kondrychyn I, Zheng W, Korzh V, Gong Z. 2009. Development of zebrafish swimbladder: The requirement of Hedgehog signaling in specification and organization of the three tissue layers. Developmental biology **331:**222-236.

Wright S, Hwang Y, Oertel D. 2014. Synaptic transmission between end bulbs of Held and bushy cells in the cochlear nucleus of mice with a mutation in Otoferlin. Journal of neurophysiology **112:**3173-3188.

Wu W, Rahman MN, Guo J, Roy N, Xue L, Cahill CM, Zhang S, Jia Z. 2015. Function coupling of otoferlin with GAD65 acts to modulate GABAergic activity. Journal of molecular cell biology **7:**168-179.

Yasunaga S, Grati M, Chardenoux S, Smith TN, Friedman TB, Lalwani AK, Wilcox ER, Petit C. 2000. OTOF encodes multiple long and short isoforms: genetic evidence that the long ones underlie recessive deafness DFNB9. American journal of human genetics **67:**591-600.

Yasunaga S, Grati M, Cohen-Salmon M, El-Amraoui A, Mustapha M, Salem N, El-Zir E, Loiselet J, Petit C. 1999. A mutation in OTOF, encoding otoferlin, a FER-1-like protein, causes DFNB9, a nonsyndromic form of deafness. Nature genetics **21:**363-369.

Zak M, Bress A, Brandt N, Franz C, Ruth P, Pfister M, Knipper M, Blin N. 2012. Ergic2, a brain specific interacting partner of Otoferlin. Cellular physiology and biochemistry : international journal of experimental cellular physiology, biochemistry, and pharmacology **29:**941-948.

Zenisek D, Davila V, Wan L, Almers W. 2003. Imaging calcium entry sites and ribbon structures in two presynaptic cells. The Journal of neuroscience **23:**2538-2548

.

Zhao Y, Araki S, Wu J, Teramoto T, Chang YF, Nakano M, Abdelfattah AS, Fujiwara M, Ishihara T, Nagai T, Campbell RE. 2011. An expanded palette of genetically encoded Ca(2)(+) indicators. Science **333:**1888-1891.